

UNCLASSIFIED

AD NUMBER

AD919085

LIMITATION CHANGES

TO:

Approved for public release; distribution is unlimited.

FROM:

Distribution authorized to U.S. Gov't. agencies only; Administrative/Operational Use; MAR 1974. Other requests shall be referred to Air Force Aero Propulsion Lab., Wright-Patterson AFB, OH 45433.

AUTHORITY

AFWAL ltr 9 Jun 1076

THIS PAGE IS UNCLASSIFIED

THIS REPORT HAS BEEN DELIMITED
AND CLEARED FOR PUBLIC RELEASE
UNDER DOD DIRECTIVE 5200.20 AND
NO RESTRICTIONS ARE IMPOSED UPON
ITS USE AND DISCLOSURE,

DISTRIBUTION STATEMENT A

APPROVED FOR PUBLIC RELEASE;
DISTRIBUTION UNLIMITED,

AFAPL-TR-73-106

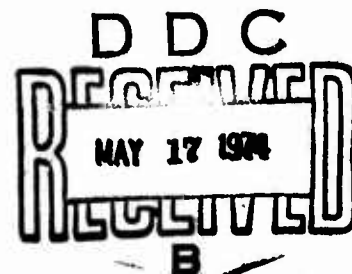
AD919085

AN EVALUATION OF A SPACE FLIGHT TEST OF HARDENED SOLAR ARRAY TECHNOLOGY

JOHN M. GREEN, 1st LT, USAF

TECHNICAL REPORT AFAPL-TR-73-106

MARCH 1974



Distribution limited to U.S. Government agencies only; Test and Evaluation;
Sept. 1973. Other requests for this document must be referred to AF Aero
Propulsion Laboratory (POE-2), WPAFB, Ohio 45433.

**AIR FORCE AERO PROPULSION LABORATORY
AIR FORCE SYSTEMS COMMAND
WRIGHT-PATTERSON AIR FORCE BASE, OHIO 45433**

NOTICE

When government drawings, specifications or other data are used for any purpose other than in connection with a definitely related government procurement operation, the United States Government thereby incurs no responsibility nor any obligation whatsoever; and the fact that the government may have formulated, furnished, or in any way supplied the said drawings, specifications, or other data, is not to be regarded by implication or otherwise as in any manner licensing the holder or any other person or corporation, or conveying any rights or permission to manufacture, use, or sell any patented invention that may in any way be related thereto.

Copies of this report should not be returned unless return is required by security considerations, contractual obligations, or notice on a specific document.

AFAPL-TR-73-106

**AN EVALUATION OF A SPACE FLIGHT TEST
OF HARDENED SOLAR ARRAY TECHNOLOGY**

JOHN M. GREEN, 1st LT, USAF

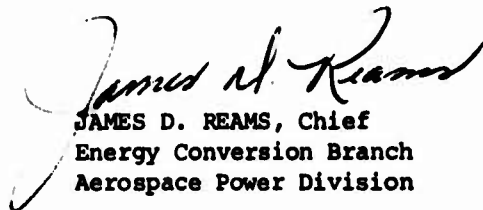
Distribution limited to U.S. Government agencies only; Test and Evaluation;
Sept. 1973. Other requests for this document must be referred to AF Aero
Propulsion Laboratory (POE-2), WPAFB, Ohio 45433.

FOREWORD

This Technical Report covers all work performed under an in-house effort from 15 January 1972 to 15 April 1973. The work was initiated under Project Nr. 3145, Task Nr. 19, Work Unit Nr. 33, "Support of TRIAD I Radiation Hardened Solar Cells for Space Flight Test."

The work of this effort was conducted by Lt John M. Green, AFAPL/POE-2, Energy Conversion Branch, Aerospace Power Division of the Air Force Aero Propulsion Laboratory, Wright-Patterson Air Force Base, Ohio. Mr. W. E. Ray of the Applied Physics Laboratory of Johns Hopkins University (APL), provided valuable assistance and functioned as the APL focal point for this effort. The satellite vehicle for this experiment was a Navy navigational satellite of the Transit Series. FY71 Laboratory Director's Funds were used to initiate procurement of the hardened solar cells for the flight test in order to meet a tight launch schedule.

This technical report has been reviewed and is approved for publication.


JAMES D. REAMS, Chief
Energy Conversion Branch
Aerospace Power Division

ABSTRACT

Hardened solar array panel segments and experimental modules fabricated by TRW for the Air Force Aero Propulsion Laboratory are described. Preflight tests and data reduction techniques used for this experiment are explained and the results reported. The flight test, which was conducted by the Applied Physics Laboratory of Johns Hopkins University, yielded very little data due to a telemetry system failure of the host satellite (a Navy navigation satellite of the Transit series). Data which was obtained in the 30 days of flight prior to the failure is presented and discussed.

TABLE OF CONTENTS

| SECTION | PAGE |
|--|------|
| I INTRODUCTION | 1 |
| II DISCUSSION | 2 |
| 1.0 Solar Panel Segments | 2 |
| 1.1 Test Procedure | 2 |
| 1.2 Test Results | 2 |
| 1.3 Flight Data | 2 |
| 2.0 Experimental Modules | 3 |
| 2.1 I-V Characteristics | 4 |
| 2.2 Angle of Incidence | 4 |
| 2.2.1 Data Corrections | 4 |
| 2.2.1.1 Temperature Variations | 6 |
| 2.2.1.2 Ambient Light | 6 |
| 2.2.1.3 Variations in Light Intensity | 6 |
| 2.2.2 Experimental Procedure | 7 |
| 2.2.3 Results | 7 |
| 2.2.3.1 Current | 7 |
| 2.2.3.2 Voltage | 9 |
| 2.3 Flight Data | 9 |
| III CONCLUSIONS | 10 |
| APPENDIX A. DERIVATION OF CO-ORDINATE TRANSFORMATIONS FOR CALCULATIONS OF INTENSITY CORRECTIONS | 58 |
| APPENDIX B. COMPUTER PROGRAM FOR TRIAD DATA REDUCTION | 63 |

ILLUSTRATIONS

| FIGURE | PAGE |
|---|------|
| 1. Panel Layout and Nomenclature | 11 |
| 2. Relative Intensity of Solar Simulator Beam | 12 |
| 3. V vs. I For Panel Segment 1A | 13 |
| 4. V vs. I For Panel Segment 2A | 14 |
| 5. V vs. I For Panel Segment 3A | 15 |
| 6. V vs. I For Panel Segment 4A | 16 |
| 7. V vs. I For Panel Segment 1B | 17 |
| 8. V vs. I For Panel Segment 2B | 18 |
| 9. V vs. I For Panel Segment 3B | 19 |
| 10. V vs. I For Panel Segment 4B | 20 |
| 11. Environment Survey Panel (ESP) | 21 |
| 12. V vs. I For Module 1 | 22 |
| 13. V vs. I For Module 2 | 23 |
| 14. V vs. I For Module 3 | 24 |
| 15. V vs. I For Module 4 | 25 |
| 16. V vs. I For Module 5 | 26 |
| 17. V vs. I For Module 6 | 27 |
| 18. TRIAD Telemetry Simulation Loads Schematic Diagram | 28 |
| 19. Normalizing Factors vs. Sensistor Resistance to Correct Data to 25°C | 29 |
| 20. Contribution of Ambient Light to Short Circuit Current Output | 30 |
| 21. Short Circuit Current vs. Solar Attitude Angle For Module 1 | 31 |
| 22. Short Circuit Current vs. Solar Attitude Angle for Module 2 | 32 |

ILLUSTRATIONS (CONTD)

| FIGURE | PAGE |
|---|------|
| 23. Short Circuit Current vs. Solar Attitude Angle for Module 3 | 33 |
| 24. Short Circuit Current vs. Solar Attitude Angle for Module 4 | 34 |
| 25. Short Circuit Current vs. Solar Attitude Angle for Module 5 | 35 |
| 26. Short Circuit Current vs. Solar Attitude Angle for Module 6 | 36 |
| 27. Module 1 Current vs. Solar Attitude Angle at Load Point One | 37 |
| 28. Module 2 Current vs. Solar Attitude Angle at Load Point One | 38 |
| 29. Module 3 Current vs. Solar Attitude Angle at Load Point One | 39 |
| 30. Module 4 Current vs. Solar Attitude Angle at Load Point One | 40 |
| 31. Module 5 Current vs. Solar Attitude Angle at Load Point One | 41 |
| 32. Module 6 Current vs. Solar Attitude Angle at Load Point One | 42 |
| 33. Module 1 Current vs. Solar Attitude Angle at Load Point Two | 43 |
| 34. Module 2 Current vs. Solar Attitude Angle at Load Point Two | 44 |
| 35. Module 3 Current vs. Solar Attitude Angle at Load Point Two | 45 |
| 36. Module 4 Current vs. Solar Attitude Angle at Load Point Two | 46 |
| 37. Module 5 Current vs. Solar Attitude Angle at Load Point Two | 47 |
| 38. Module 6 Current vs. Solar Attitude Angle at Load Point Two | 48 |

ILLUSTRATIONS (CONTD)

| FIGURE | PAGE |
|---|------|
| 39. Open Circuit Voltage vs. Solar Attitude Angle for Module Group 1 | 49 |
| 40. Open Circuit Voltage vs. Solar Attitude Angle for Module Group 2 | 50 |
| 41. Open Circuit Voltage vs. Solar Attitude Angle for Module Group 3 | 51 |
| 42. Module Group 1 Voltage vs. Solar Attitude Angle at Load Point One | 52 |
| 43. Module Group 2 Voltage vs. Solar Attitude Angle at Load Point One | 53 |
| 44. Module Group 3 Voltage vs. Solar Attitude Angle at Load Point One | 54 |
| 45. Module Group 1 Voltage vs. Solar Attitude Angle at Load Point Two | 55 |
| 46. Module Group 2 Voltage vs. Solar Attitude Angle at Load Point Two | 56 |
| 47. Module Group 3 Voltage vs. Solar Attitude Angle at Load Point Two | 57 |
| 48. Inertial Coordinate System with Panel in the Unrotated Position | 59 |
| 49. Pitch Rotation | 60 |
| 50. Roll Rotation | 60 |
| 51. Computer Program Flowchart | 64 |
| 52. Program Printout | 65 |

LIST OF SYMBOLS

| | |
|-------------|--|
| Eff. | Efficiency of a Solar Cell |
| \bar{i} | X-axis Unit Vector of the Inertial Coordinate System |
| I | Current |
| I_m | Current at Maximum Power Point |
| I_{sc} | Short Circuit Current of Solar Cell Array |
| I'_{sc} | Short Circuit Current Corrected for Ambient Light |
| \bar{j} | Y-axis Unit Vector of the Inertial Coordinate System |
| \bar{k} | Z-axis Unit Vector of the Inertial Coordinate System |
| \bar{M}_1 | Position Vector of Module 1 |
| \bar{M}_2 | Position Vector of Module 2 |
| \bar{M}_3 | Position Vector of Module 3 |
| \bar{M}_4 | Position Vector Of Module 4 |
| \bar{M}_5 | Position Vector of Module 5 |
| \bar{M}_6 | Position Vector of Module 6 |
| \bar{p} | Vector Perpendicular to Module Surface |
| P_M | Power at Maximum Power Point |
| V_m | Voltage at Maximum Power Point |
| V_{oc} | Open Circuit Voltage of Solar Cell Array |
| x_B | X-axis Unit Vector of the Local Coordinate System |
| x_{Ba} | X-axis Unit Vector After Pitch Rotation Only |
| x_{Bb} | X-axis Unit Vector After Roll Rotation Only |
| y_B | Y-axis Unit Vector of the Local Coordinate System |
| y_{Ba} | Y-axis Unit Vector After Pitch Rotation Only |
| y_{Bb} | Y-axis Unit Vector After Roll Rotation Only |

LIST OF SYMBOLS (CONT'D)

| | |
|------------|---|
| Z_B | Z-axis Unit Vector of the Local Coordinate System |
| Z_{Ba} | Z-axis Unit Vector After Pitch Rotation Only |
| Z_{Bb} | Z-axis Unit Vector After Roll Rotation Only |
| θ_p | Pitch Rotation Angle |
| θ_R | Roll Rotation Angle |
| θ_s | Solar Attitude Angle |

SECTION I

INTRODUCTION

On 2 September 1972, the Navy launched a navigational satellite of the Transit series. This satellite, which was called TRIAD during its development, has a radioisotope thermal generator (RTG) for its main power source; however, it has an auxiliary power source consisting of four experimental hardened solar panel segments. Another one of the experiments on board the spacecraft is a set of six solar cell modules designated the Environmental Survey Panel (ESP). This report will describe the pre-flight tests that were conducted on the solar power experiments, the results of those tests, and the flight data that are available.

Four solar panel segments were built by TRW under AFAPL Contract F33615-71-C-1260. The panel segments had been tested by TRW and were considered qualified for space flight. Details of the fabrication and testing of these segments are available in the Contract Final Report AFAPL-TR-72-33. During flight qualification thermal cycling tests at the Applied Physics Laboratory (APL) on 18 May 1972, three of the panels failed catastrophically. Failure mechanism was debonding of the aluminum skin from the honeycomb core of the panel substrates. These substrates were supplied to TRW by APL. It was later determined that the inside of the skin had been anodized by mistake; this prevented good bond formation between skin and core and eventually resulted in the failure described above. The panels had previously been cycled by TRW from room temperature to low temperature and held there for a period of time; this allowed gases trapped in the substrate to out-gas. When the cycling by APL started with the high temperature first, failure occurred. The undamaged panel had been subject to a cold soak in vacuum immediately prior to the test which allowed it to out-gas as before; this accounts for its survival.

The failed panels were replaced by APL. Two of the replacements were conventional panels of Ti-Ag contacted N/P solar cells with soldered interconnects. The third panel was supplied to APL by Spectrolab and was composed of N/P and P/N lithium doped cells with aluminum contacts. The panel layout and interconnection was the same as the TRW panel, but the interconnectors were the elaborate wraparound type designed by Spectrolab rather than the notched strips used by TRW.

Thirty days after launch, the onboard analog to digital converter of the telemetry system failed. No further data could be obtained after this event. Very little flight data were obtained.

SECTION II

DISCUSSION

1.0 Solar Panel Segments

The solar panel segments were fabricated by TRW Systems under AFAPL Contract F33615-71-C-1260. The cells used for these segments have aluminum contacts. Interconnections were made using notched aluminum strips that were ultrasonically welded to the cells. These panels are the first actual space flight test of aluminum contact hardening technology.

The configuration of the panel segments is shown in Figure 1. Each panel consists of 2 sections; each section contains 40 cells connected 2 in parallel, 20 in series. Section A is made from N/P cells while Section B is made from P/N lithium doped cells. In order to distinguish between the various panel sections a code number was assigned to each section which consists of the panel number (1, 2, 3, or 4) followed by the section letter (A or B). Thus, the lithium doped cells on panel number 2 would be designated 2B.

1.1 Test Procedure

Although the intensity of the 13 inch diameter beam of the X-25 solar simulator is consistent within $\pm 2\%$, there is some variation between different locations within the beam. The intensities, as measured at locations in the beam with a balloon flight standard cell, are shown in Figure 2. In order to compensate for this problem the panels were oriented in four different positions. The I-V characteristics were plotted for each position. The curves produced by this procedure were averaged visually, and a composite curve was drawn which was most representative of the data obtained. It is these composite curves for each panel section, that are included in this report.

The solar simulator intensity was set with a balloon flight standard cell by matching its short circuit current (I_{sc}) under the simulator with that measured in the high altitude balloon flight and corrected for seasonal variation.

1.2 Test Results

The composite curves mentioned above are presented in Figures 3 through 10. The values of the parameters of interest for panels are presented in Table 1. These values were obtained directly from the composite curves.

1.3 Flight Data

As mentioned previously, only panel number four was actually flown. Due to the secondary nature of the solar power experiment, no I-V characteristics were determined for the panel segments prior to the failure of the telemetry system. The only data that are available are shown in Figure 6 and Figure 10. Since the solar panels were being used to charge the spacecraft batteries, the data were all obtained at the charging voltage of about six volts. Data was taken during each telemetry pass until the failure occurred. The flight data were only taken for solar attitude angles of less

than 45° and corrected for normal incidence using the cosine law. Although the flight data are somewhat higher than experimental data, the correlation is excellent considering the lower intensities obtained near the panel edges during laboratory measurements as indicated in Figure 1. No degradation in performance was noted during the twenty-six days in which data were obtained.

TABLE I: PRE-FLIGHT SOLAR PANEL SEGMENT PARAMETERS

| Section | V _{OC} (volts) | I _{SC} (ma) | V _m (volts) | I _m (ma) | P _m (mw) | Eff.* |
|---------|-------------------------|----------------------|------------------------|---------------------|---------------------|-------|
| 1A | 10.61 | 265 | 8.45 | 247 | 2.09 | 9.3% |
| 2A | 10.66 | 265 | 8.60 | 247 | 2.13 | 9.5% |
| 3A | 10.71 | 261 | 8.60 | 247 | 2.12 | 9.5% |
| 4A | 10.66 | 261 | 8.53 | 249 | 2.12 | 9.5% |
| 1B | 11.59 | 264 | 8.90 | 247 | 2.20 | 9.8% |
| 2B | 11.66 | 268 | 9.03 | 244 | 2.20 | 9.8% |
| 3B | 11.65 | 268 | 9.01 | 245 | 2.21 | 9.9% |
| 4B | 11.60 | 266 | 8.88 | 248 | 2.20 | 9.8% |

* Based on 4.0 cm² per cell of active area and calculated at max power; solar intensity assumed to be 140.0mw/cm²

2.0 Experimental Modules

There were six experimental modules, each consisting of six solar cells, mounted on the Environmental Survey Panel (ESP) of the TRIAD spacecraft. The layout of this panel is shown in Figure 11.

The cell types used for each of the modules are as follows:

| | | |
|----------|-----|----------------------------|
| Module 1 | N/P | No cover glass |
| Module 2 | N/P | 6 mil fused silica covers |
| Module 3 | N/P | Integral 1720 glass covers |
| Module 4 | P/N | Lithium doped cells |
| Module 5 | N/P | 20 mil fused silica covers |
| Module 6 | N/P | 60 mil fused silica covers |

Modules number 3 and 4 were fabricated by TRW Systems under AFAPL Contract F33615-71-C-1260. Other modules were supplied by the Applied Physics Laboratory.

2.1 I-V Characteristics

When the ESP arrived at AFAPL, it was already wired into the flight configuration which made it impossible to obtain continuous I-V characteristics of the individual modules. By using the telemetry simulation loading it was possible to obtain only the four points described in paragraph 2.2 below. For this reason, the preflight I-V curves for these modules, which appear as Figures 12 through 17, were supplied by the Applied Physics Laboratory. In addition to these curves, both calibration data points obtained at normal incidence in the angle of incidence experiment described below and available flight data, are plotted in these figures. Explanation and analysis of the flight data are presented in paragraph 2.3. The APL preflight calibration I-V curves indicate short circuit currents (I_{sc}) that are considerably lower than the AFAPL and flight data values. This can be attributed to the fact that their curves were taken using a tungsten lamp illuminator, which does not match the Air Mass Zero (AMO) spectral distribution as well as the Xenon lamp simulator which AFAPL uses. In addition, the intensity of the APL simulator is set on the conservative side (i.e., lower intensity than AMO) according to Mr. William Ray of APL. This is a reasonable explanation in view of the fact that the open circuit voltages, which are not a strong function of illumination, are accurate while the short circuit current values, which are a strong function of illumination, are low.

2.2 Angle of Incidence

Since the ESP is not oriented toward the sun, it will be only on rare occasions that the experiment is perpendicular to the sun. Thus, it is desirable to be able to obtain meaningful data regardless of the angle of the incidence of the sun's light.

In order to determine the response of the modules, they were mounted on a goniometer platform which allowed them to be positioned in the solar simulator beam with two degrees of freedom. By using a resistance network supplied by APL to simulate the spacecraft load system, the performance of the modules at each telemetry load condition could be examined. The simulated load conditions were for open circuit voltage, short circuit current, and two points in between called load point 1 and load point 2. Using these four points it is possible to get an idea of how the I-V characteristic curve should look. Figure 18 gives the schematic diagram for the telemetry simulating load and Table II gives the condition simulated by the various positions of switches S_1 and S_2 .

The solar attitude angle, θ_s , is defined as the angle between a line perpendicular to the solar cell surface and a line from the cell surface to the center of the sun. For example, if the cell surface is perpendicular to the sun, the solar attitude angle is 0° .

2.2.1 Data Reduction

Before the collected data could be analyzed, it was necessary to compensate for several factors in which the test setup was not a true simulation of space conditions. Corrective factors were determined for temperature variations, ambient lighting conditions, and variations in light intensity with distance

TABLE II

SIMULATED LOAD CONDITIONS FOR AFAPL PRE-FLIGHT TESTS

| POSITION OF SWITCH | | SIMULATED LOAD |
|--------------------|----------------|-----------------------|
| S ₁ | S ₂ | |
| A | A | Open circuit voltage |
| A | B | Load Point 2 |
| B | A | Short circuit current |
| B | B | Load Point 1 |

from the solar simulator. The techniques which were used to make these adjustments are described in the following paragraphs. All of the necessary factors were combined in a single computer program which is described in Appendix B.

2.2.1.1 Temperature Variations

The temperature of the ESP panel was determined by a device called a "sensistor". The resistance of this device is a linear function of temperature over the range of interest which makes it quite easy to evaluate the panel temperature. For the pre-flight test, the sensistor leads were connected to a digital volt-ohm meter for direct readout of the resistance instead of the usual telemetry circuit. The necessary corrective factors needed to normalize the data to 25°C, were determined and were plotted versus sensistor resistance in Figure 19. The corrected data are obtained by multiplying the raw data by the correction factor.

2.2.1.2 Ambient Light

Due to the large size of the test setup, it was not possible to shield it from outside light sources such as room lighting. To overcome this, a standard cell was mounted on the goniometer and its response was plotted as a function of position with the solar simulator turned off. By adding the AMO short circuit current to the value recorded and dividing this number by the AMO short circuit current, the percentage change in the output due to ambient light was obtained. This plot is shown in Figure 20. The dotted line represents an empirical approximation of the observed data. The formula for the approximation is:

$$I'_{sc} = \left(\frac{100}{101.5 + 1.225 \sin \theta_x} \right)$$

$$\text{where } \theta_x = \frac{90 (\theta_s - 24^\circ)}{66}$$

θ_s = solar attitude angle in degrees

I_{sc} = original data

I'_{sc} = data corrected for ambient light

The numbers in the equations for both I'_{sc} and θ_x represent the best empirical approximation to fit observed data and have no physical significance. Since small variations in ambient light do not affect the voltage, no corrective factor need be determined. (This fact was verified experimentally.)

2.2.1.3 Variations in Light Intensity

The light from the solar simulator is a very tight beam, but unfortunately it is not tight enough. Since the beam is not perfectly collimated, the intensity of the light is a function of distance from the simulator. By placing a standard cell in the beam and measuring short circuit current, the variation of intensity was found to be 1.88% per inch for ± 10 inches from the standard distance of 96 inches. As with ambient light, the voltage is unaffected by these variations.

In order to compensate for intensity variation, it is necessary to determine the distance between the solar cells and the simulator. The equations to do this are derived in Appendix A.

The corrected currents are obtained by dividing the raw data by $(1 + .0188M)$ where M is defined such that $(96-M)$ is the distance in inches from the solar cell surface to the solar simulator.

2.2.2 Experimental Procedure

After the panel was positioned properly on the goniometer, the goniometer was rotated to a specified angle about one axis and then was rotated through 180° about the other axis of rotation. During the run through the second rotation, the current and voltage outputs of the modules were recorded on a multichannel strip chart recorder. Due to the limited number of telemetry channels onboard the spacecraft, the modules were divided into three groups, and only the group voltages are measured. Group one consists of the parallel combination of modules 1, 2, and 3; group 2 is module 4, while group 3 is modules 5 and 6 in parallel. The current from each module is transmitted making a total of nine tracks of information recorded during each run. Since four load resistances were used, it was necessary to make four runs at each pitch angle to obtain the required data. The circuit diagram showing how the modules are connected is presented in Figure 18.

2.2.3 Results

After the reduction techniques described in the previous section were applied to the data, various plots were made to help evaluate it. A summary of the responses is presented in Table II, and each of the findings is discussed briefly in the paragraphs that follow.

2.2.3.1 Current

The responses of the modules for short circuit current were all typical of what has been found by earlier experimenters. The output was found to vary with the cosine of the solar attitude angle. These plots are shown in Figures 21 through 26.

Since load point one has a relatively low load impedance, the load point was past the knee of the I-V curve which means the current output was very close to short circuit current. Figures 27 through 32 present these curves.

At load point two, the cell output was almost independent of the solar attitude angle up to about 30° . The slight decrease with increasing angle can be approximated by the linear function given in Table III. The current output of each of the modules at load point two is given in Figures 33 through 38.

TABLE III

RESPONSE OF ESP MODULES AS A FUNCTION OF THE SOLAR ATTITUDE ANGLE, θ_s

| MODULE LOAD CONDITION | V_1 | V_2 | V_3 |
|--------------------------|--------------------------------|--------------------------------|--------------------------------|
| I_{sc} | * | * | * |
| Load Point 1 | $.590 - \frac{\theta_s}{C_1}$ | $.530 - \frac{\theta_s}{C_1}$ | $.560 - \frac{\theta_s}{C_1}$ |
| Load Point 2 | $1.480 - \frac{\theta_s}{C_2}$ | $1.580 - \frac{\theta_s}{C_2}$ | $1.530 - \frac{\theta_s}{C_2}$ |
| V_{oc} | 1.735 | 1.870 | 1.765 |

| MODULE LOAD CONDITION | I_1 | I_2 | I_3 | I_4 | I_5 | I_6 |
|--------------------------|------------------------------|------------------------------|------------------------------|------------------------------|------------------------------|------------------------------|
| I_{sc} | $275 \cos \theta_s$ | $273 \cos \theta_s$ | $252 \cos \theta_s$ | $264 \cos \theta_s$ | $278 \cos \theta_s$ | $280 \cos \theta_s$ |
| Load Point 1 | $275 \cos \theta_s$ | $273 \cos \theta_s$ | $252 \cos \theta_s$ | $264 \cos \theta_s$ | $278 \cos \theta_s$ | $280 \cos \theta_s$ |
| Load Point 2 | $133 - \frac{\theta_s}{C_3}$ | $132 - \frac{\theta_s}{C_3}$ | $130 - \frac{\theta_s}{C_3}$ | $130 - \frac{\theta_s}{C_4}$ | $123 - \frac{\theta_s}{C_4}$ | $135 - \frac{\theta_s}{C_4}$ |
| V_{oc} | * | * | * | * | * | * |

*Approximately zero

Notes: 1. Voltages are in volts; currents are in milliamps; θ_s is in degrees
 2. $C_1 = 500^\circ/\text{volt}$; $C_2 = 1000^\circ/\text{volt}$; $C_3 = 8^\circ/\text{milliamp}$; $C_4 = 4^\circ/\text{milliamp}$

2.2.3.2 Voltage

Little variation was noted in any of the voltages for solar attitude angles of less than 30° . Above 30° the voltage began falling off rather rapidly. Figures 39, 40, and 41 are the open circuit voltage plots while Figures 42 through 44 are for load point one and Figures 45 through 47 are for load point two.

2.3 Flight Data

Data were obtained from the solar modules on days 4, 13, 25 and 26 after launch. Due to the short exposure time, no degradation in performance was noted except for the bare cells in module 1. Data points were corrected to normal incidence and 28°C and were plotted in Figures 12 through 17. The degradation observed in module 1 was approximately 12% in open circuit voltage, 6% in short circuit current, and 22% in maximum power; this can be clearly seen in Figure 12. The degradation was probably due to low energy proton irradiation.

It was observed during preflight testing that short circuit current was a cosine function of the angle of solar incidence. This fact was verified using flight data. Since all of the modules behaved in a similar fashion, only Figure 22, which is for module 2, contains a plot of flight data.

The agreement between calibration data and flight data for open circuit voltage (VOC) is good (about 5% difference), which indicates that temperature corrections for the cells are reasonably good since VOC is a strong function of temperature but is not a strong function of intensity. On the other hand, the agreement is not so good (about 14% difference) for short circuit current (I_{sc}) which is a strong function of intensity. It seems evident that the AFAPL simulator intensity was somewhat low. This fact is further borne out by the fact that the calibration data for modules 2 and 4 which are in the center of the panel are in better agreement with flight data than are the other modules which are on the outer portion of the panel. This was to be expected since the simulator beam is less intense at the outer edges (see Figure 1). The differences between APL and AFAPL calibrations are pointed out in paragraph 2.1.

SECTION III

CONCLUSIONS

Although the quantity of flight data obtained was not great, the quality was good. In every case measured in-space performance of the hardened solar cells was higher than was predicted from ground based testing. The tests conducted by TRW on the solar panel segments and experimental modules were not discussed in this report, but their predictions were within 2% of AFAPL predictions in every case. Thus, it would seem that beam uniformity of the X-25 simulator rather than experimental procedure is probably the cause of the low predicted values.

No conclusions concerning the long-term performance of the hardened solar cells are possible due to the short period of time for which data are available.

Flight test validation of hardened space power components should continue to take a high priority. Now that initial high performance has been proven, it should be easier to convince mission planners to include hardened solar cells, perhaps even as the primary power source.

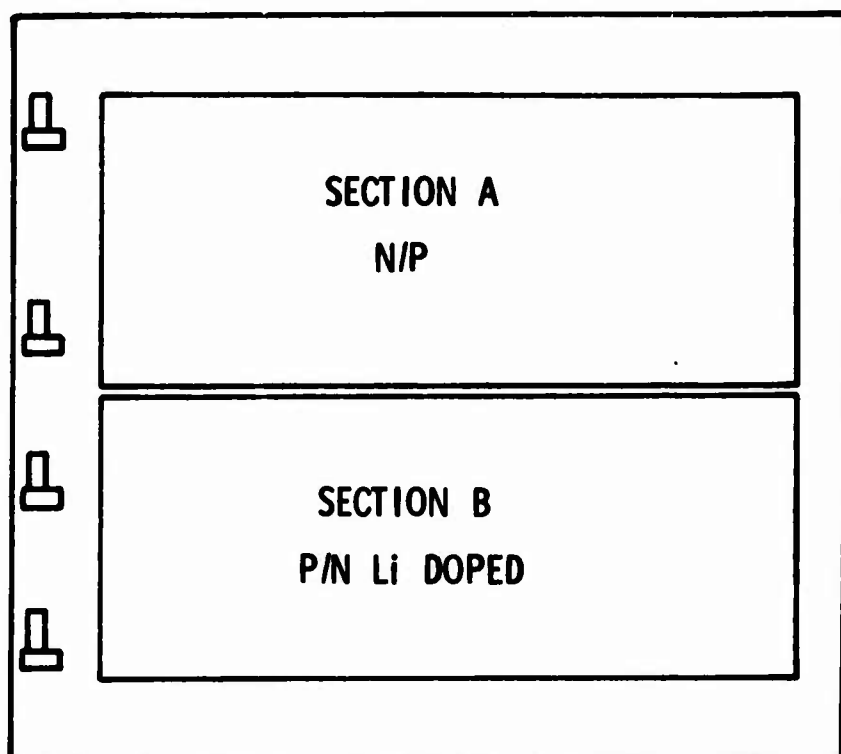
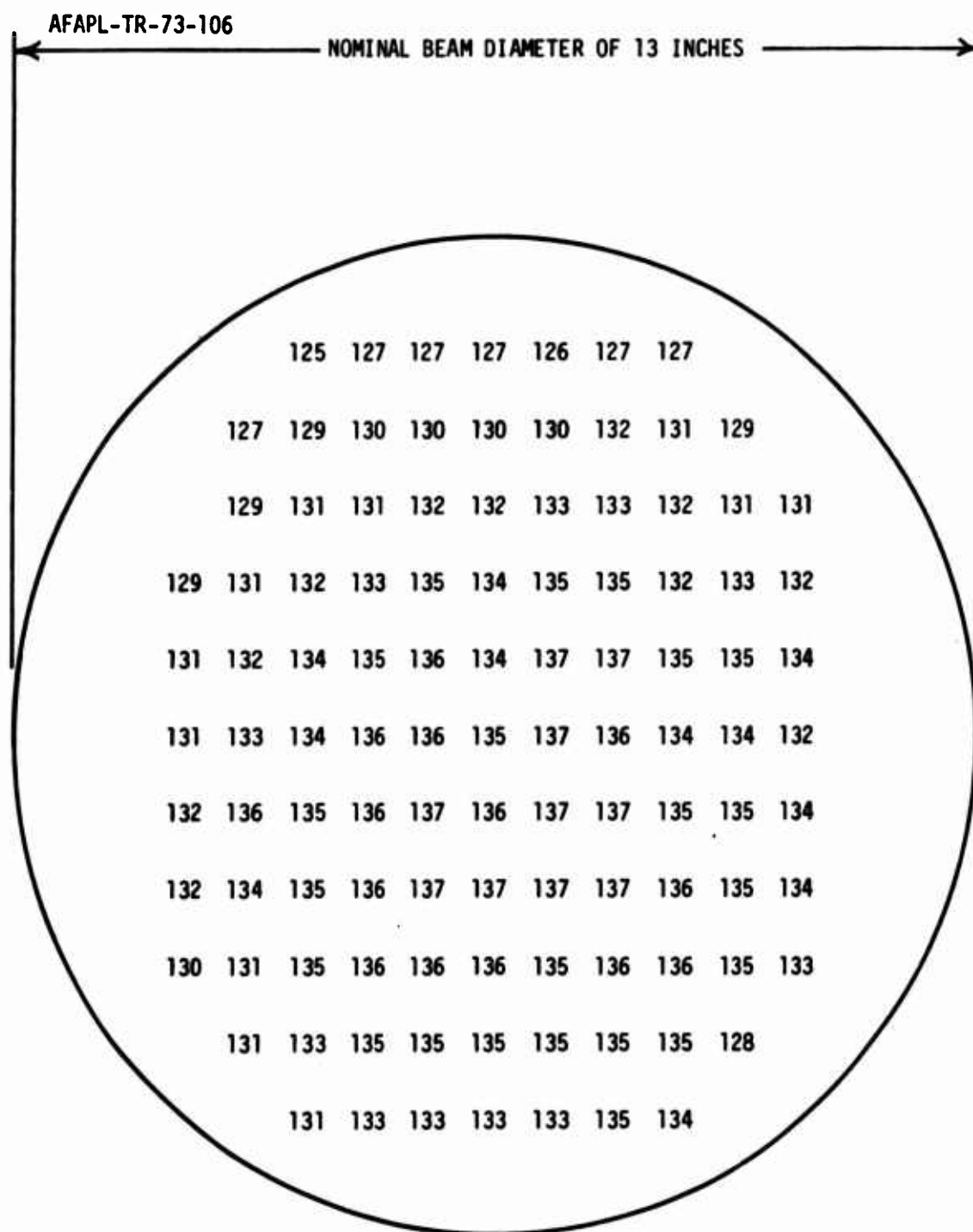


Figure 1. Panel Layout and Nomenclature



X-25 SIMULATOR SET TO AMO CONDITIONS WITH $140 \text{ mW}/\text{CM}^2$ AT THE BEAM'S CENTER USING IPC-3 BALLOON FLIGHT STANDARD.

PLOT MADE WITH $2 \times 2 \text{ CM}$ CELL MOUNTED ON A WATER COOLED BLOCK (78°F). CELL WAS N/P, NUMBERS INDICATE I_{sc} FOR THE CELL. (NOMINAL $I_{sc} = 136$ at AMO)

Figure 2. Relative Intensity of Solar Simulator Beam

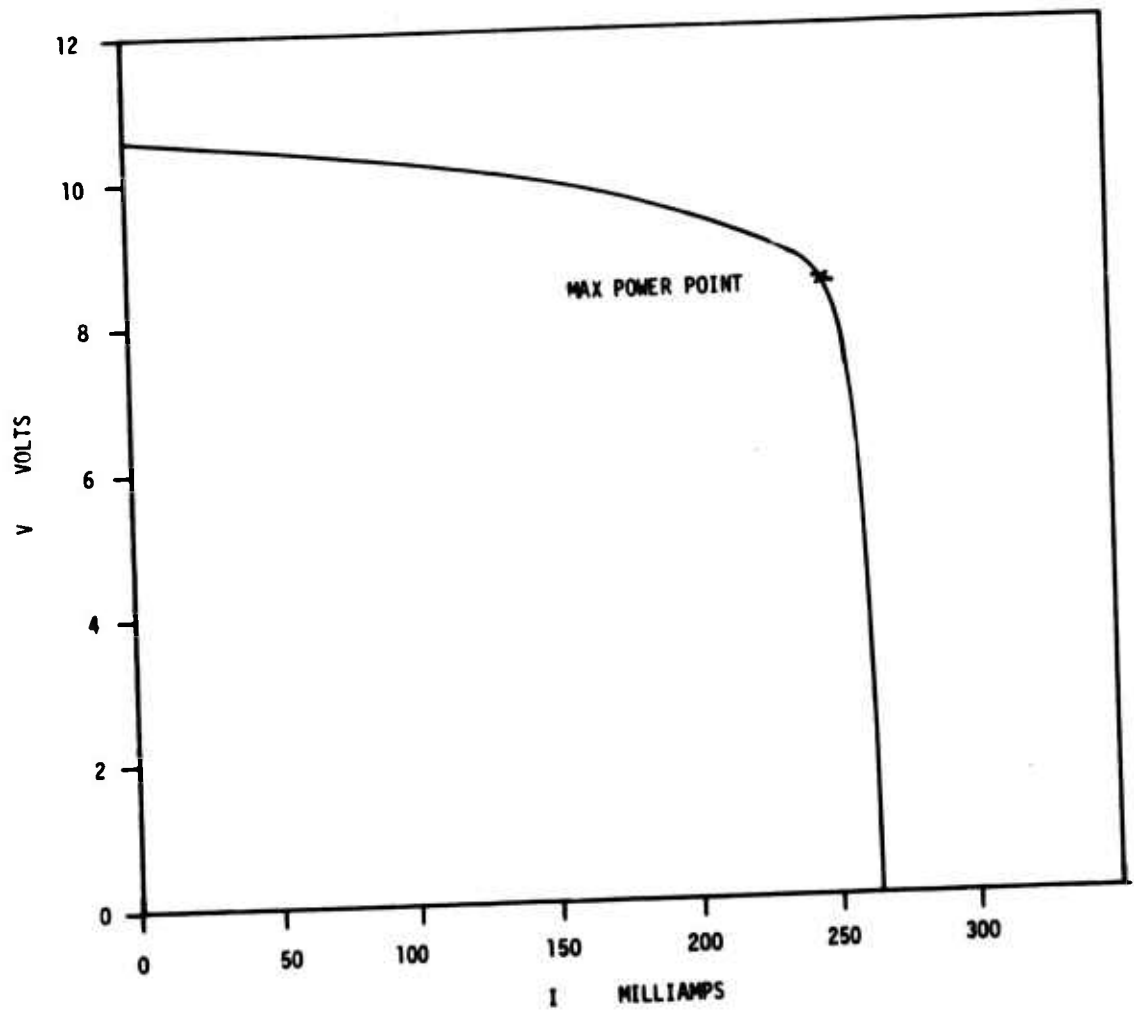


Figure 3. V vs. I For Panel Segment 1A

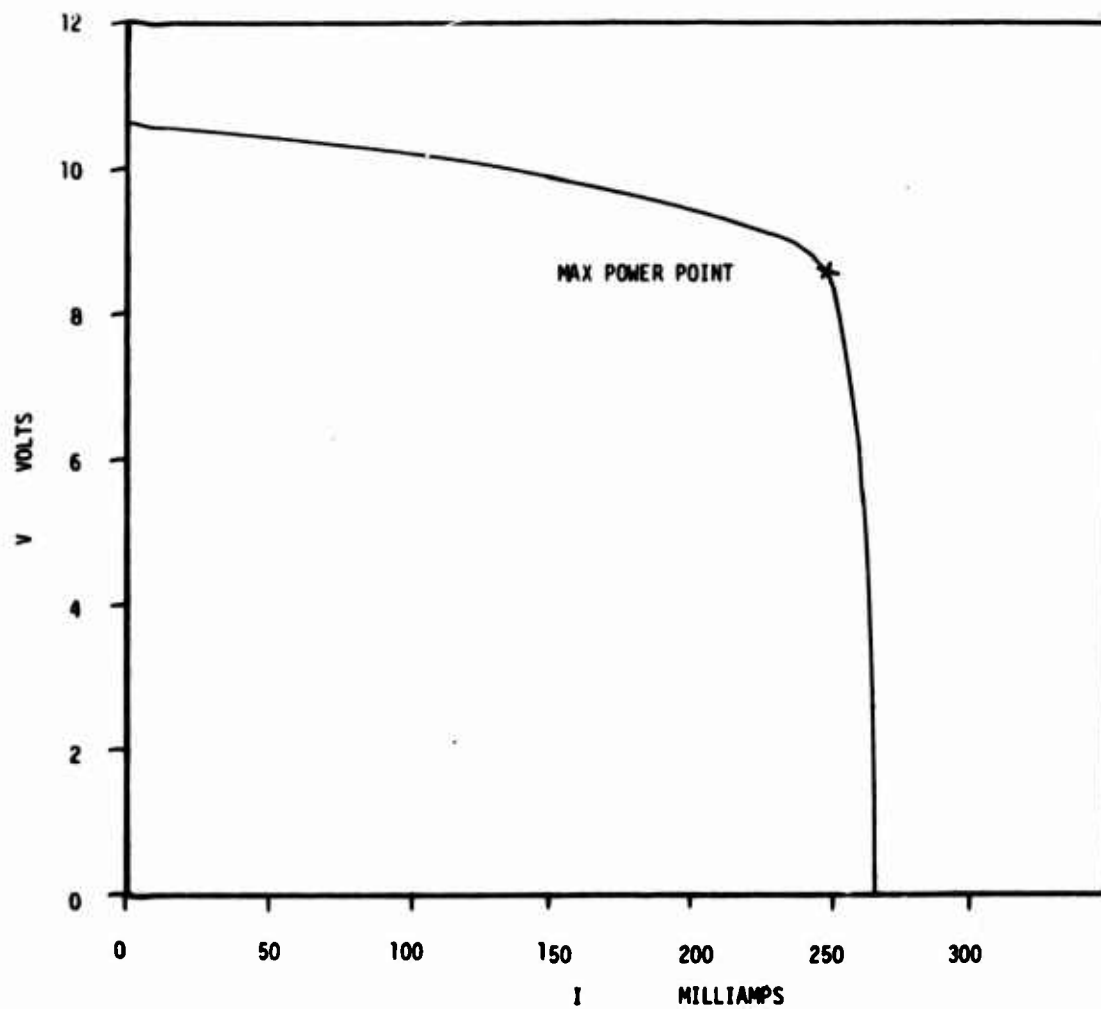


Figure 4. V vs. I For Panel Segment 2A

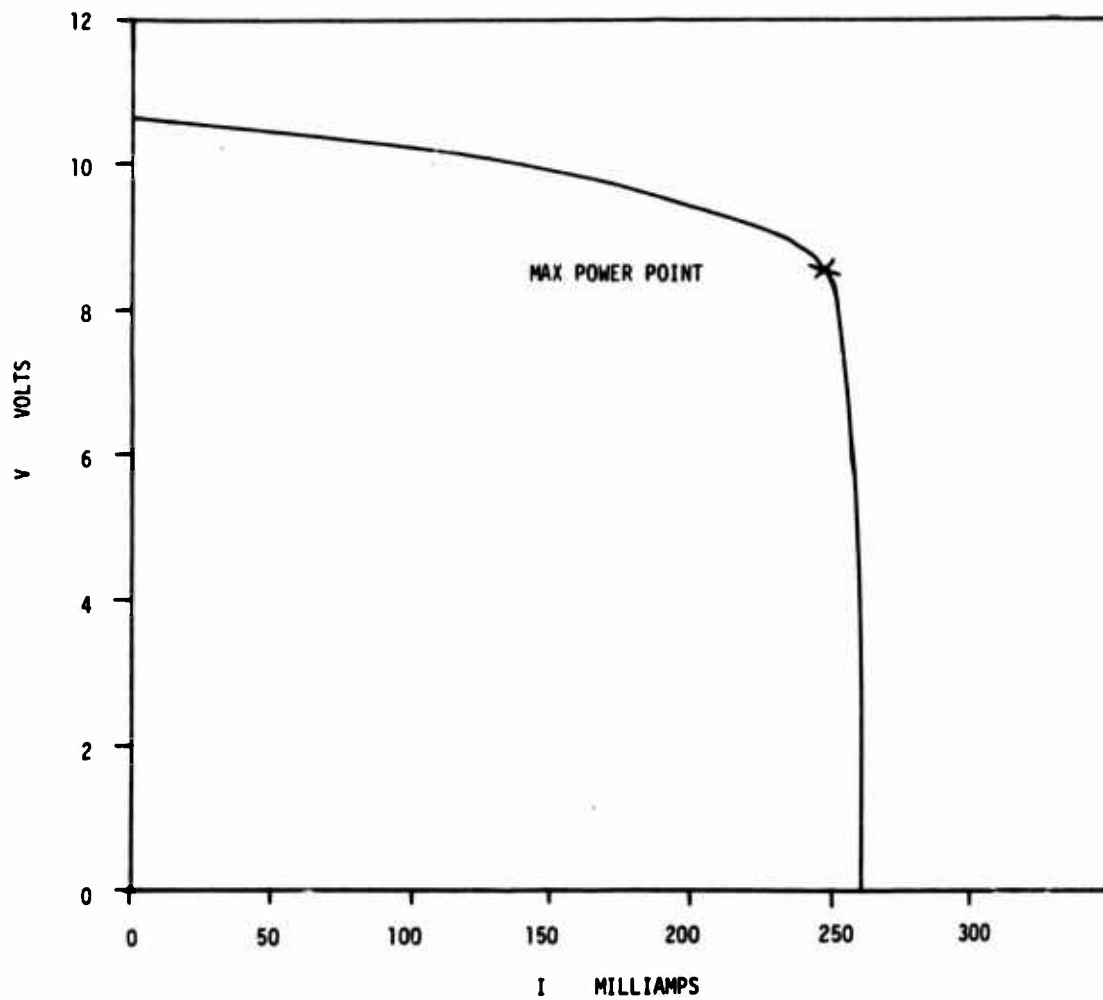


Figure 5. V vs. I For Panel Segment 3A

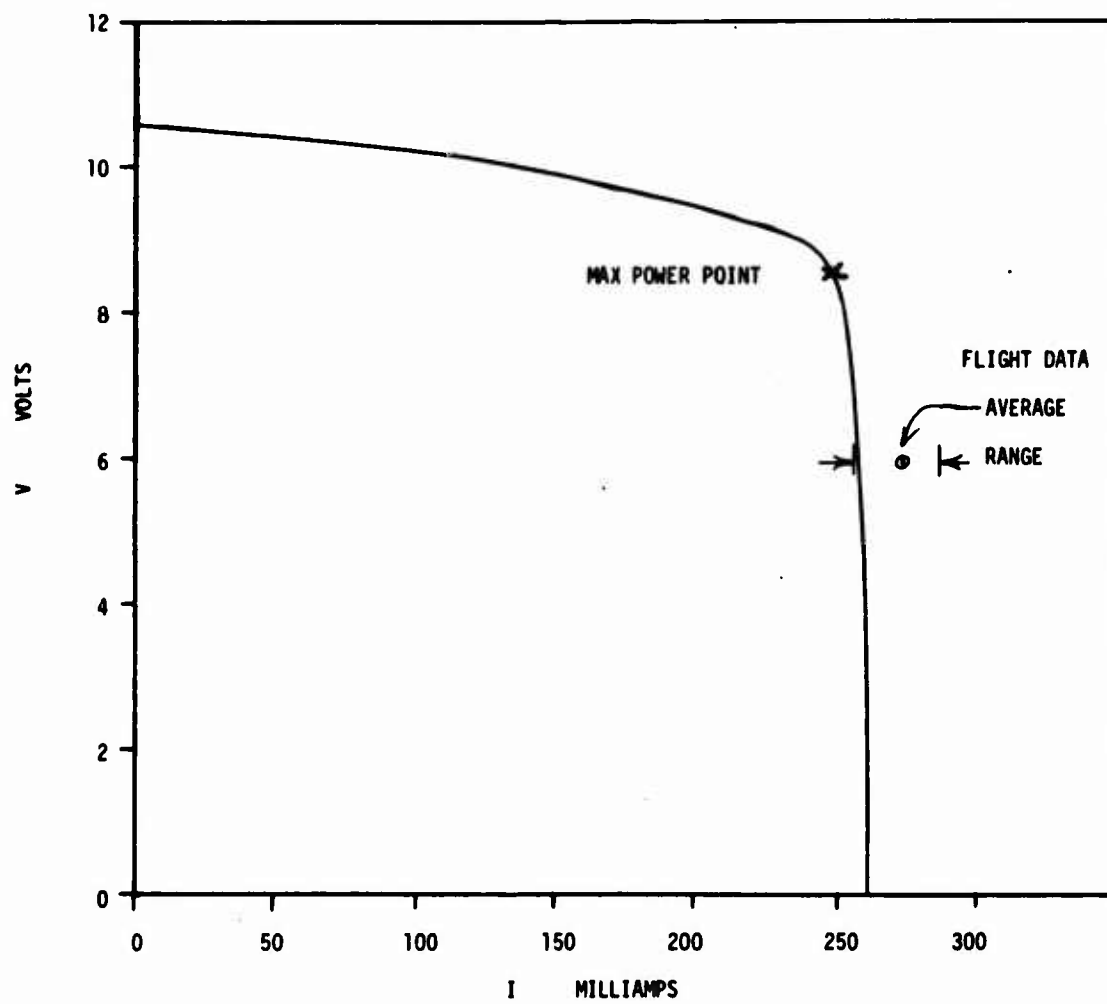


Figure 6. V vs. I For Panel Segment 4A

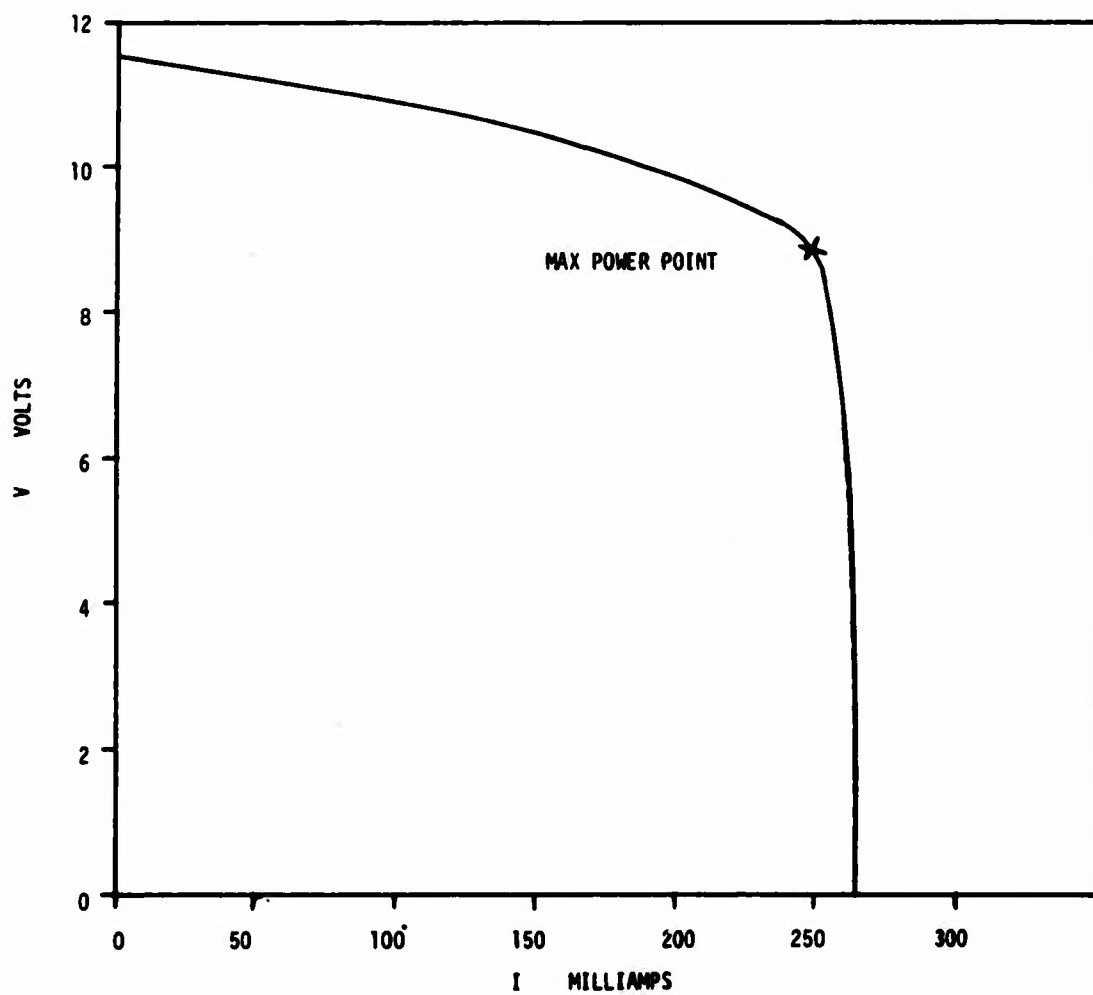


Figure 7. V vs. I For Panel Segment 1B

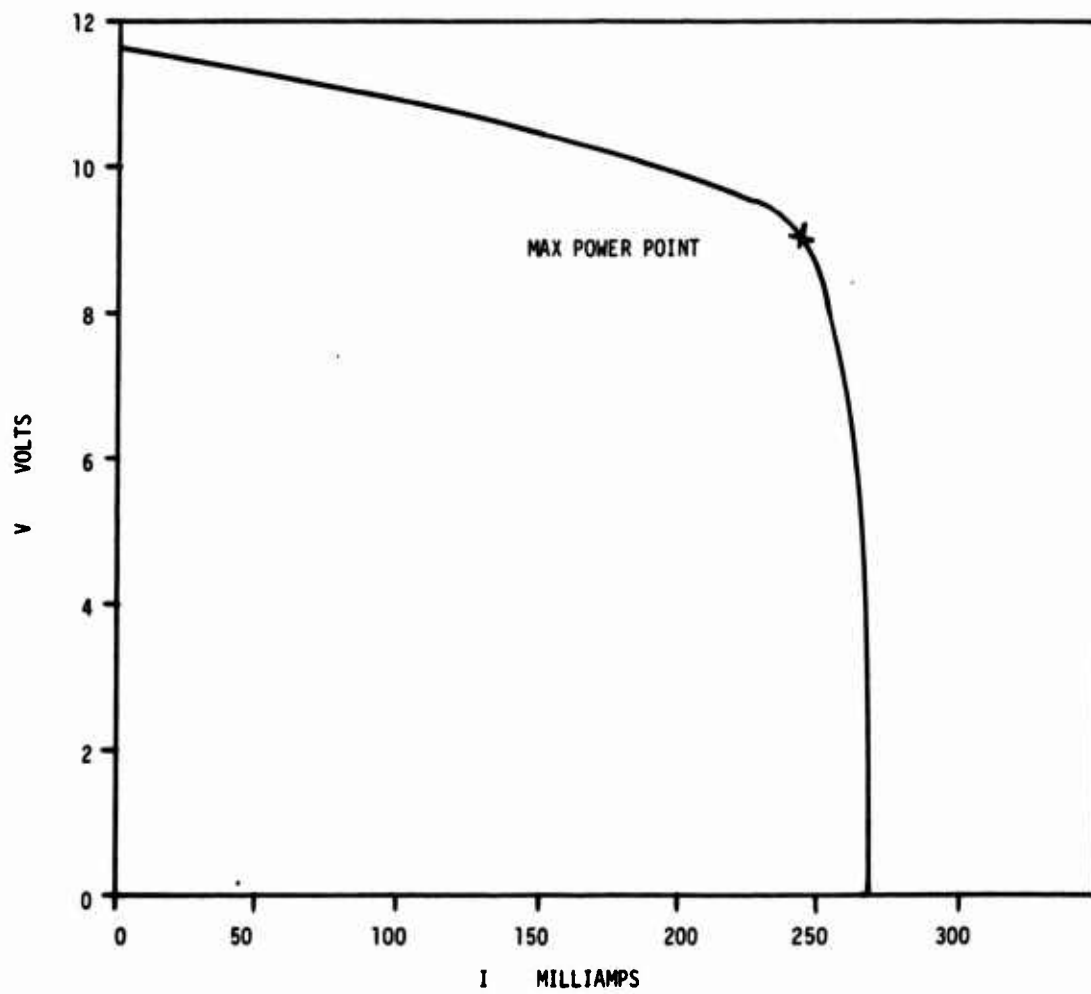


Figure 8. V vs. I For Panel Segment 2B

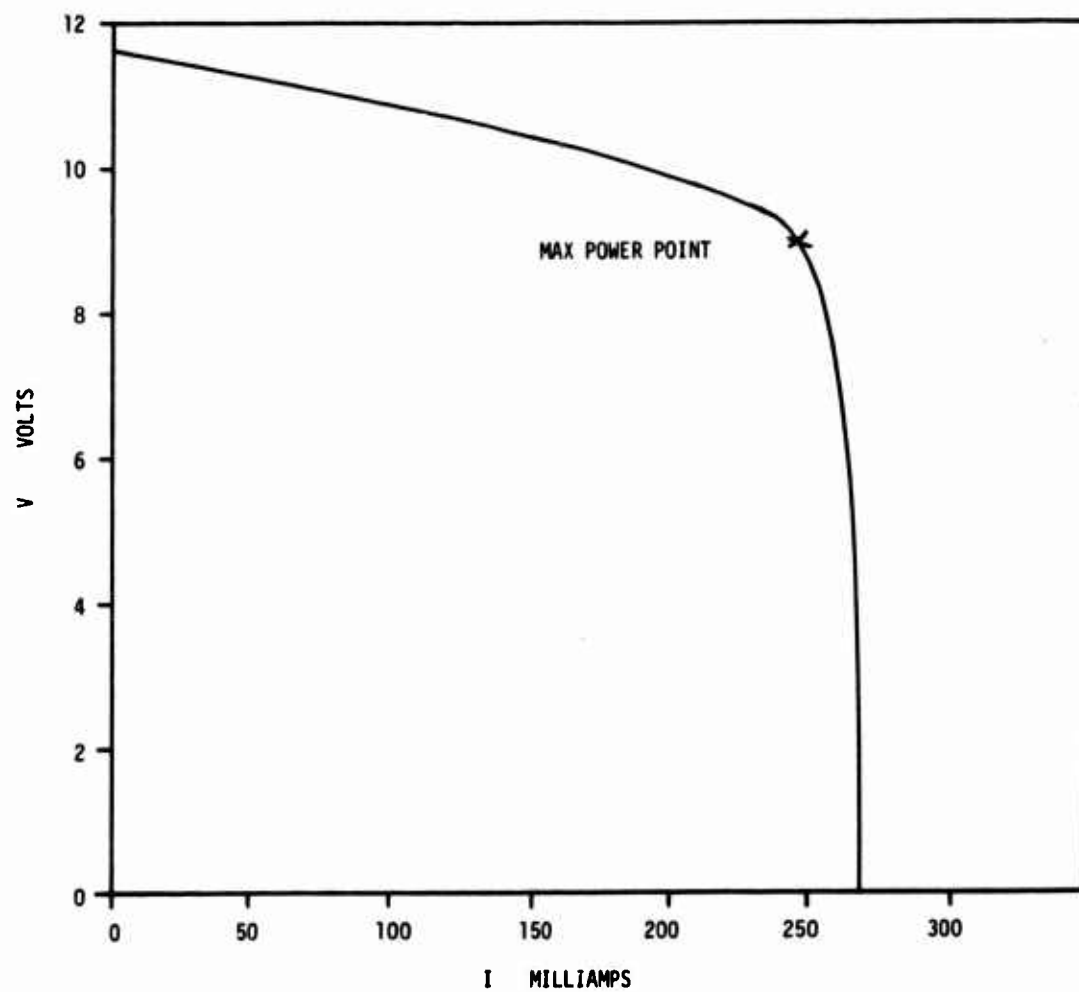


Figure 9. V vs. I For Panel Segment 3B

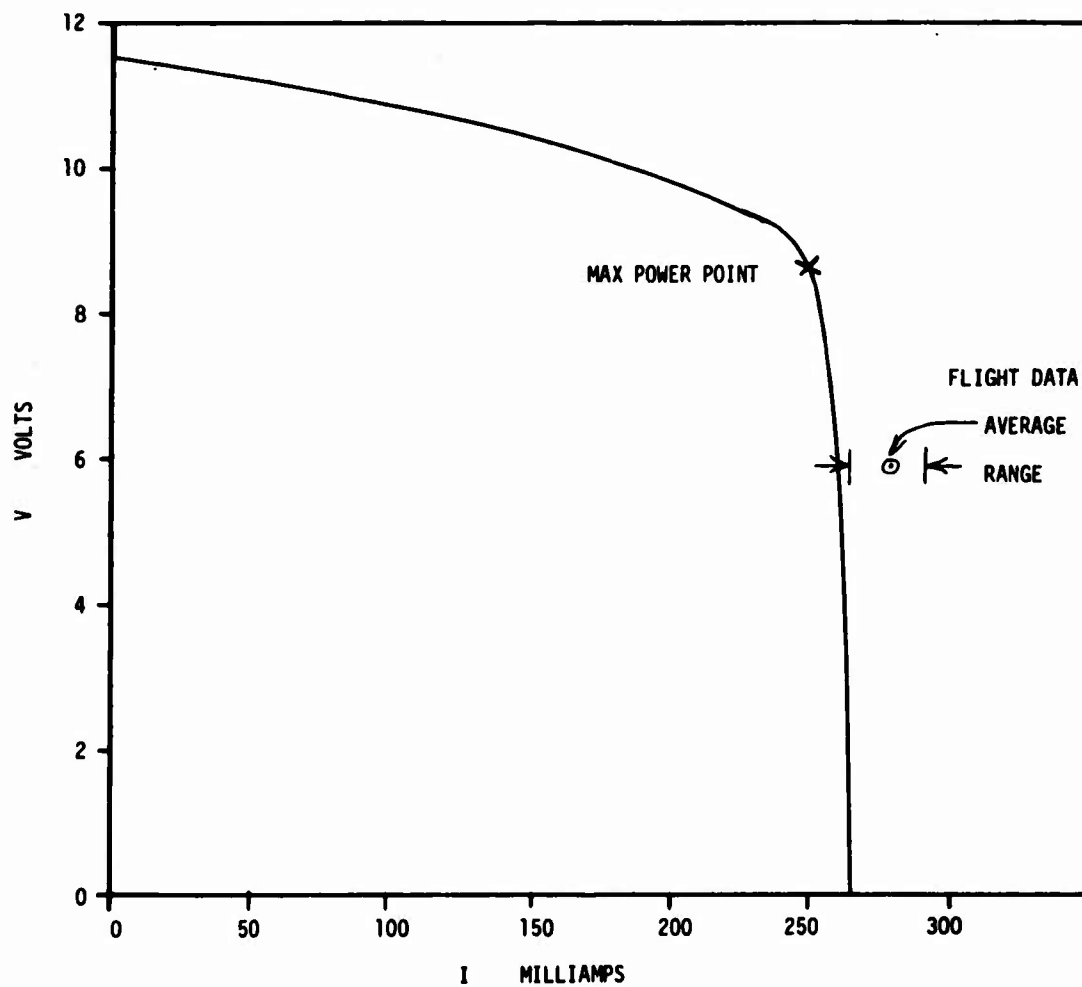


Figure 10. V vs. I For Panel Segment 4B

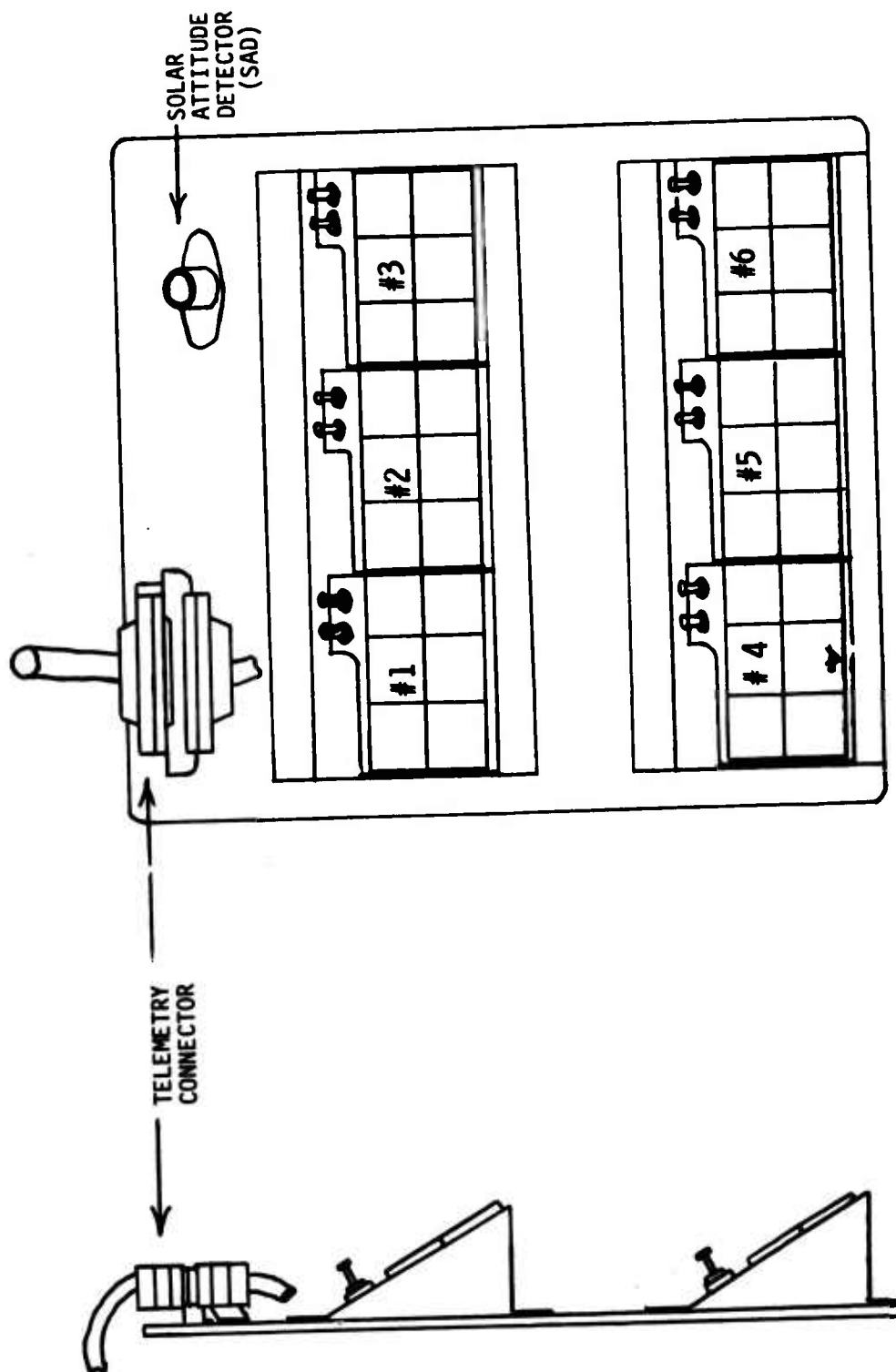


Figure 11. Environment Survey Panel 1 (ESP)

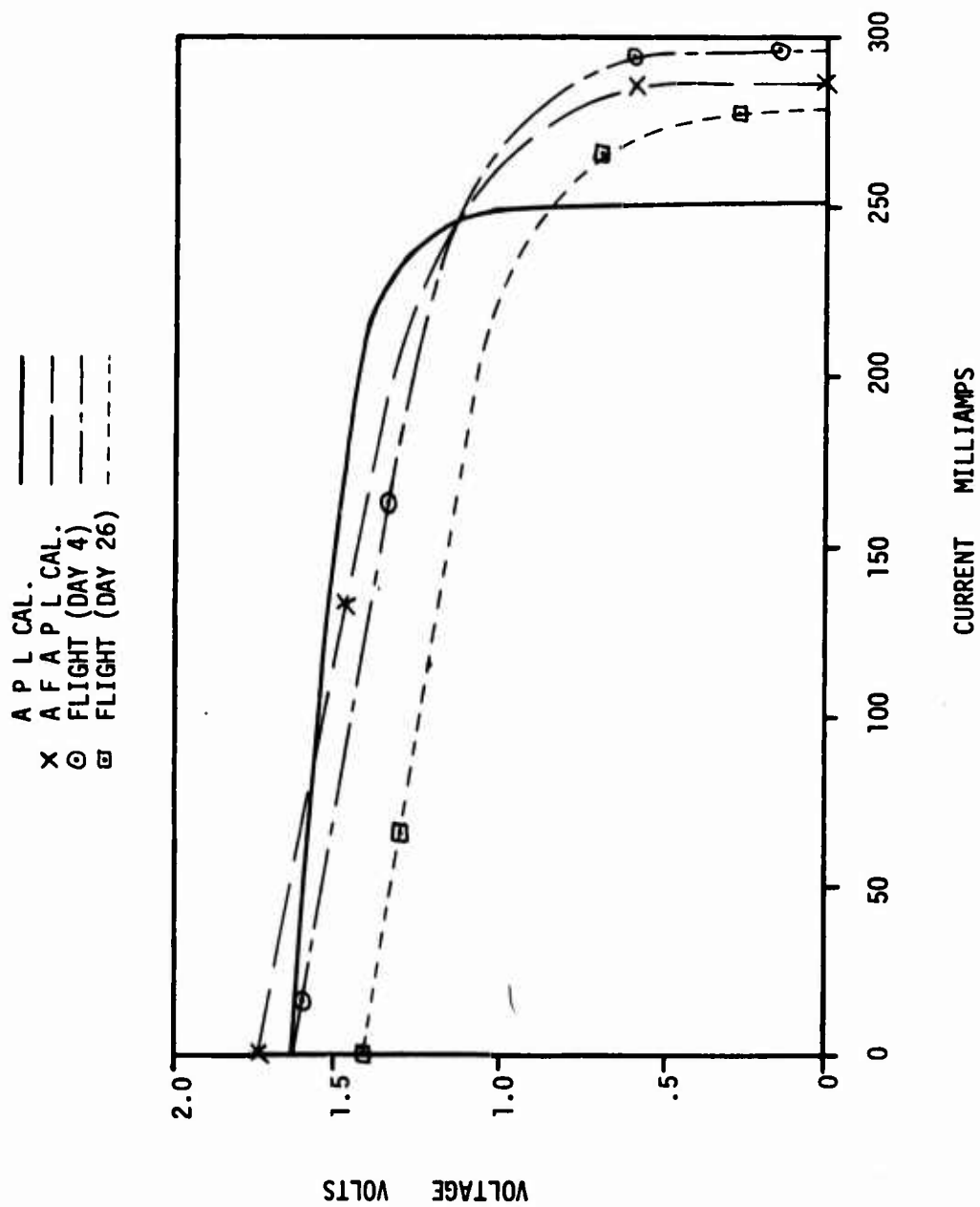


Figure 12. V vs. I For Module 1

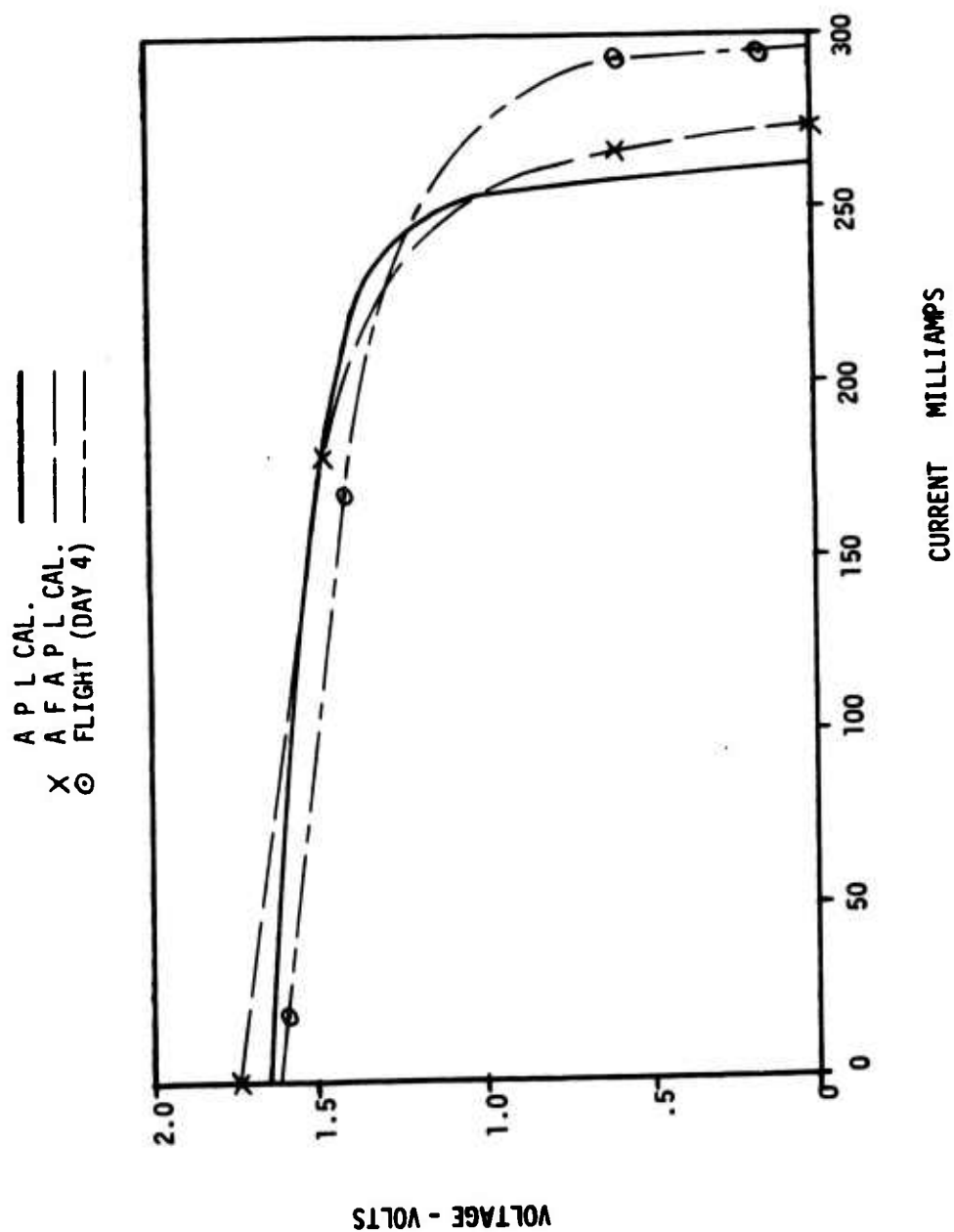


Figure 13. V vs. I For Module 2

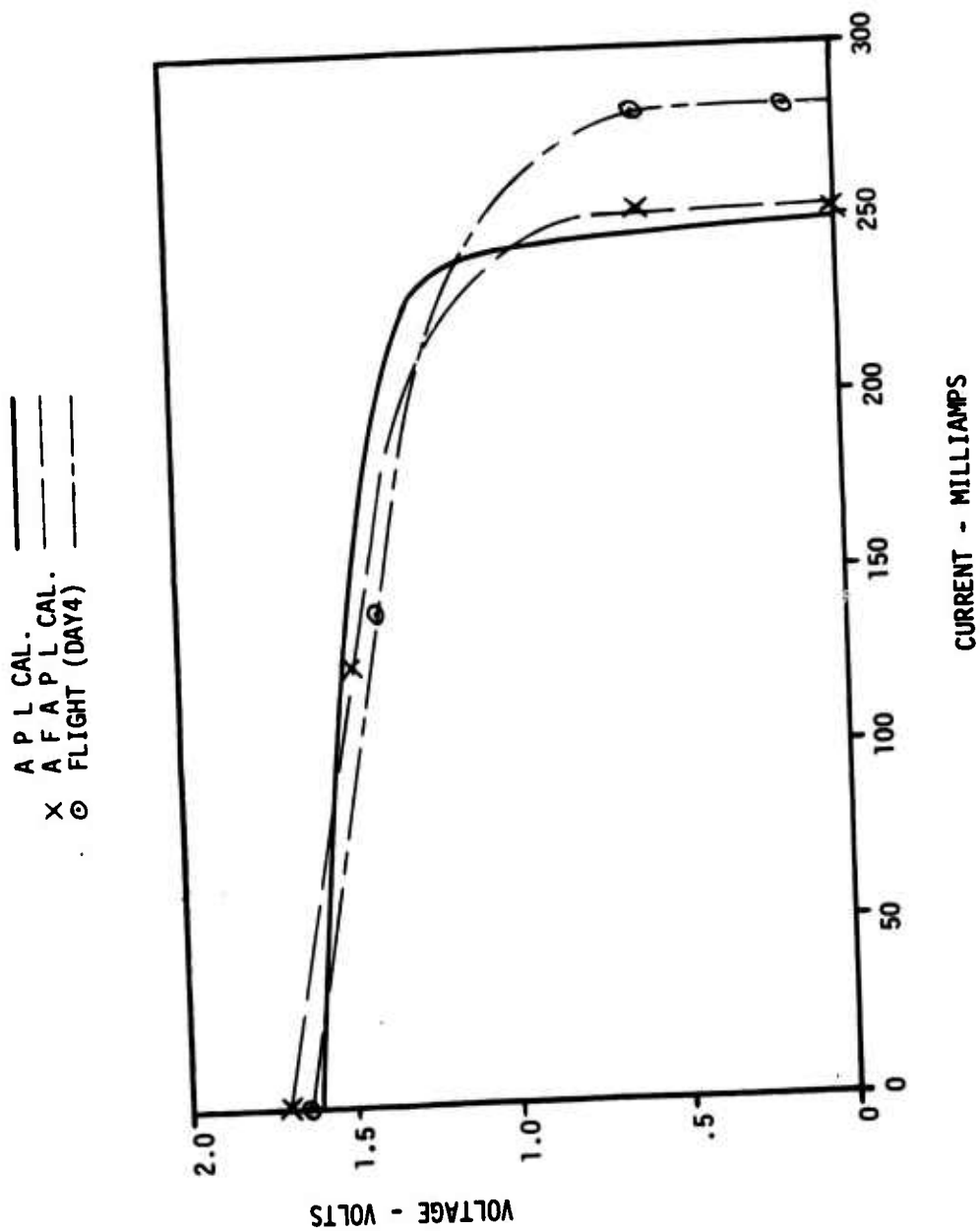


Figure 14. V vs. I For Module 3

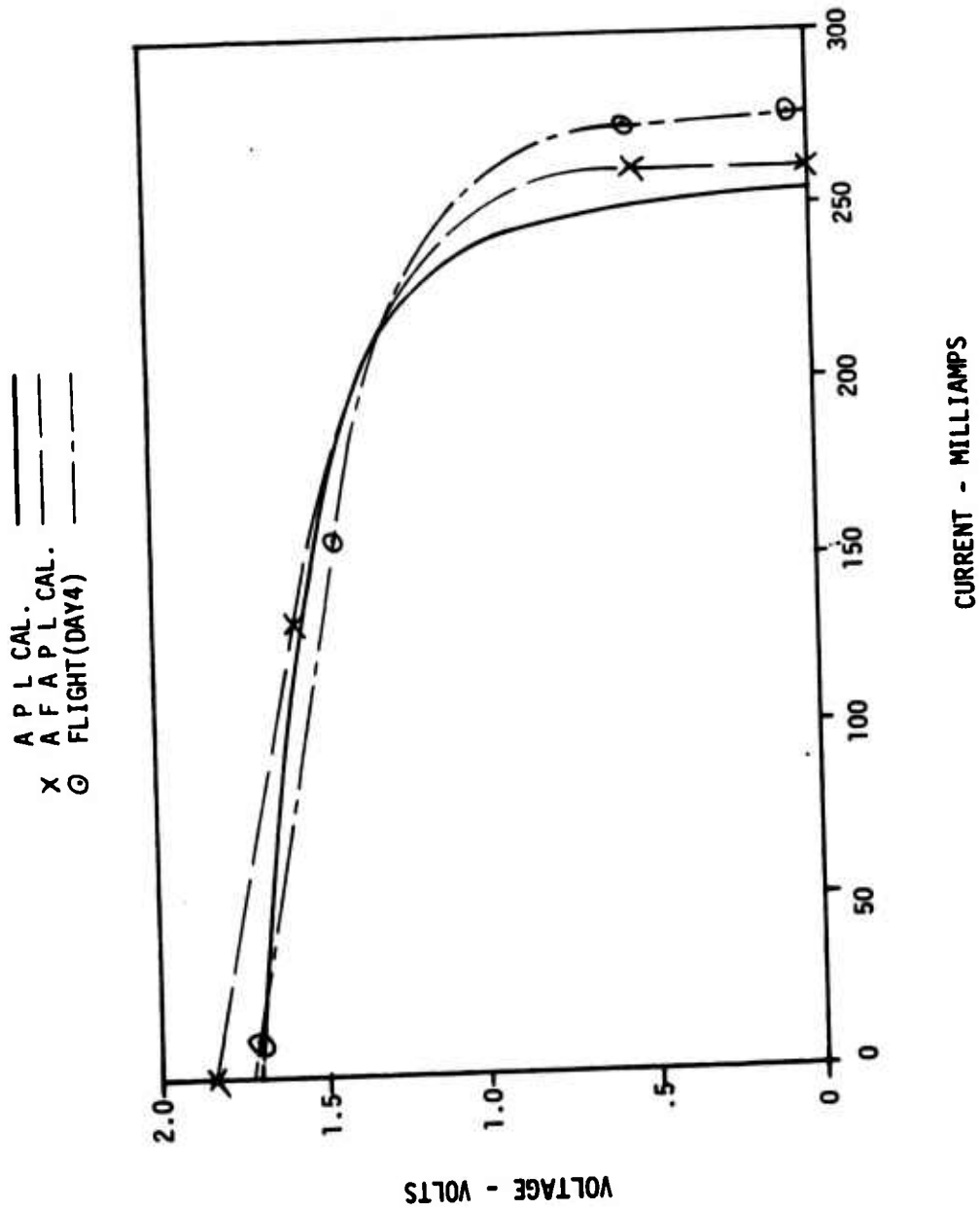


Figure 15. V vs. I For Module 4

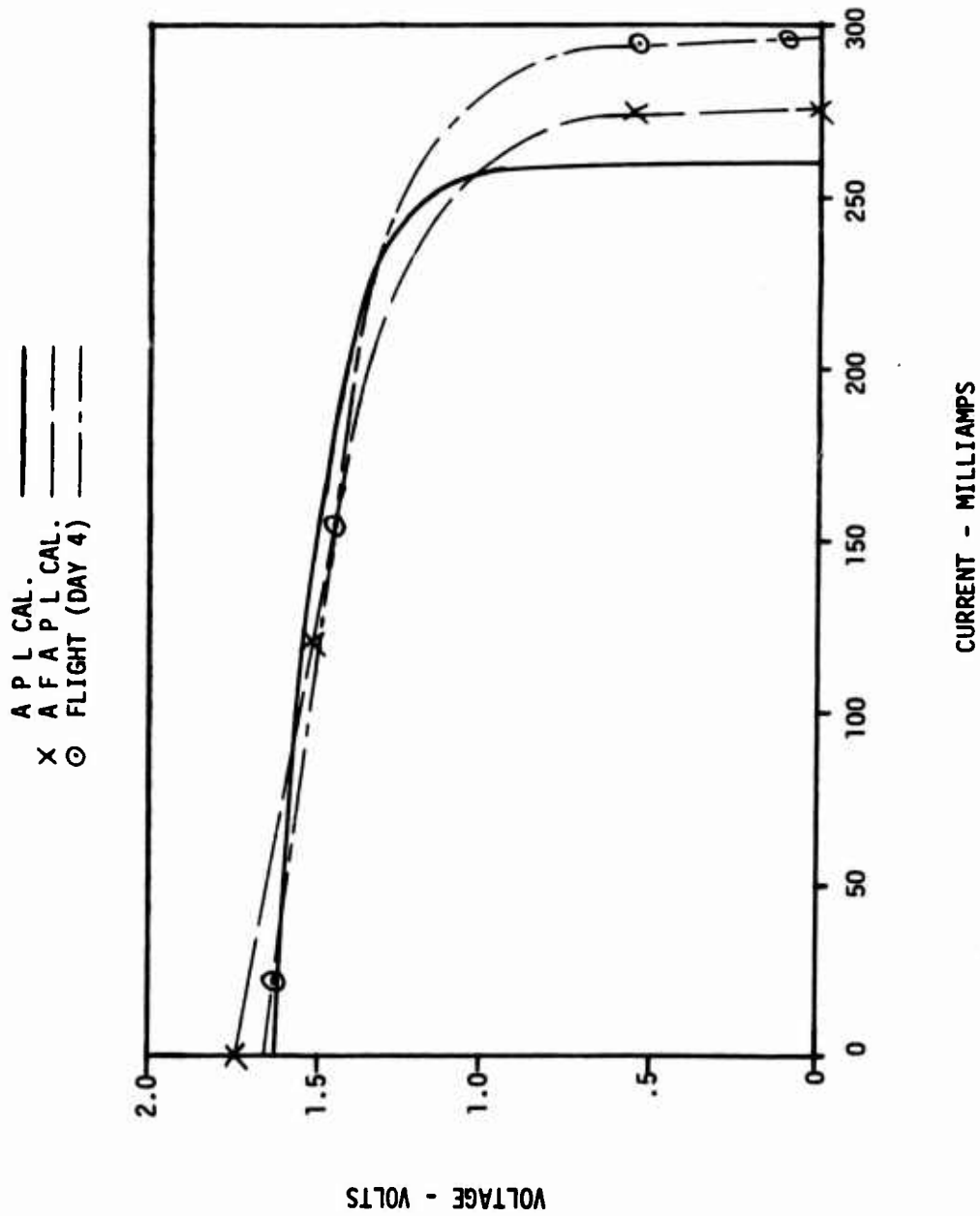


Figure 16. V vs. I For Module 5

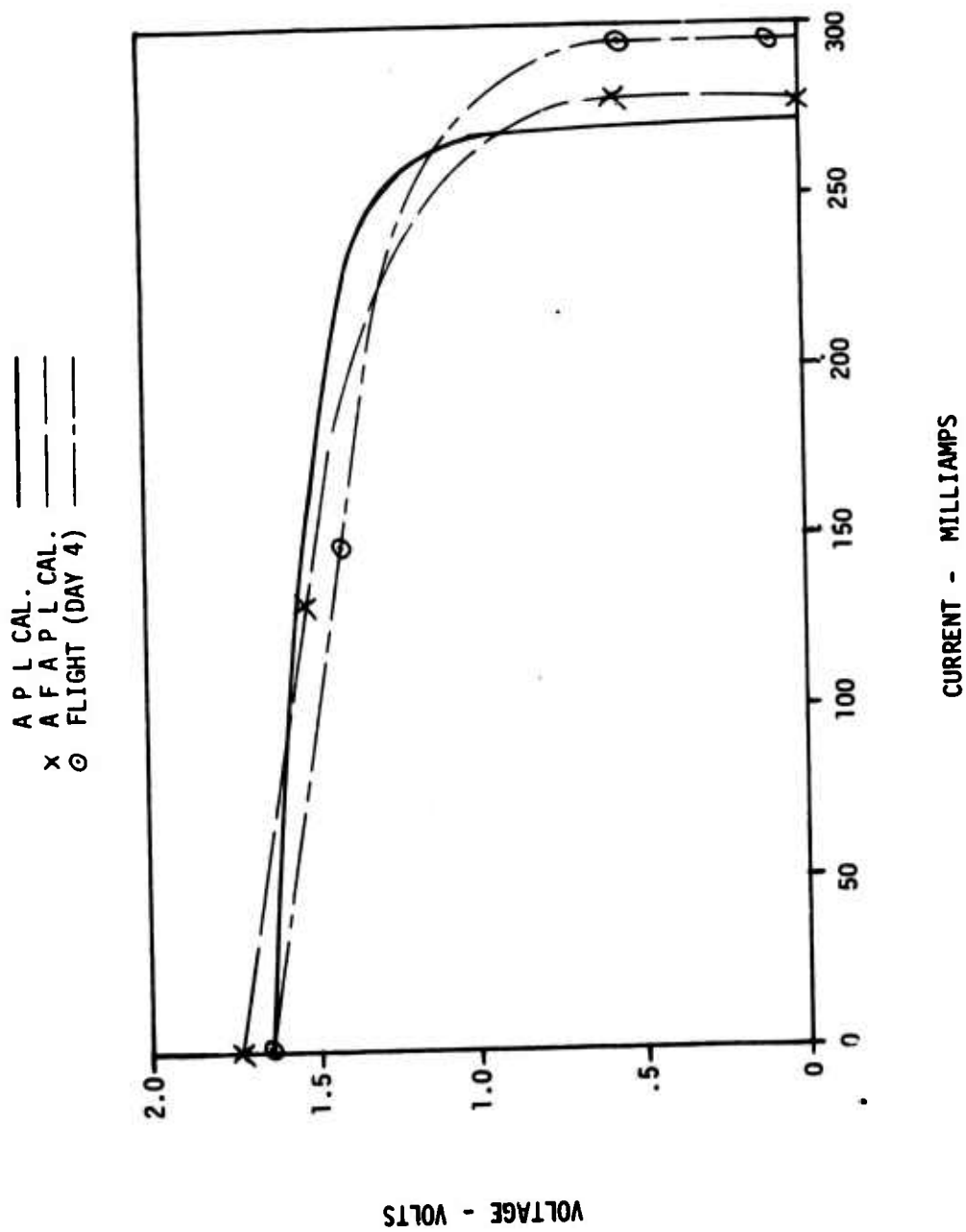


Figure 17. V vs. I For Module 6

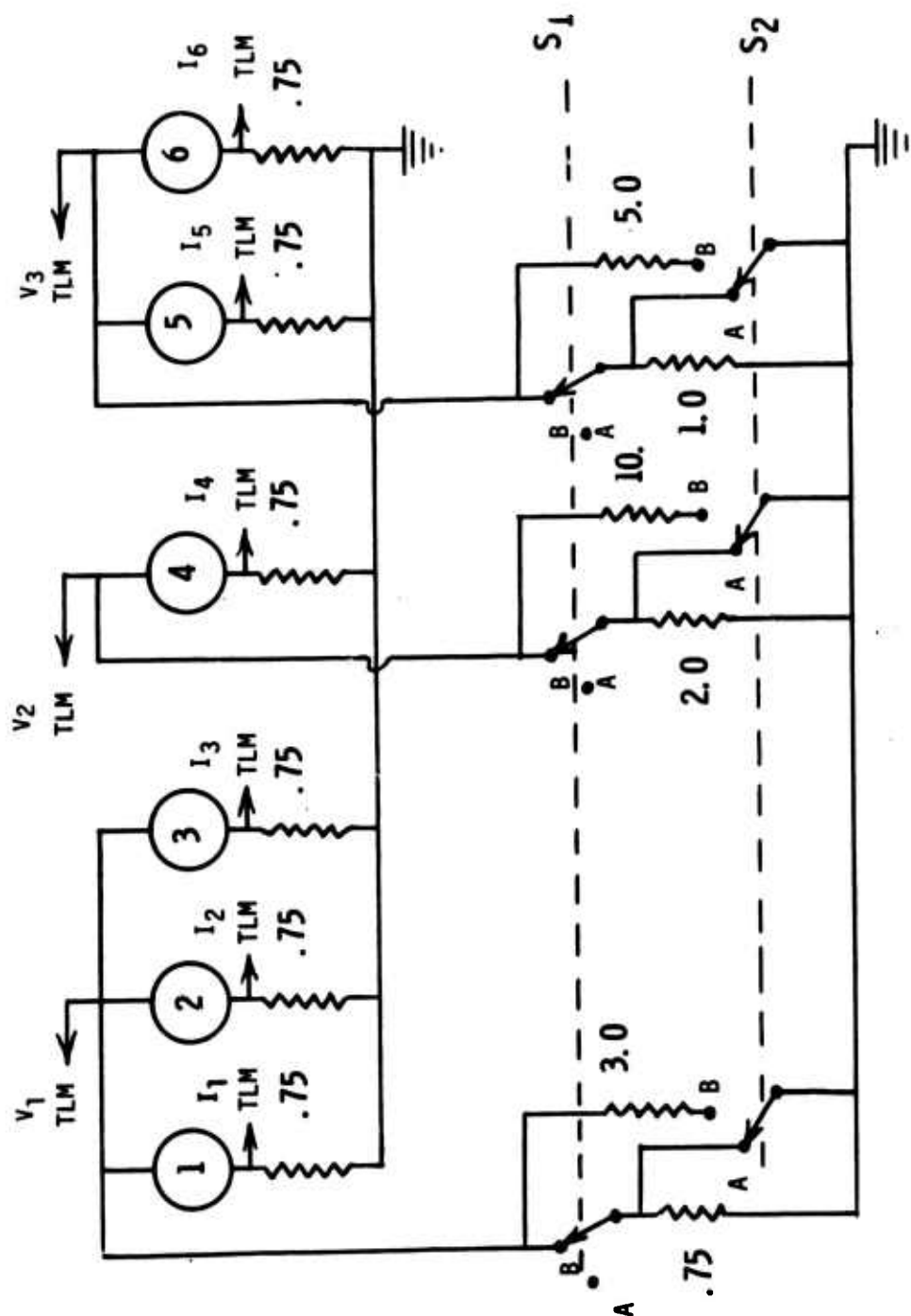


Figure 18. TRIAD Telemetry Simulation Loads Schematic Diagram

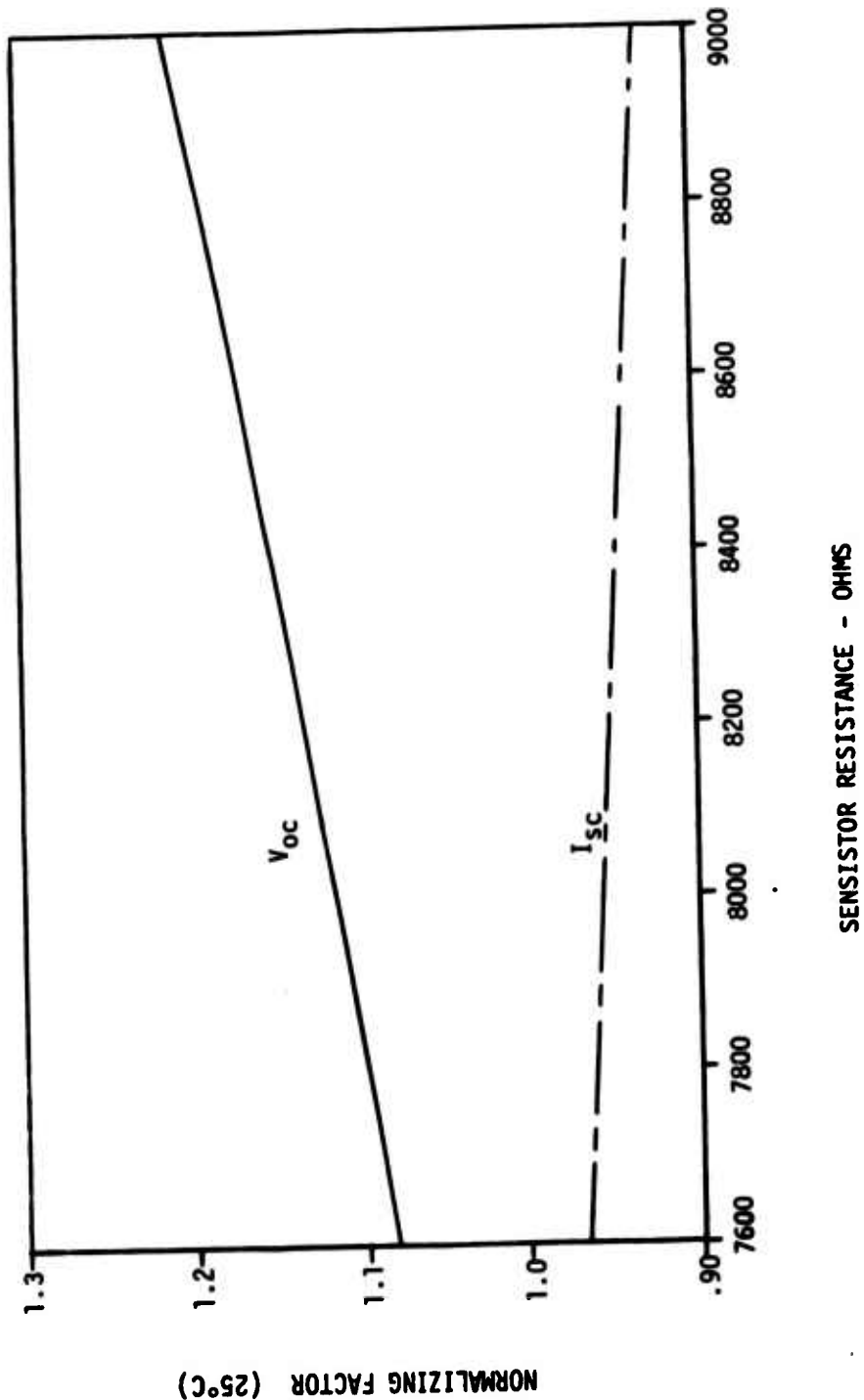


Figure 19. Normalizing Factors vs. Sensor Resistance to Correct Data to 25°C

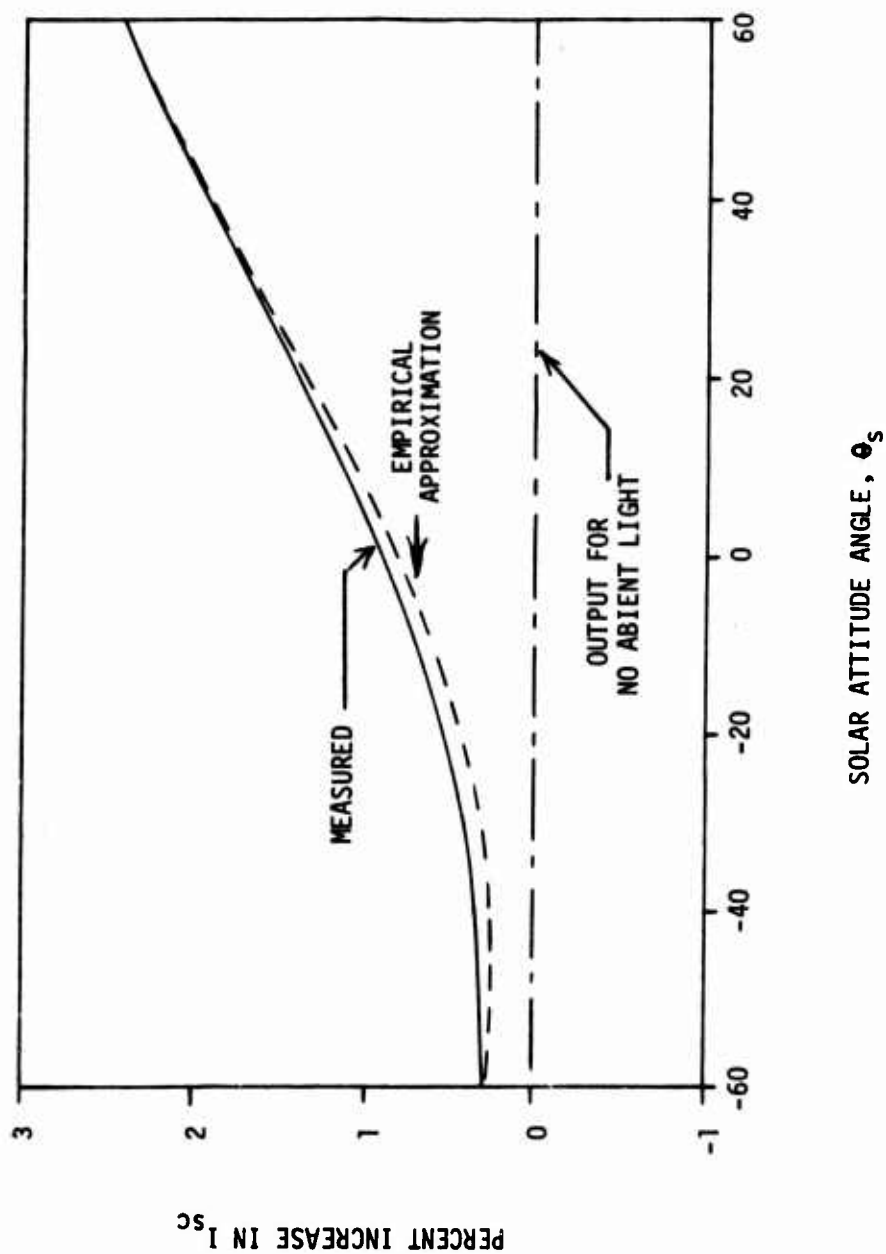


Figure 20. Contribution of Ambient Light to Short Circuit Current Output

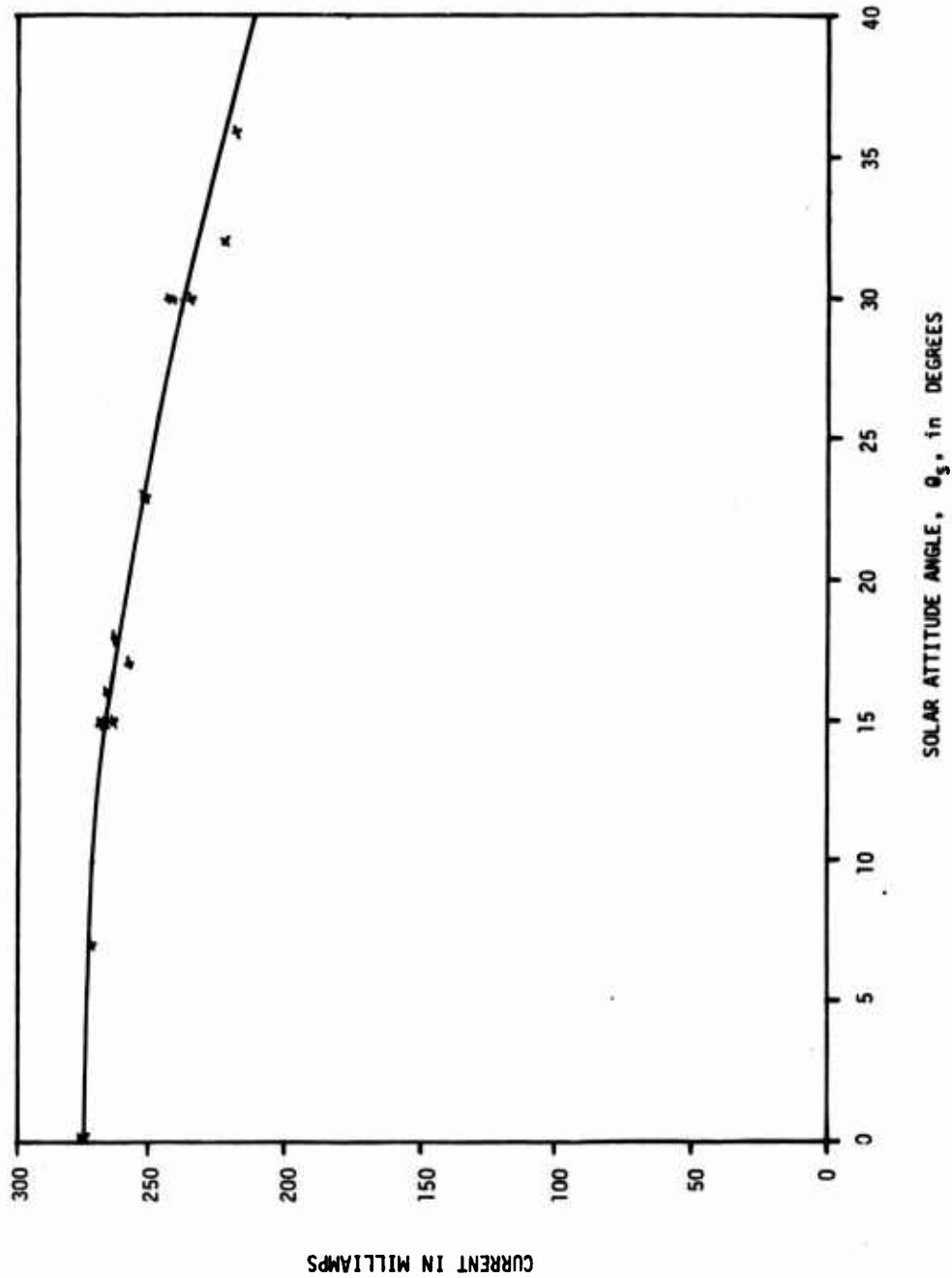


Figure 21. Short Circuit Current vs. Solar Attitude Angle for Module 1

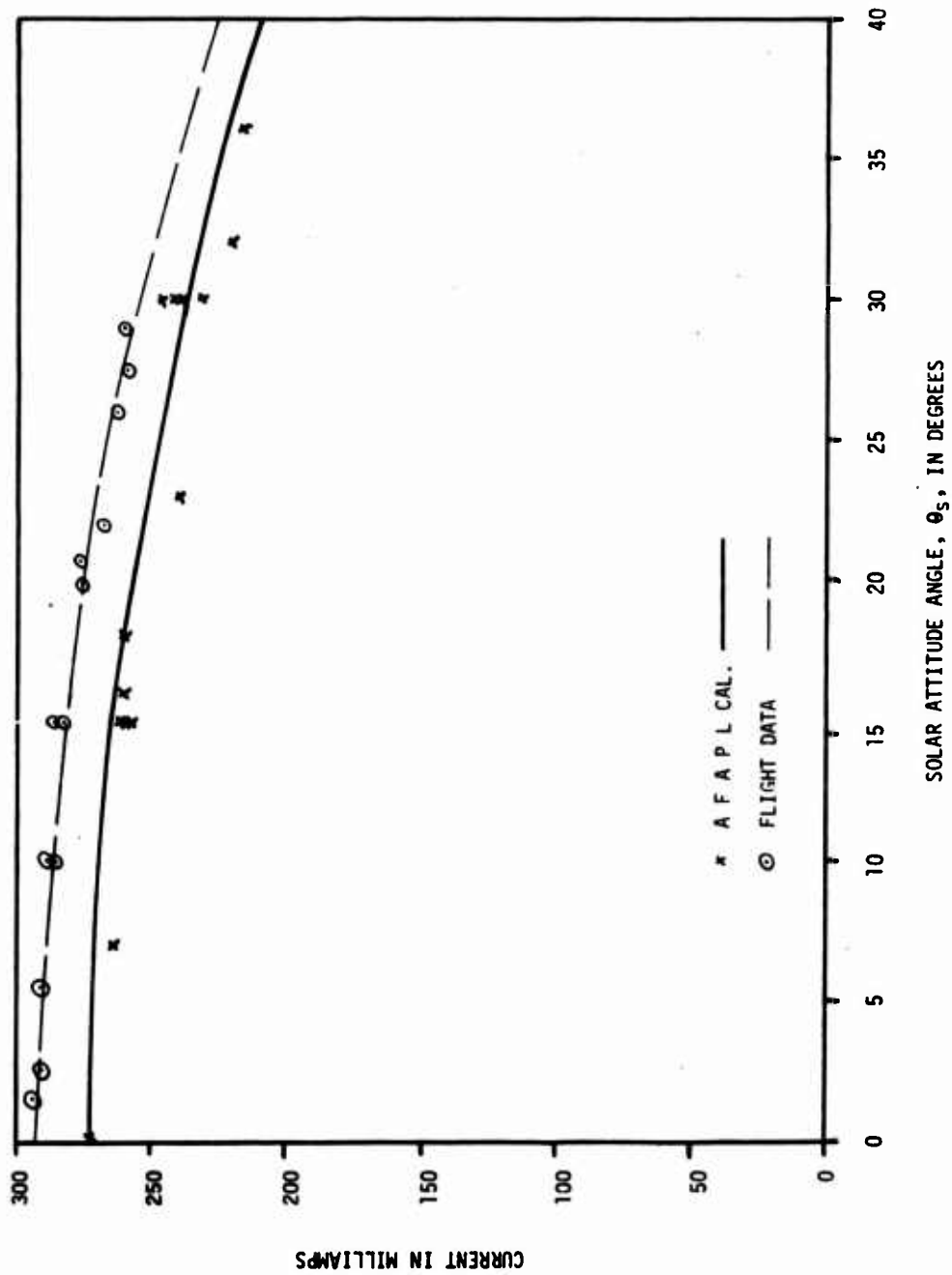


Figure 22. Short Circuit Current vs. Solar Attitude Angle for Module 2

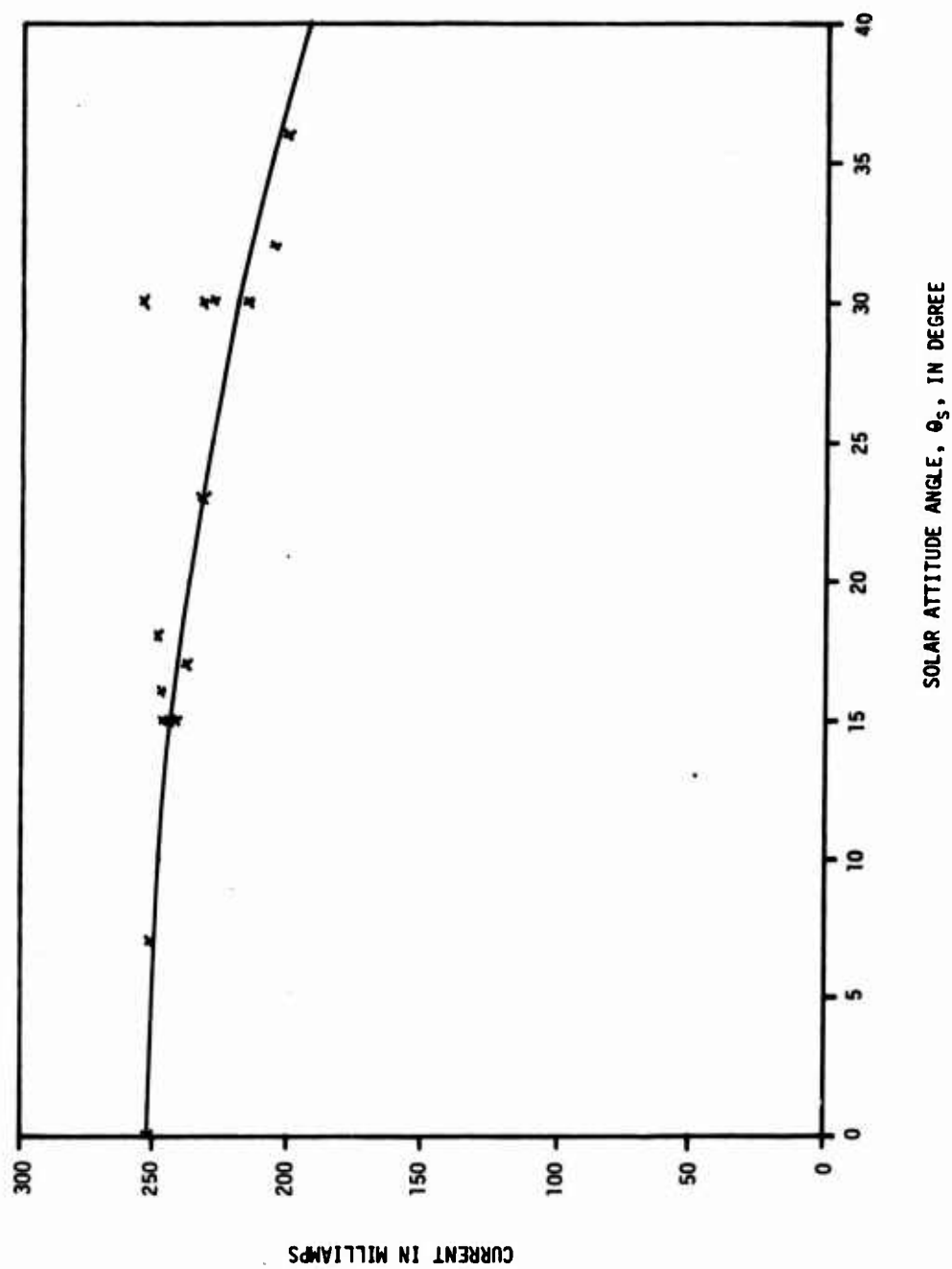


Figure 23. Short Circuit Current vs. Solar Attitude Angle for Module 3

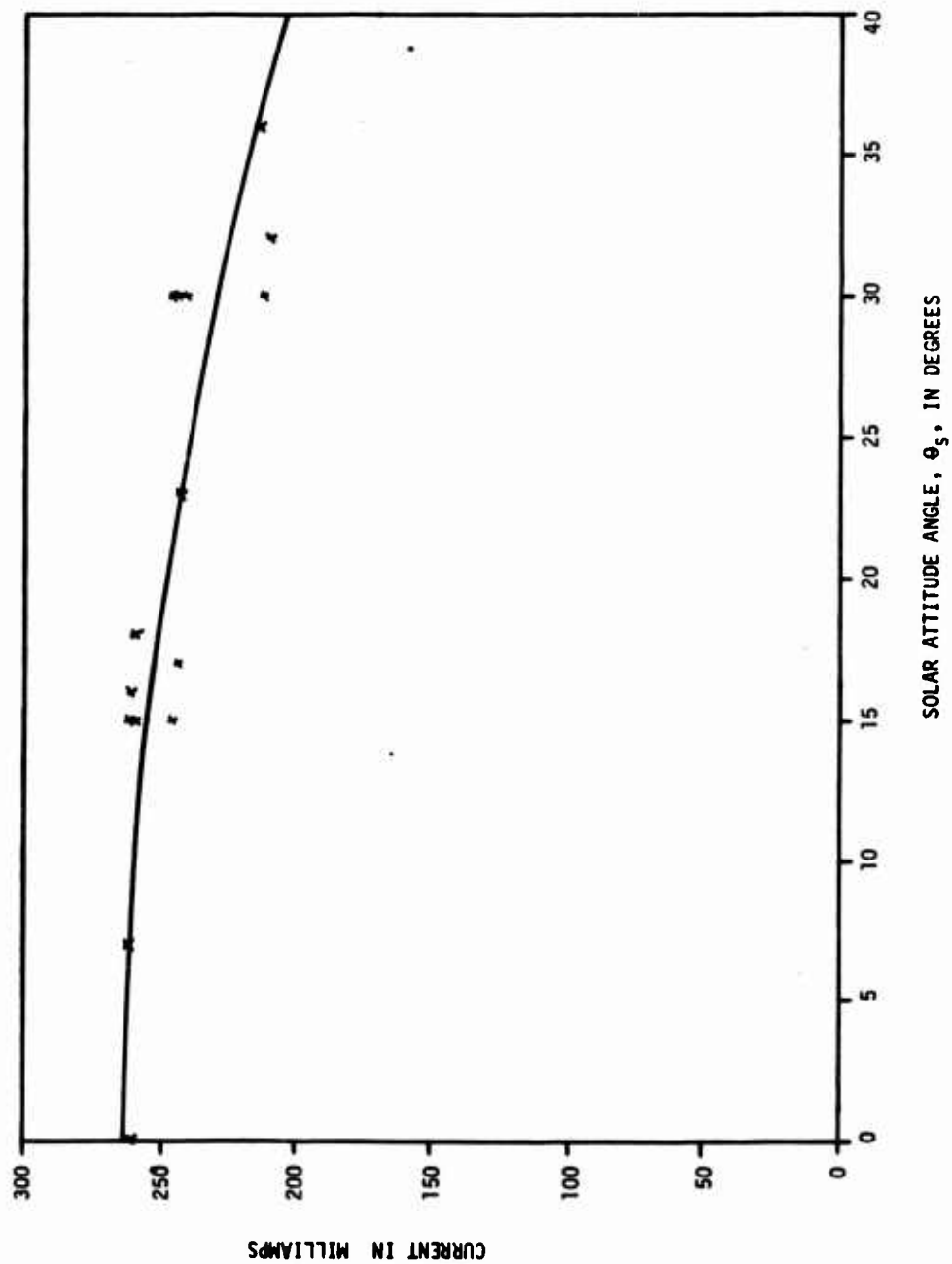


Figure 24. Short Circuit Current vs. Solar Attitude Angle for Module 4

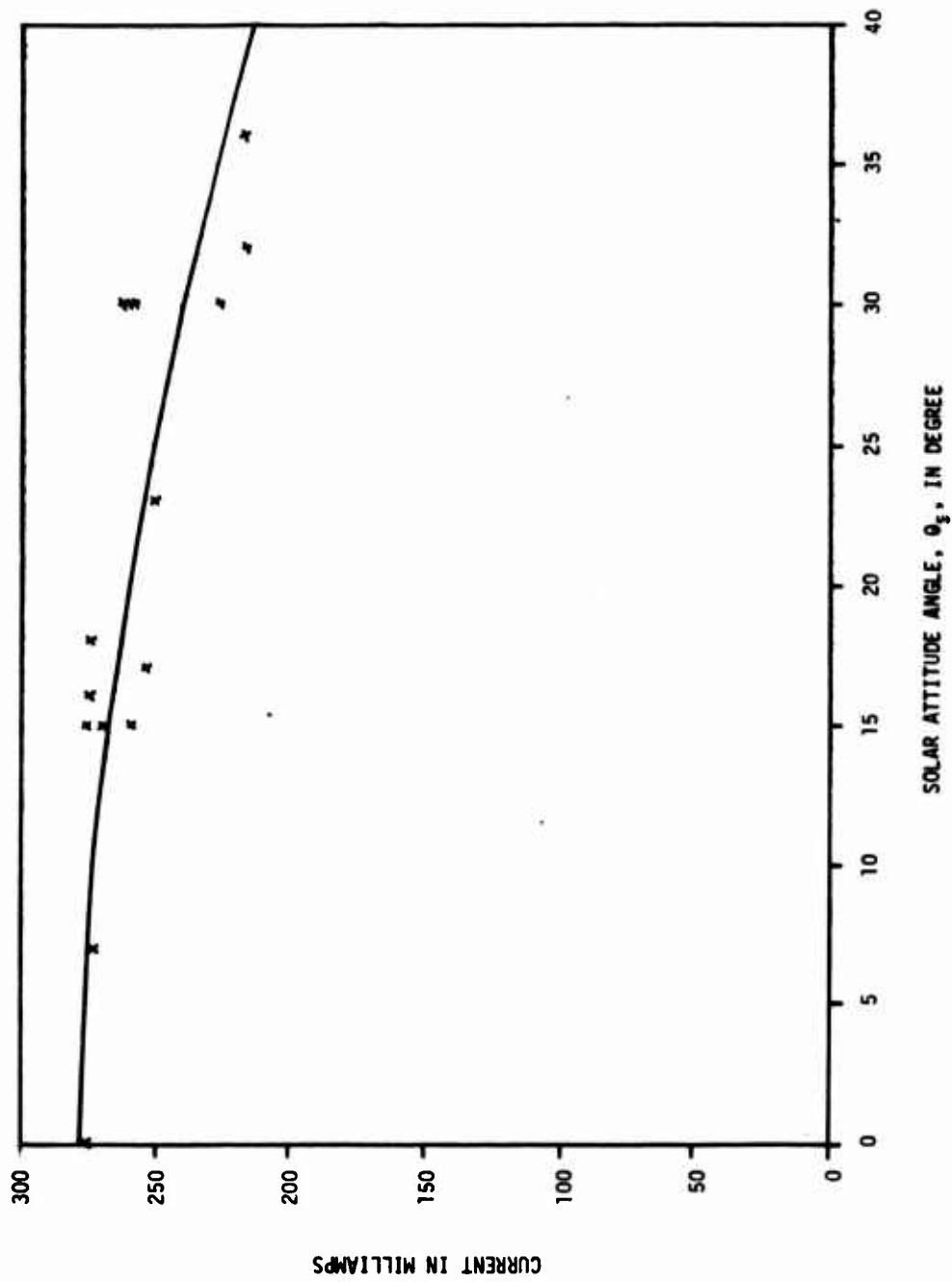


Figure 25. Short Circuit Current vs. Solar Attitude Angle for Module 5

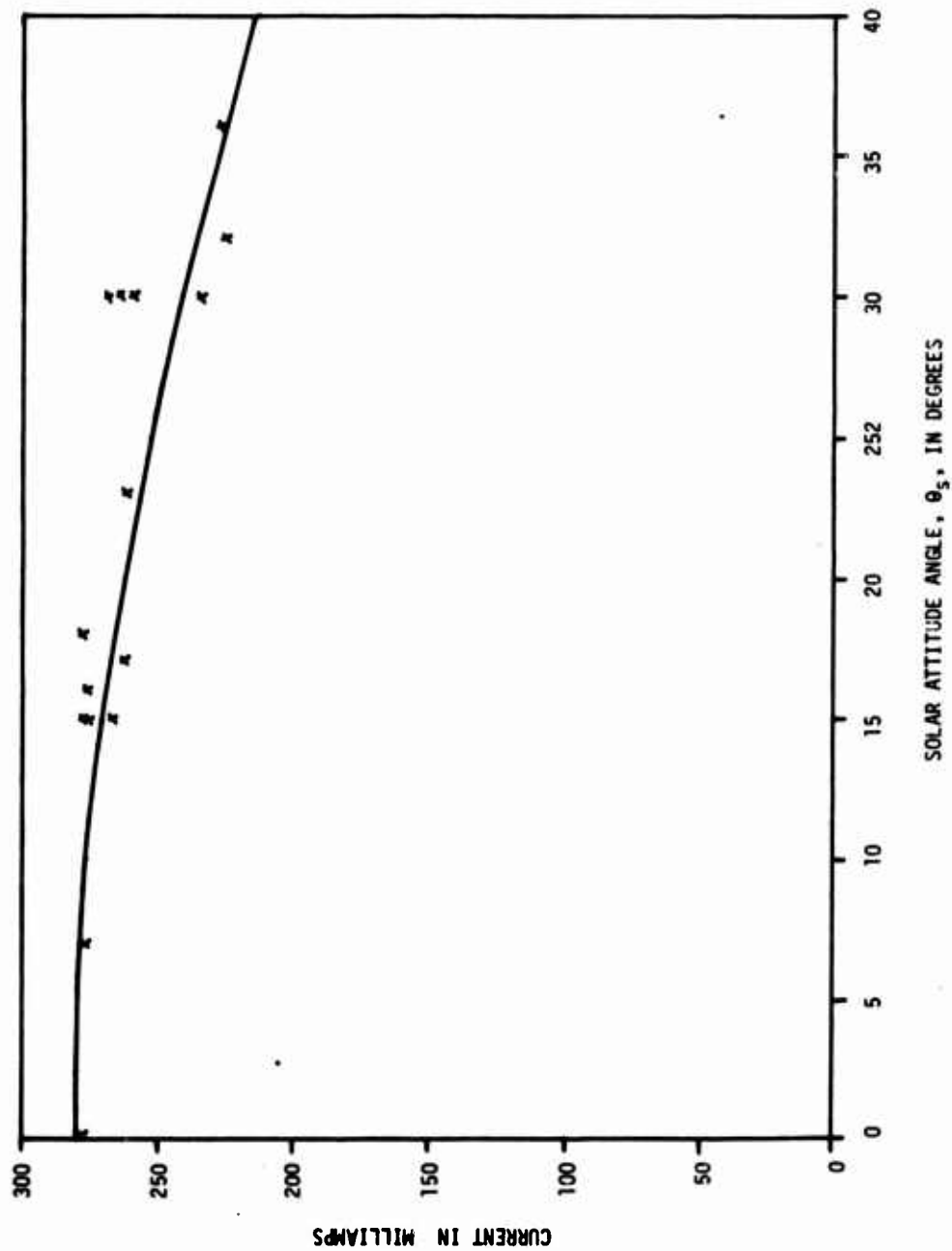


Figure 26. Short Circuit Current vs. Solar Attitude Angle for Module 6

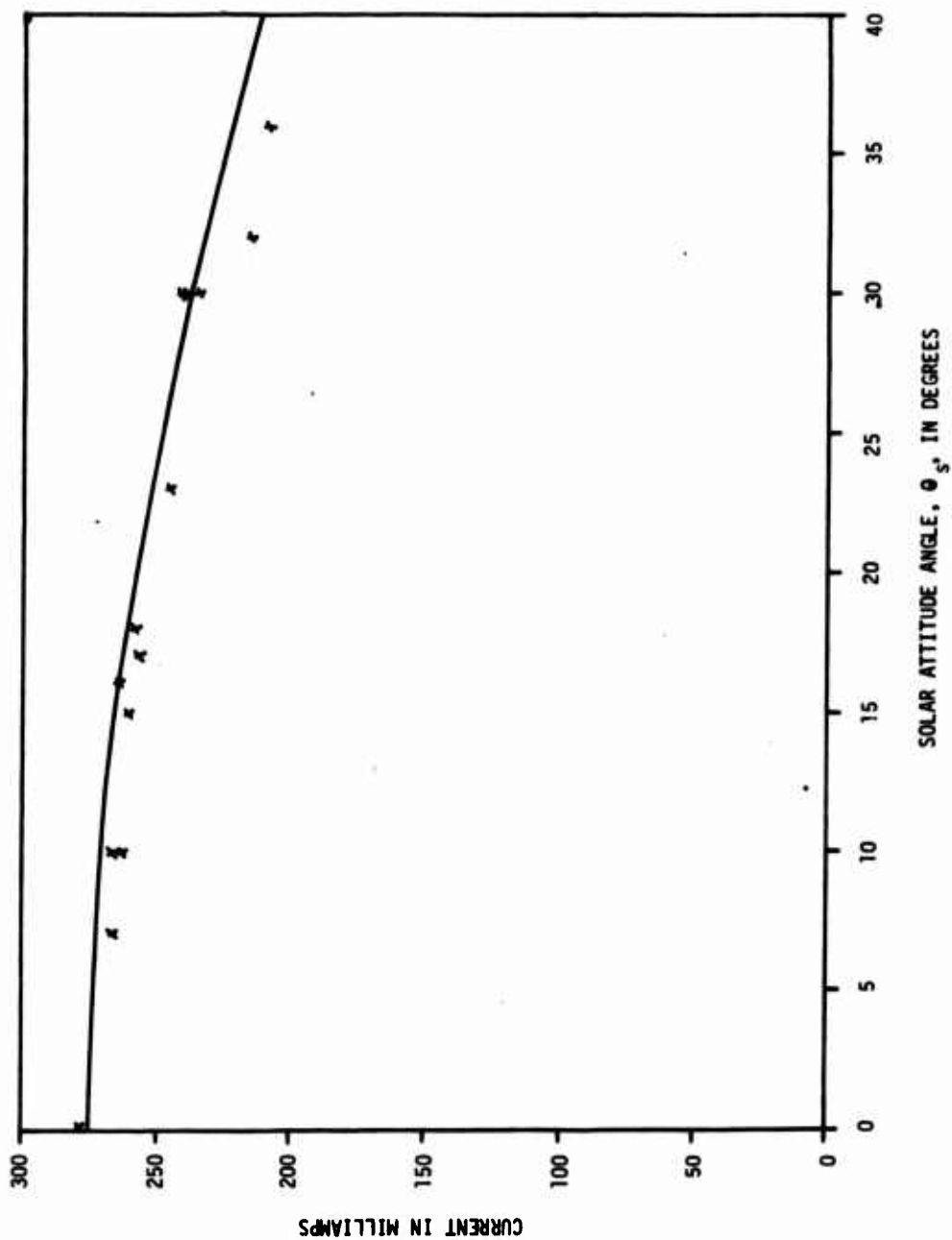


Figure 27. Module 1 Current vs. Solar Attitude Angle at Load Point One

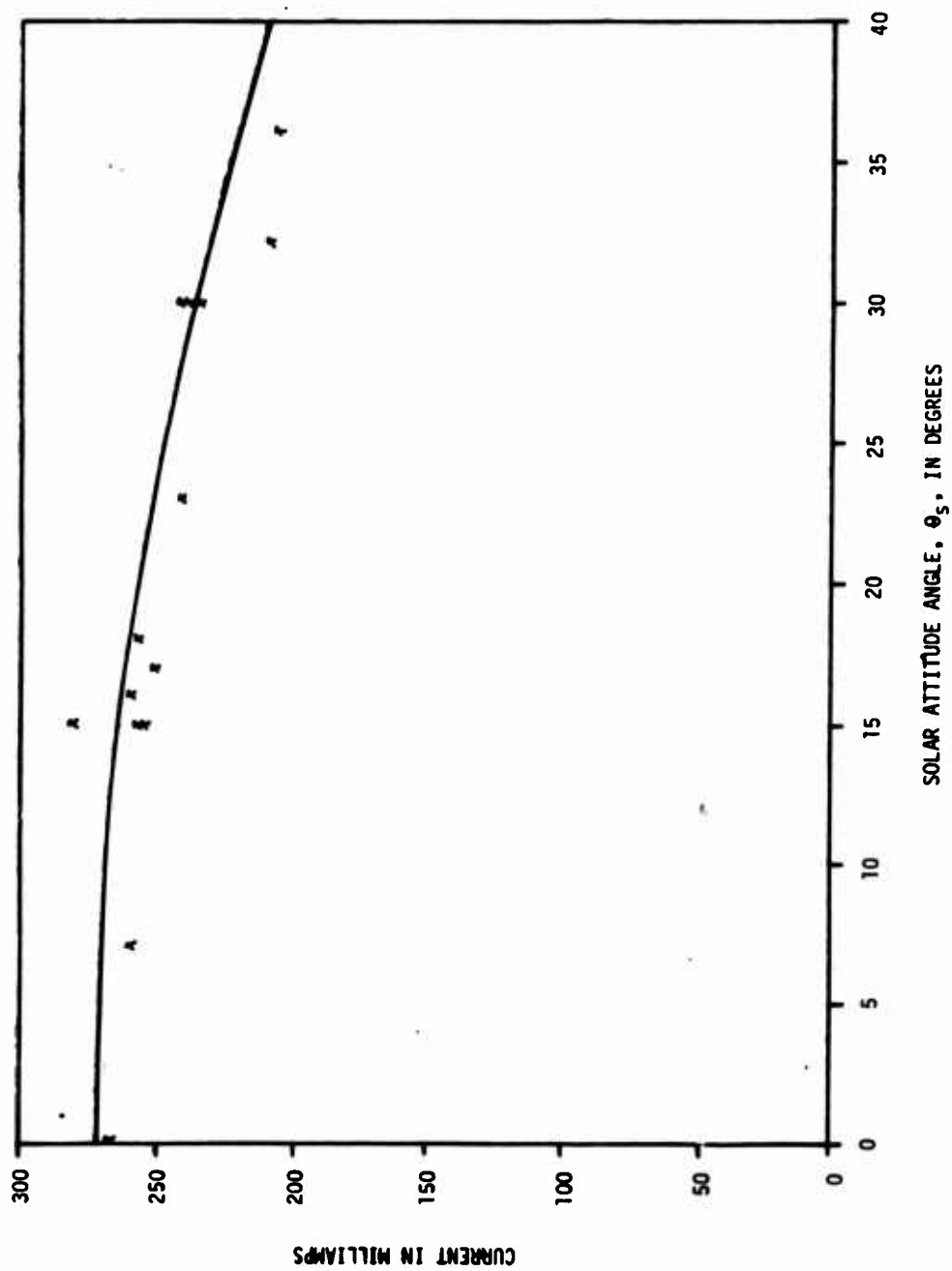


Figure 28. Module 2 Current vs. Solar Attitude Angle at Load Point One

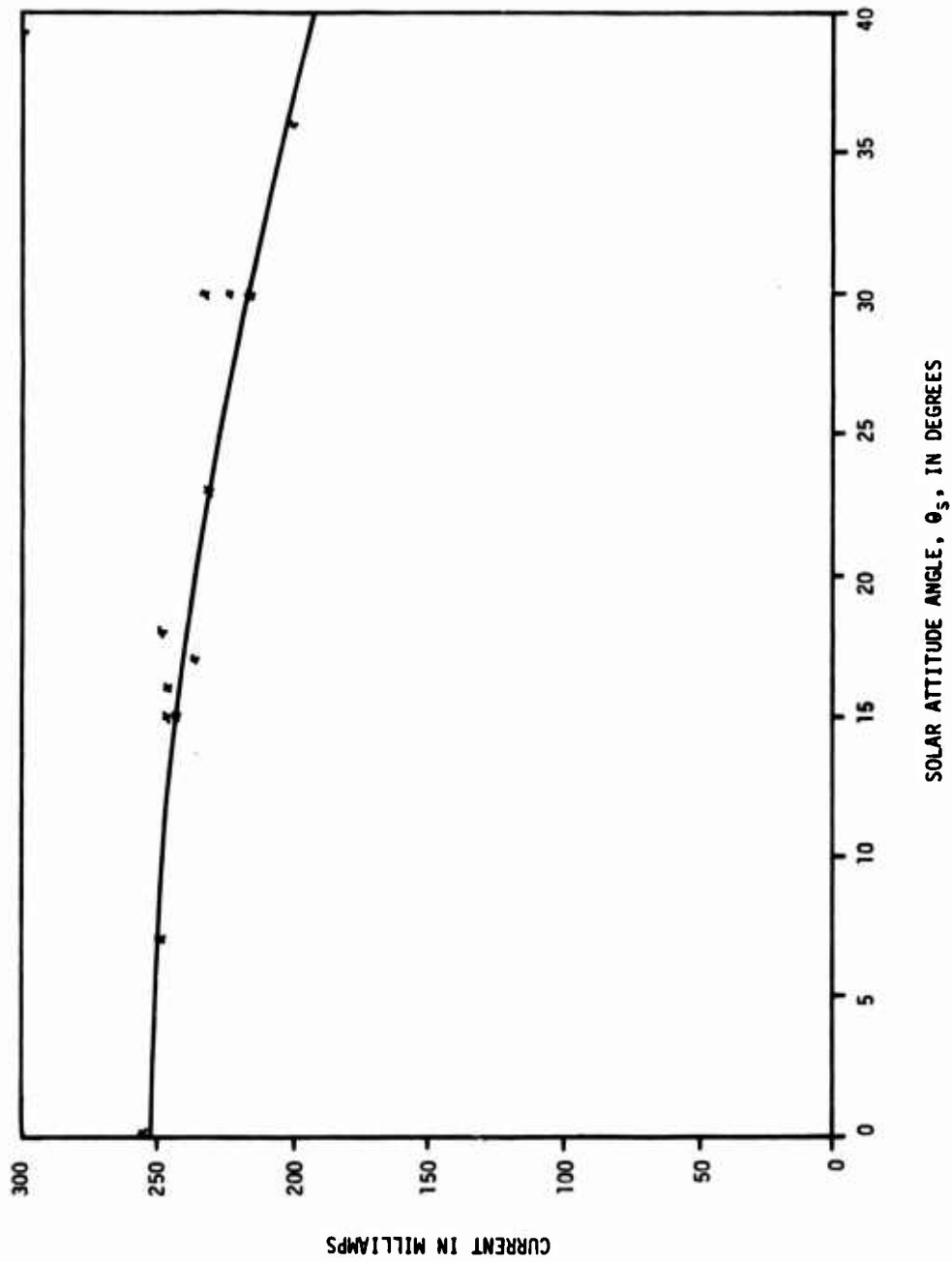


Figure 29. Module 3 Current vs. Solar Attitude Angle at Load Point One

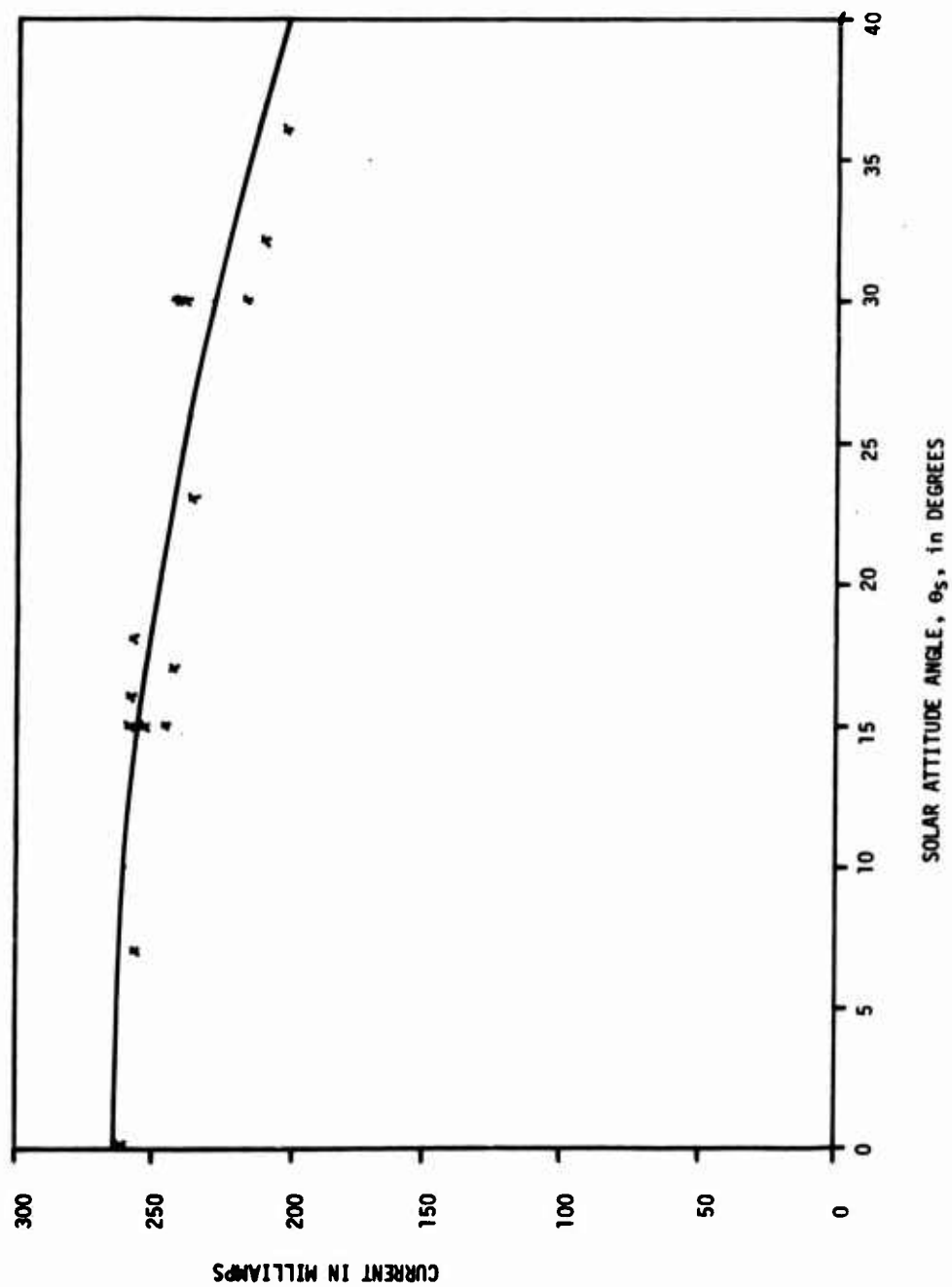


Figure 30. Module 4 Current vs. Solar Attitude Angle at Load Point One

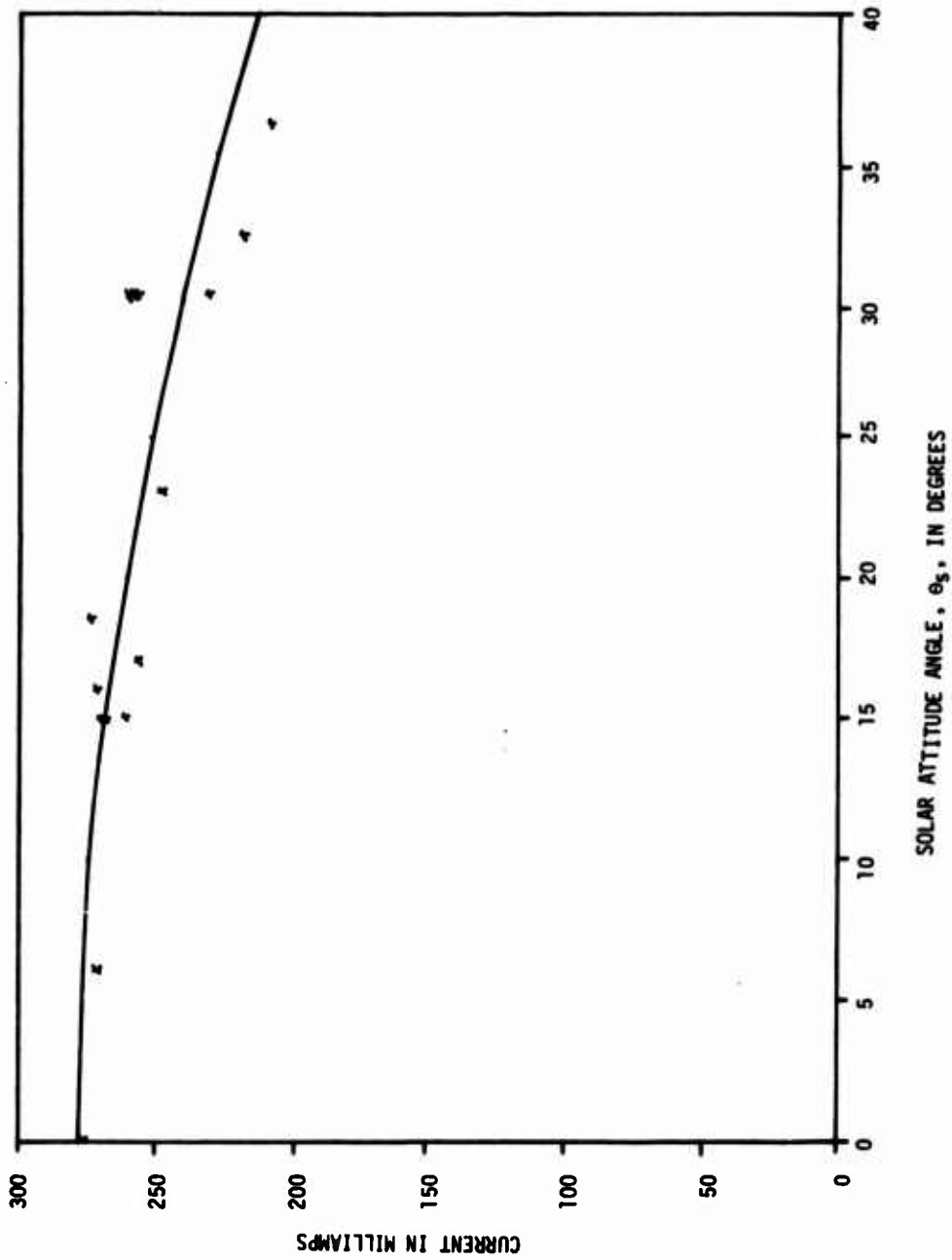


Figure 31. Module 5 Current vs. Solar Attitude Angle at Load Point One

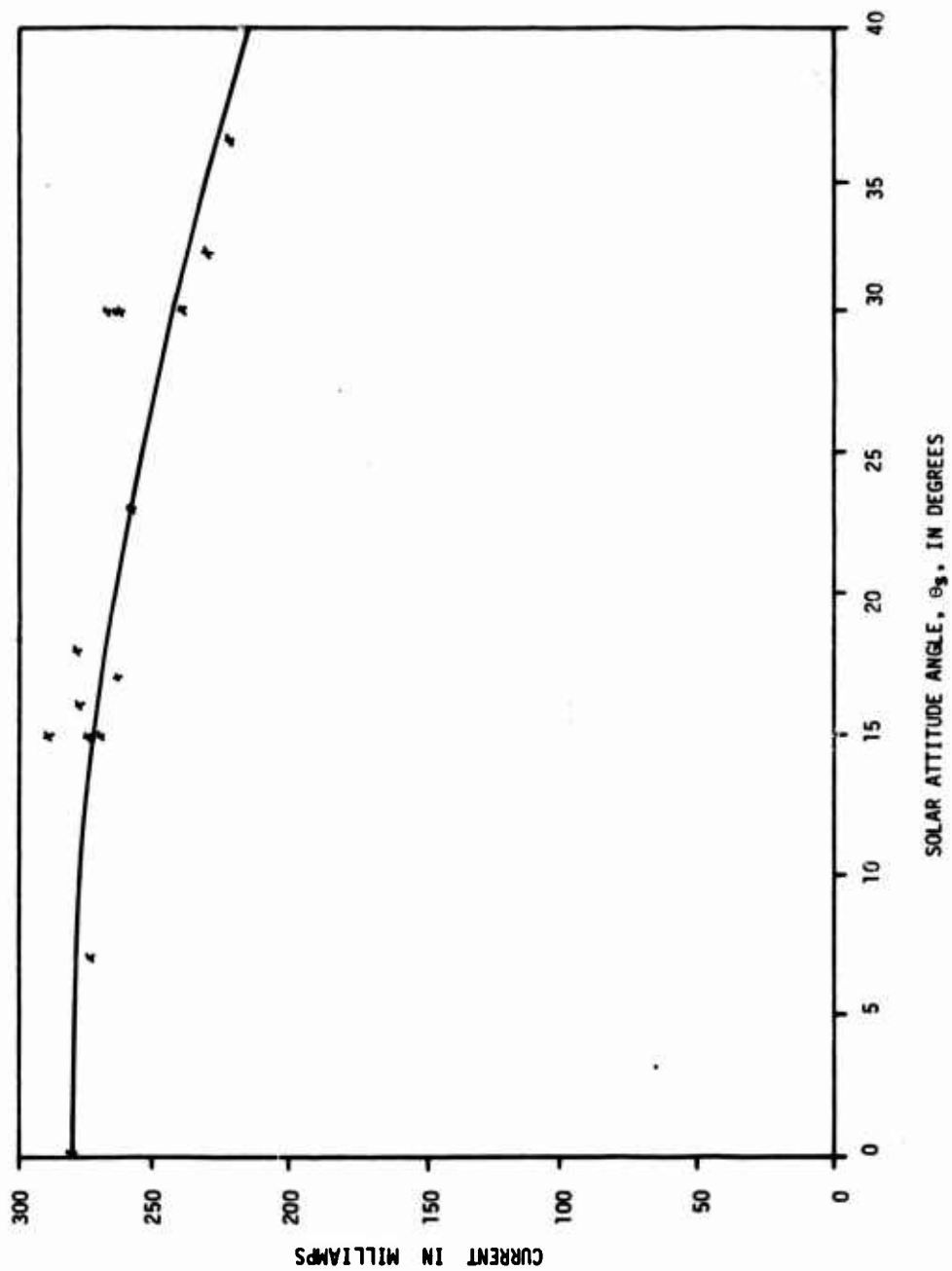


Figure 32. Module 6 Current vs. Solar Attitude Angle at Load Point One

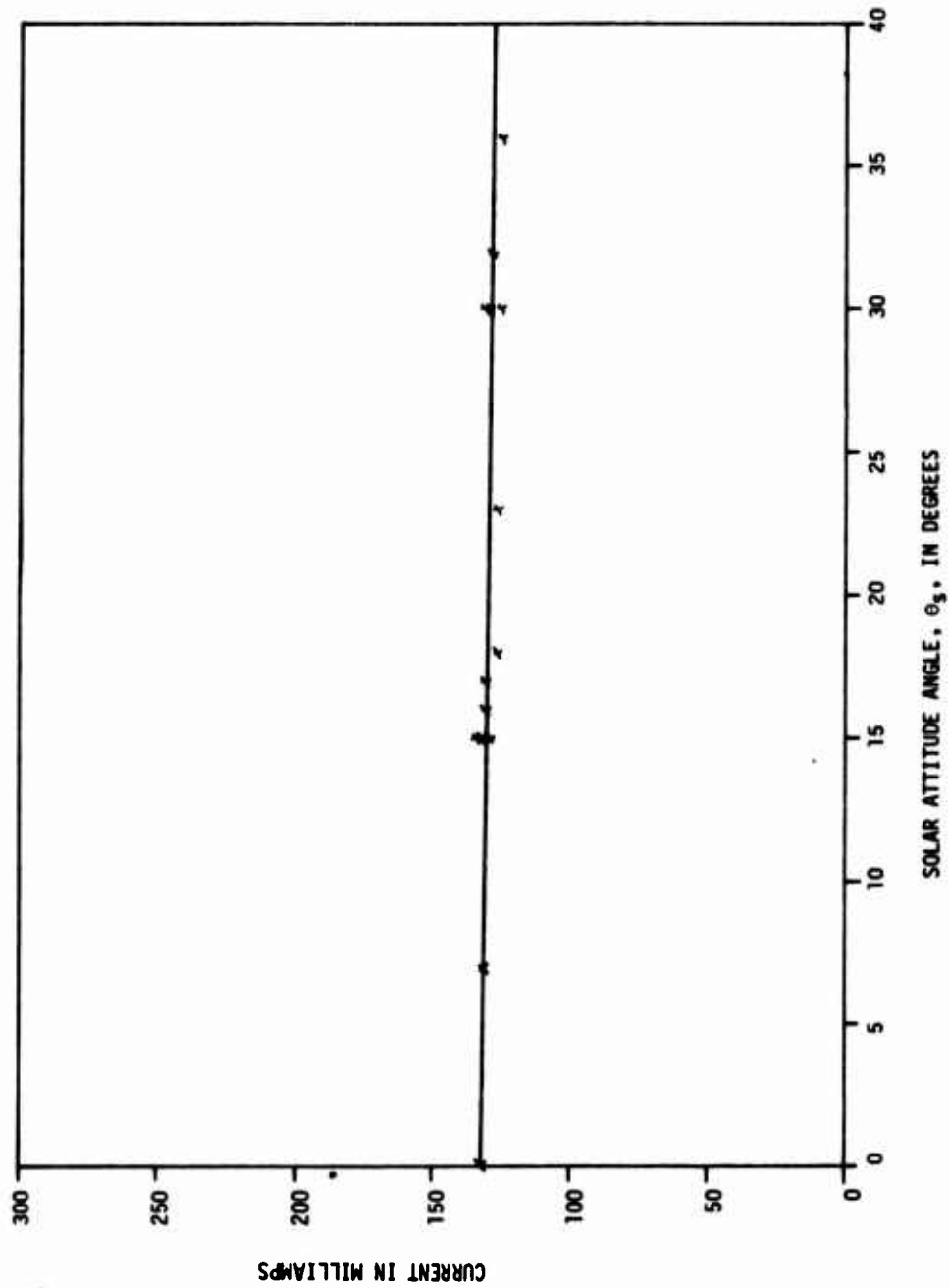


Figure 33. Module 1 Current vs. Solar Attitude Angle at Load Point Two

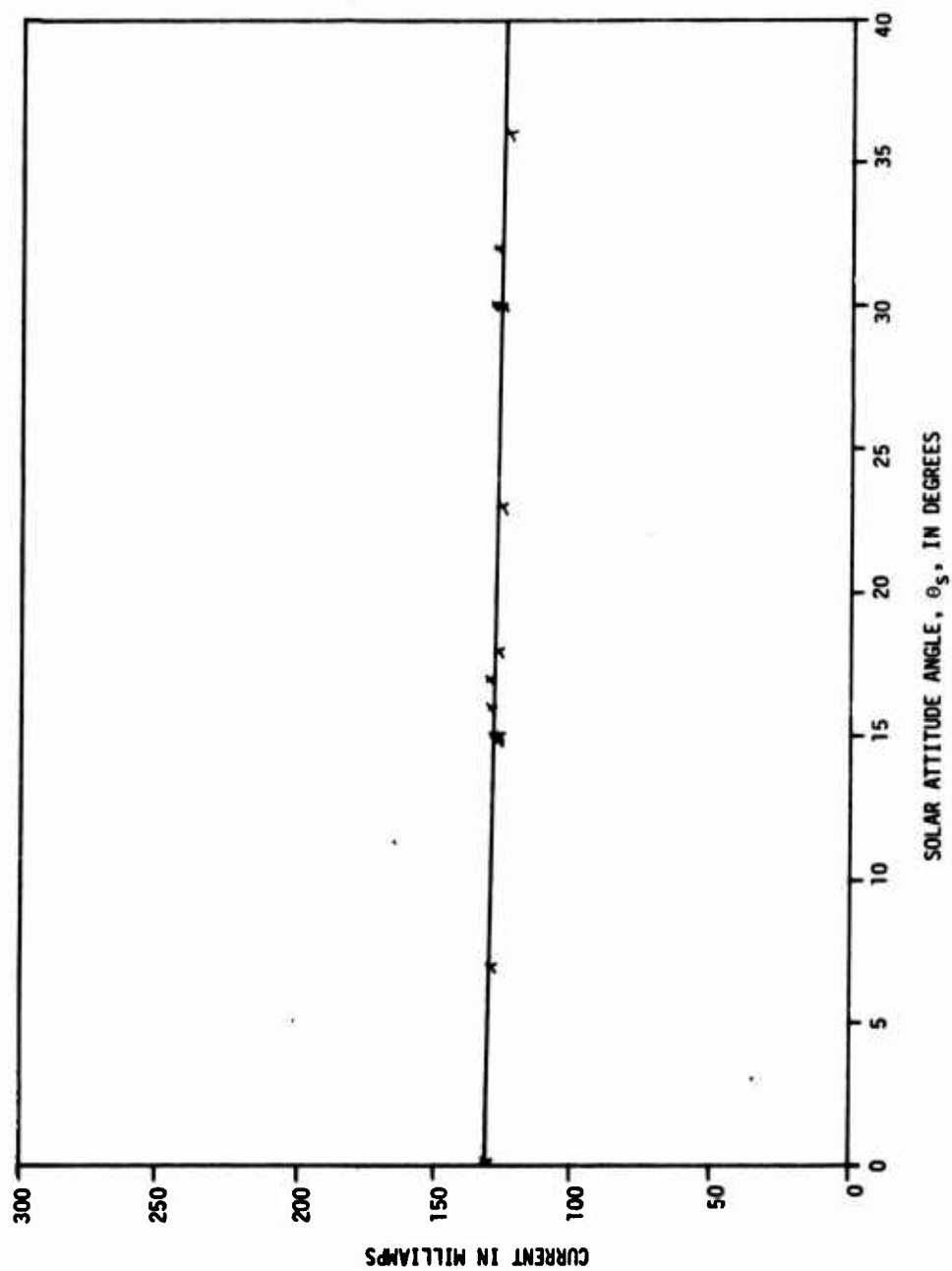


Figure 34. Module 2 Current vs. Solar Attitude Angle at Load Point Two

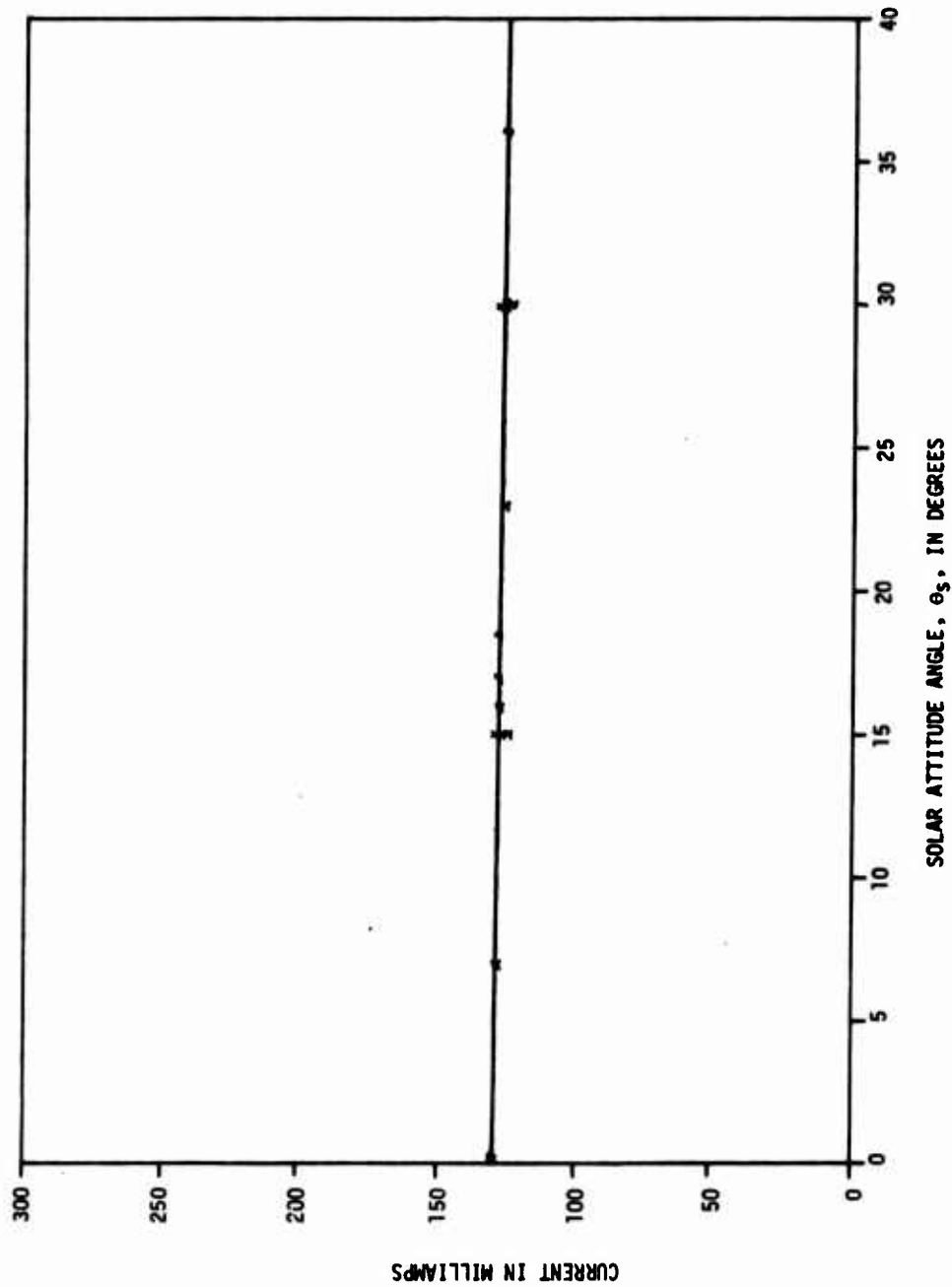


Figure 35. Module 3 Current vs. Solar Attitude Angle at Load Point Two

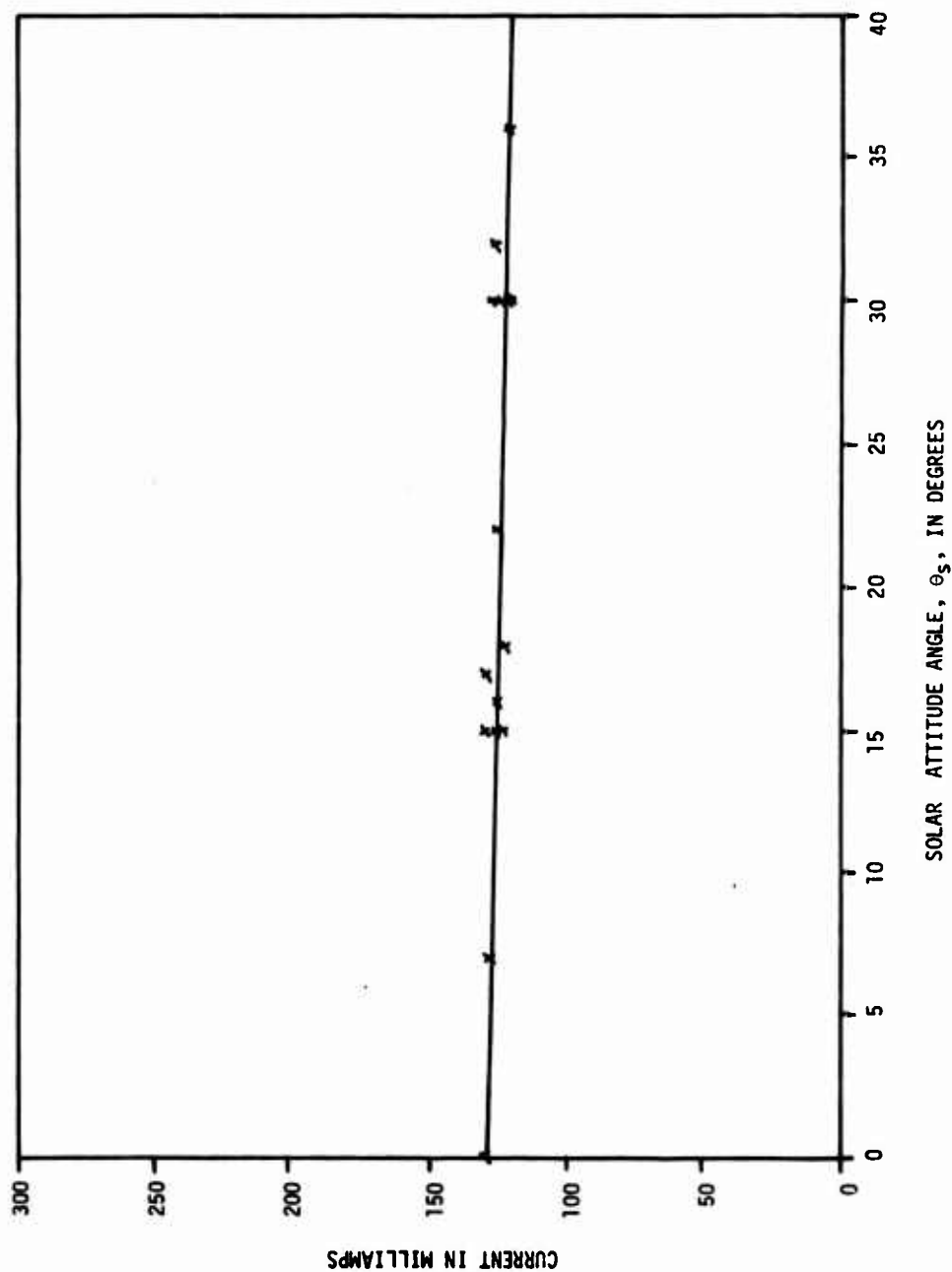


Figure 36. Module 4 Current vs. Solar Attitude Angle at Load Point Two

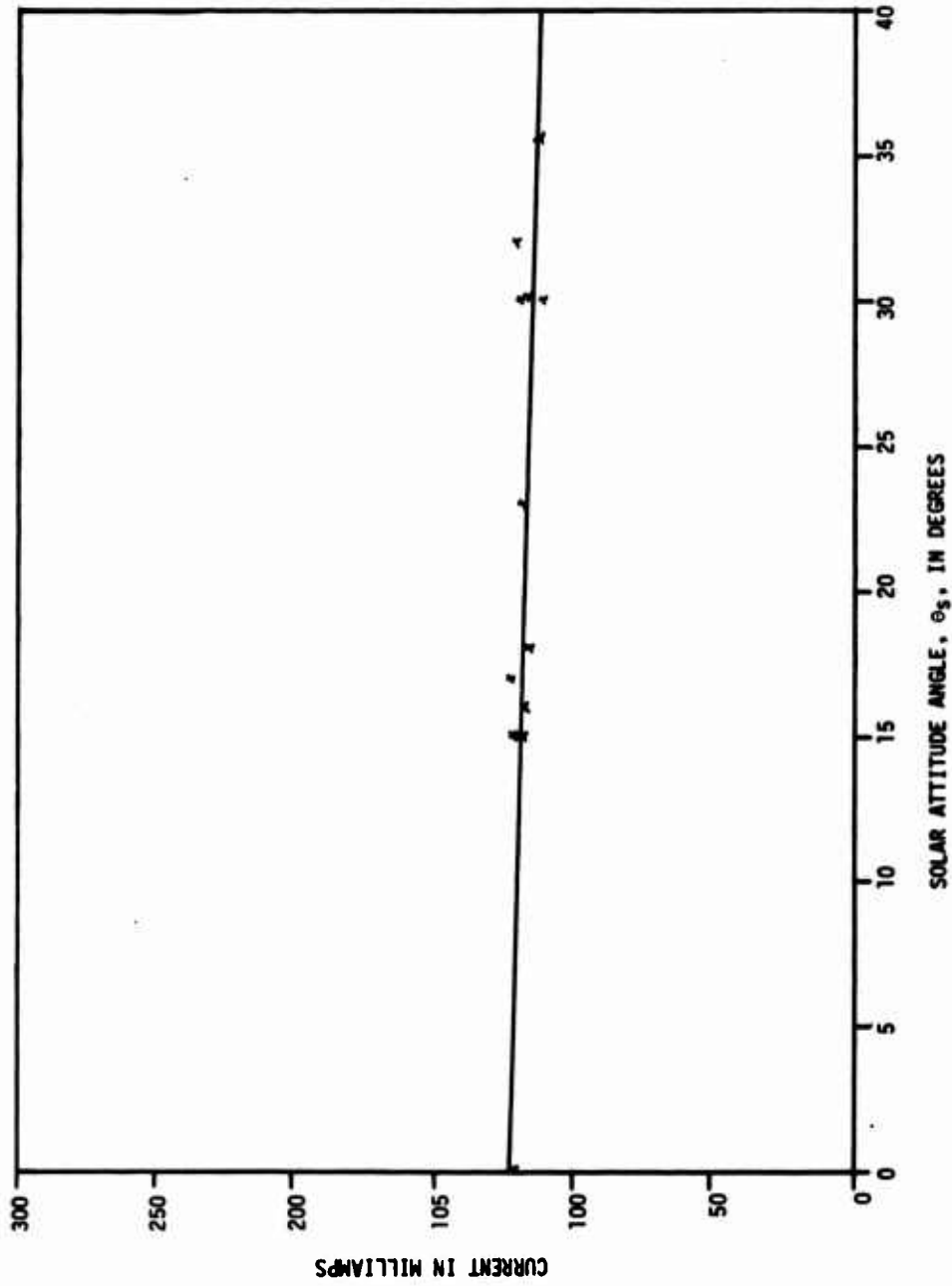


Figure 37. Module 5 Current vs. Solar Attitude Angle at Load Point Two

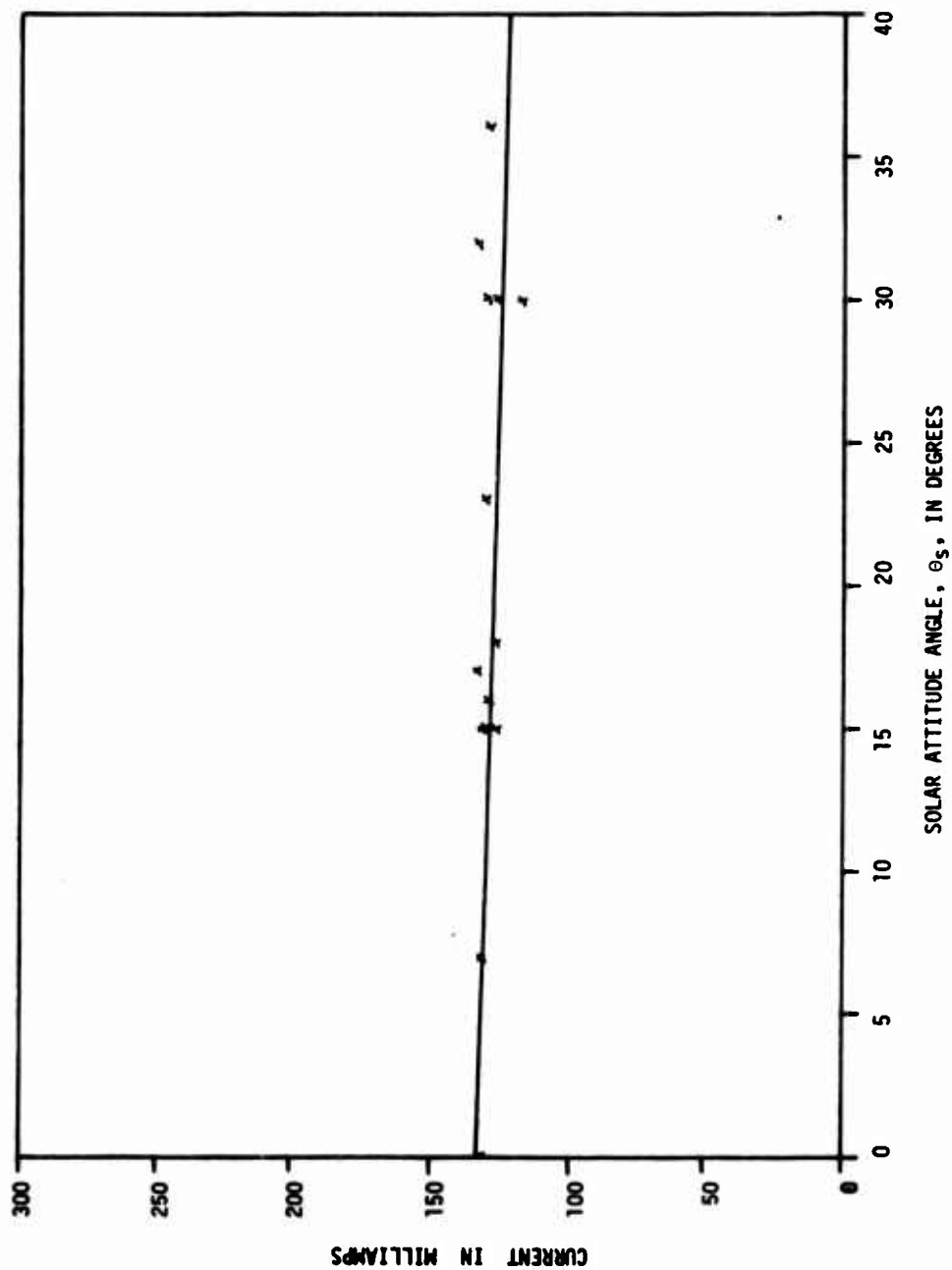


Figure 38. Module 6 Current vs. Solar Attitude Angle at Load Point Two

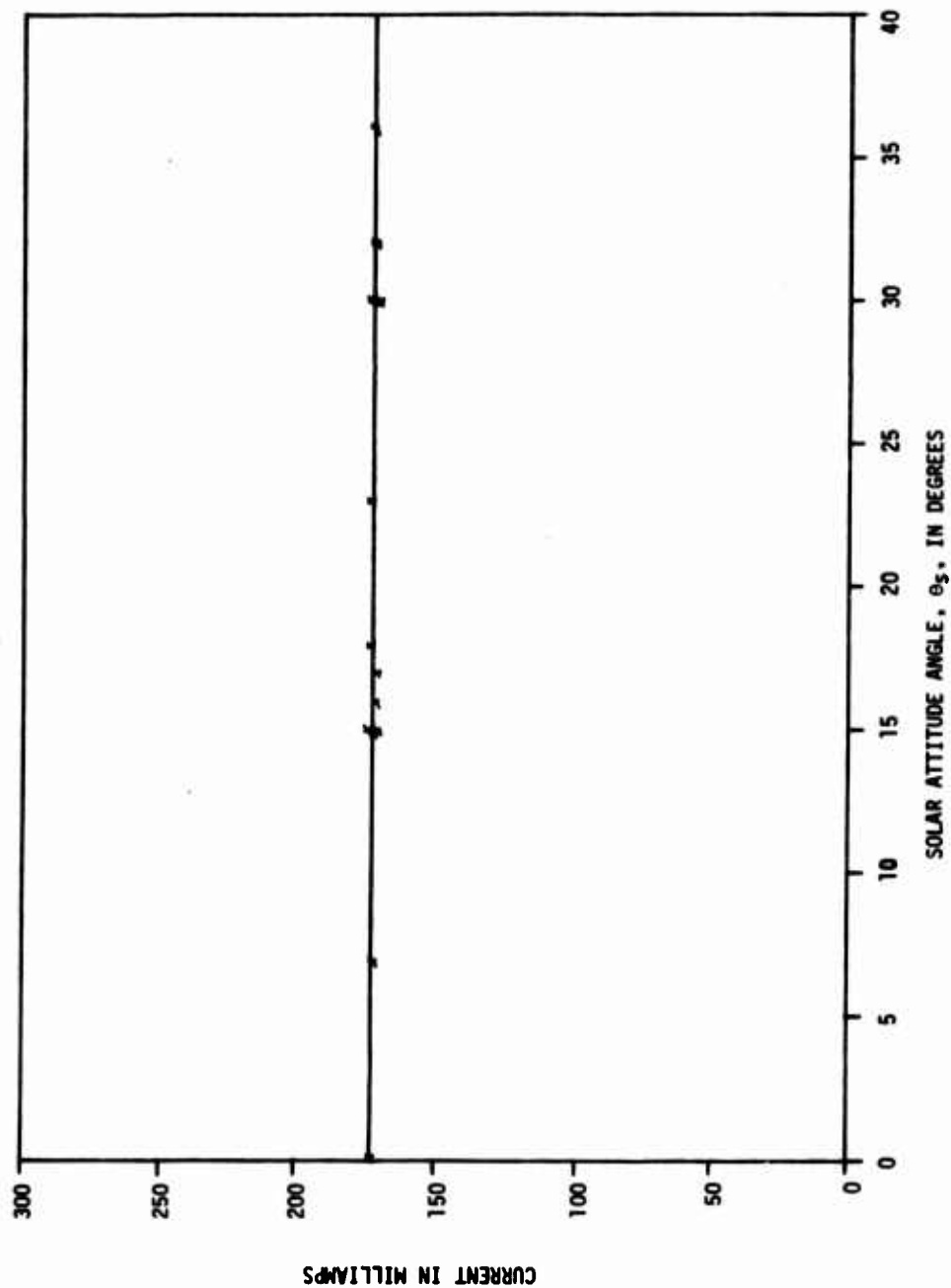


Figure 39. Open Circuit Voltage vs. Solar Attitude Angle for Module Group 1

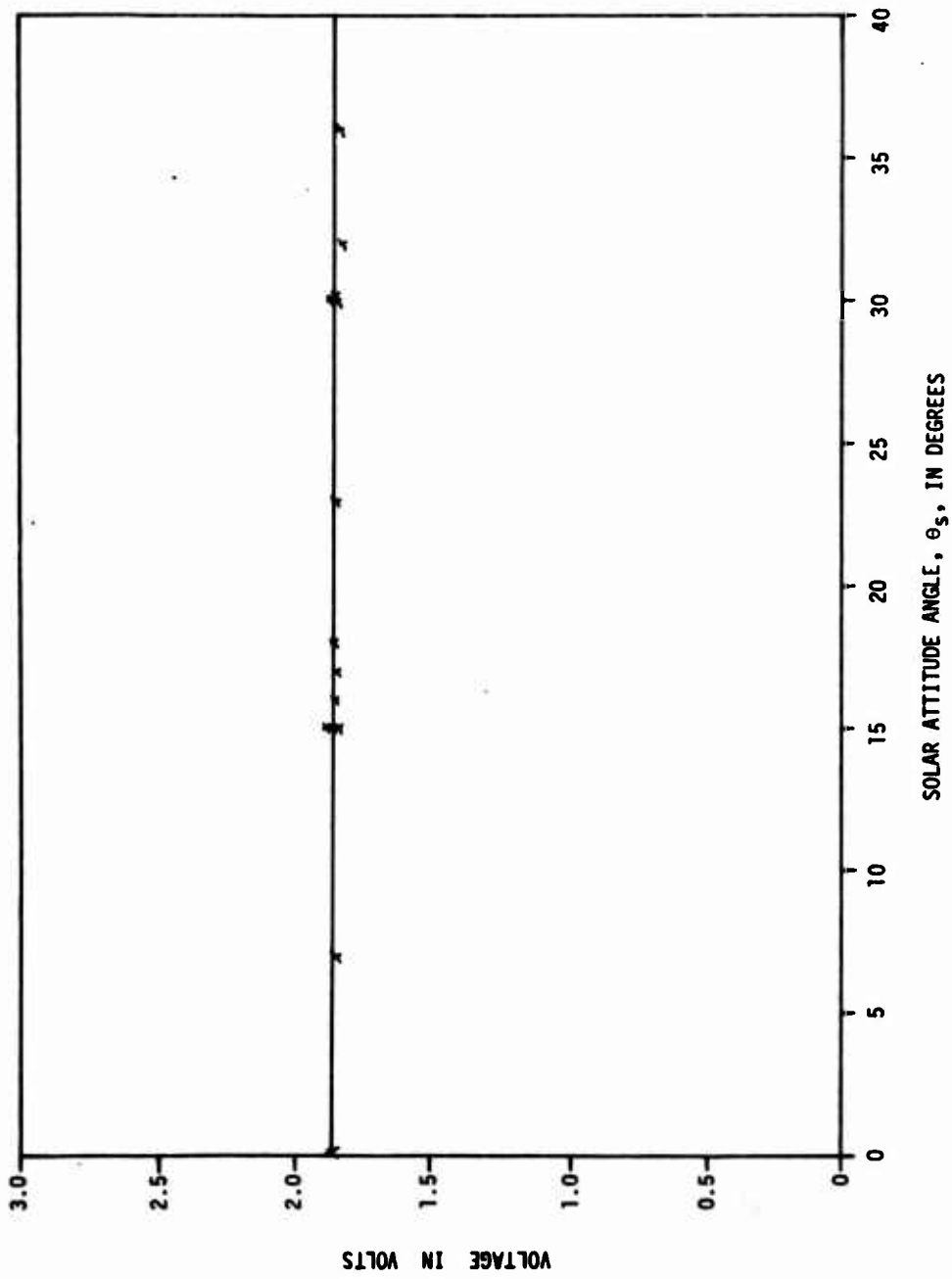


Figure 40. Open Circuit Voltage vs. Solar Attitude Angle for Module Group 2

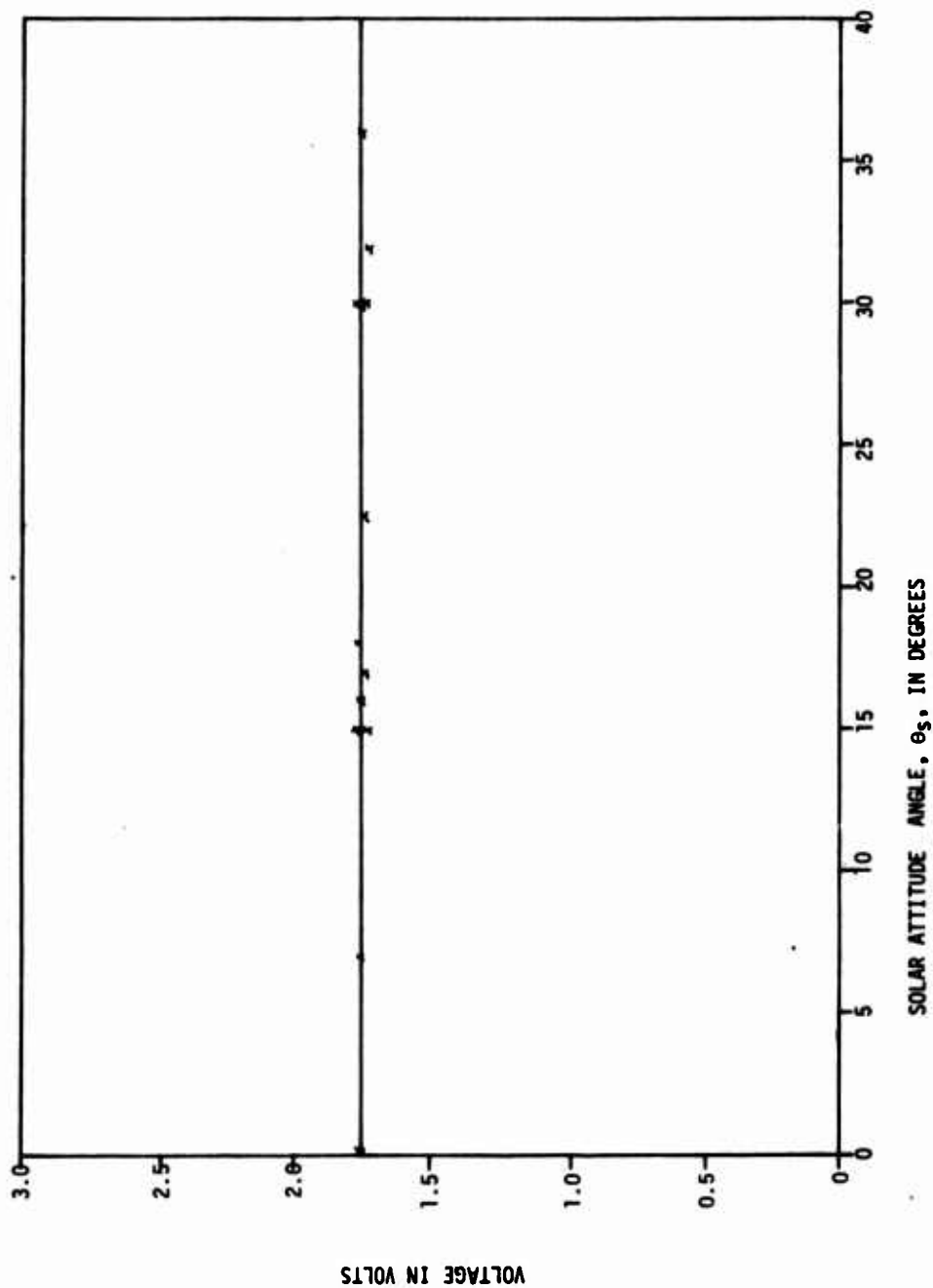


Figure 41. Open Circuit Voltage vs. Solar Attitude Angle for Module Group 3

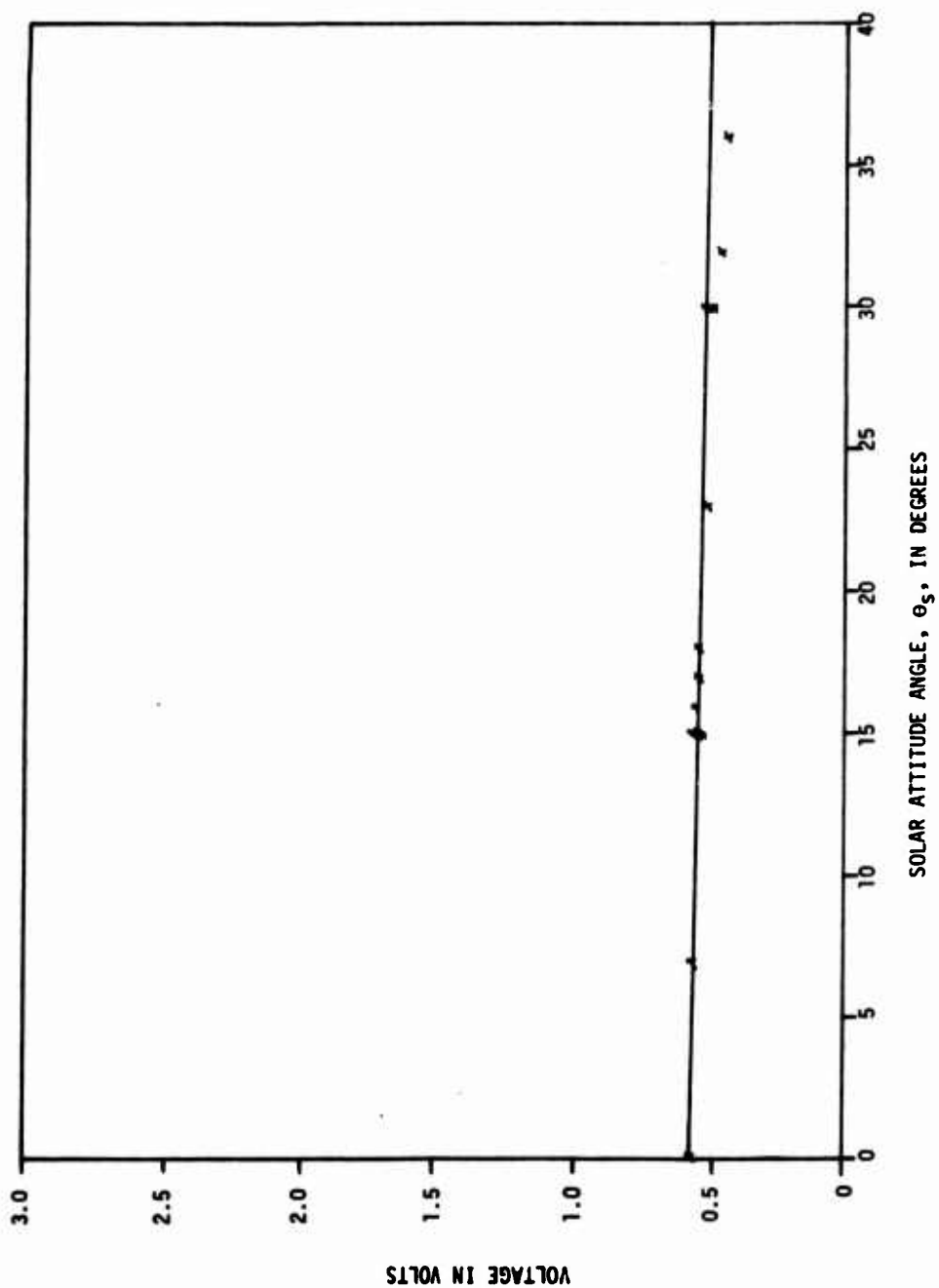


Figure 42. Module Group 1 Voltage vs. Solar Attitude Angle at Load Point One

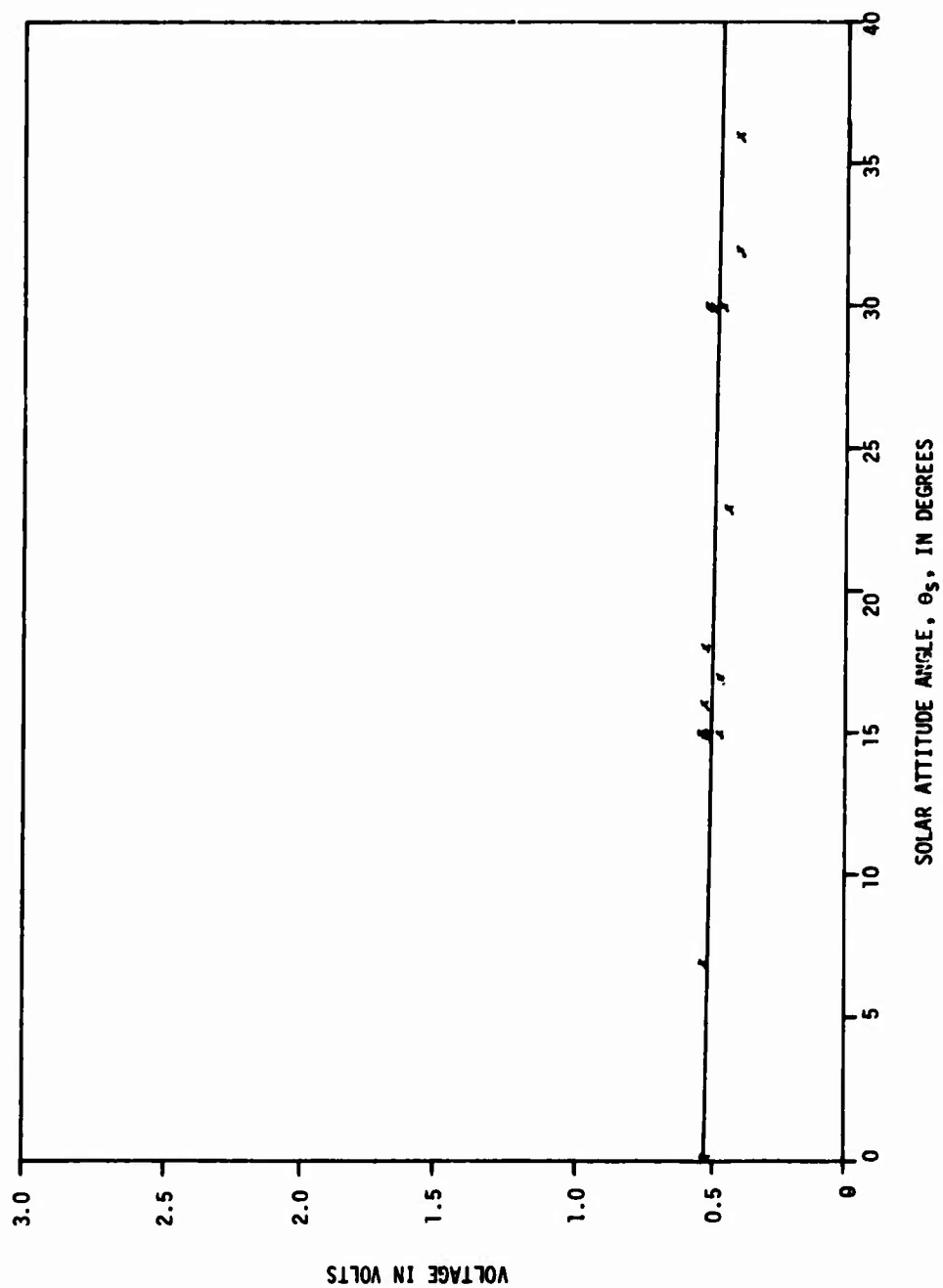


Figure 43. Module Group 2 Voltage vs. Solar Attitude Angle at Load Point One

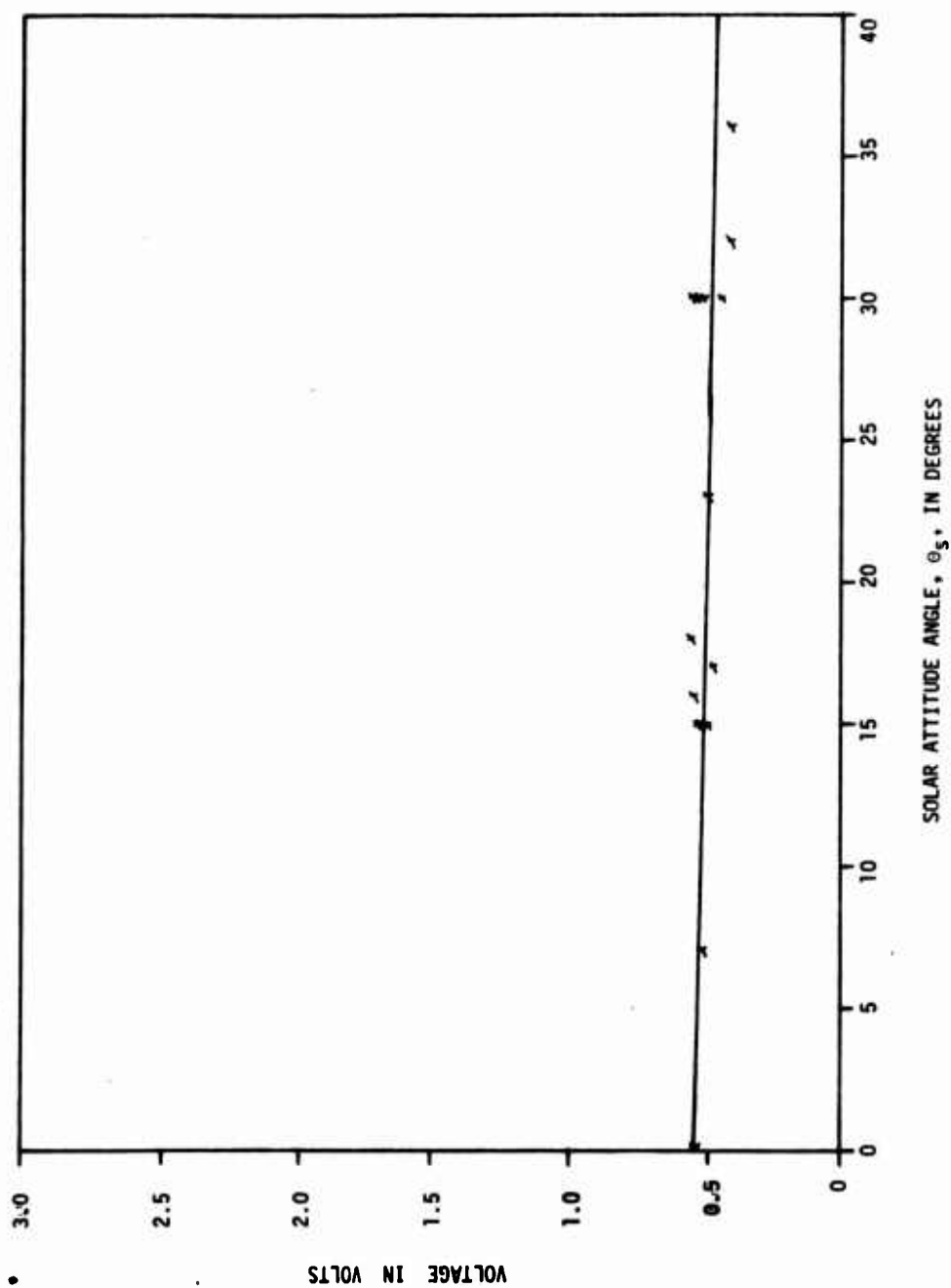


Figure 44. Module Group 3 Voltage vs. Solar Attitude Angle at Load Point

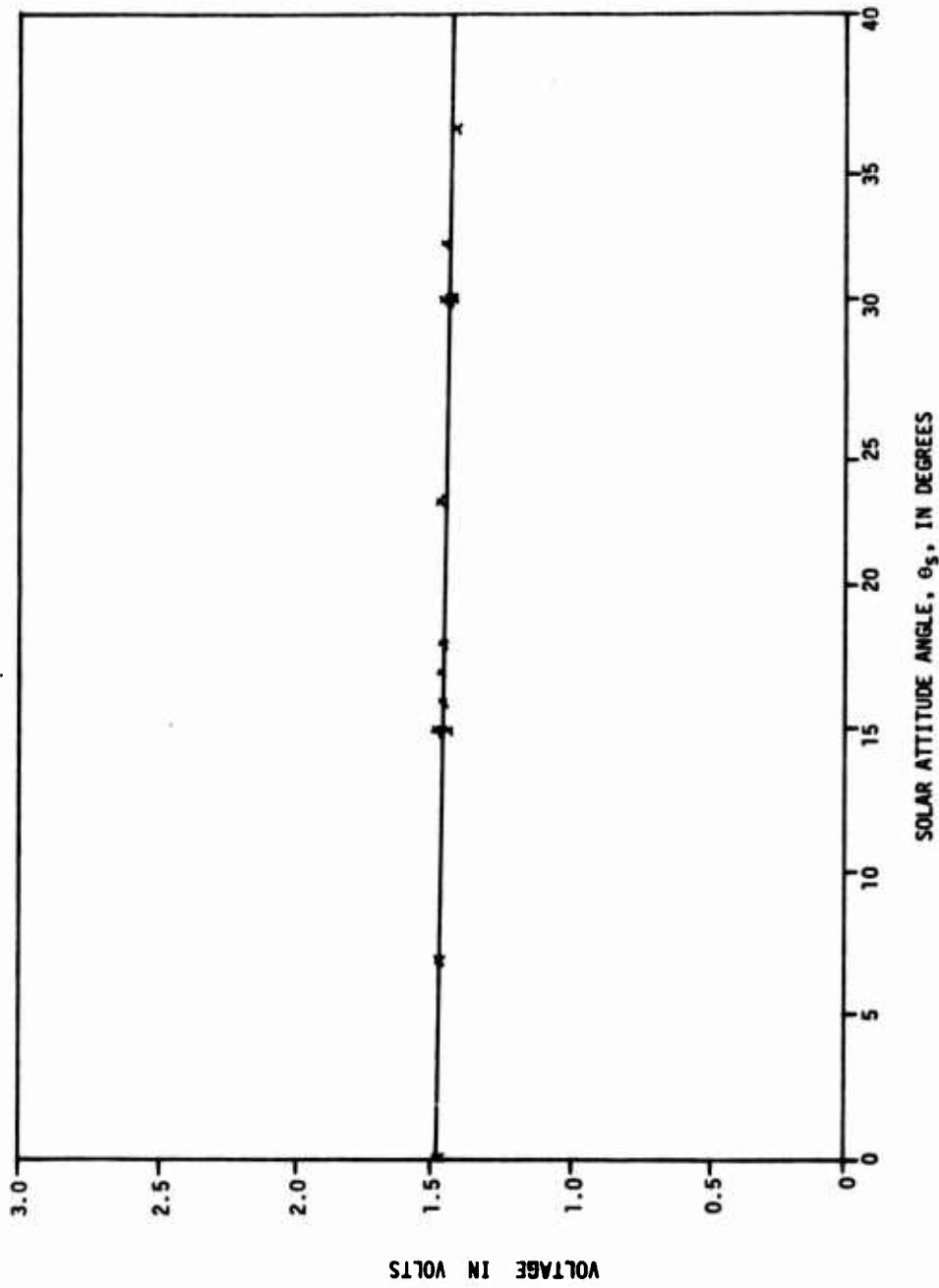


Figure 45. Module Group 1 Voltage vs. Solar Attitude Angle at Load Point Two

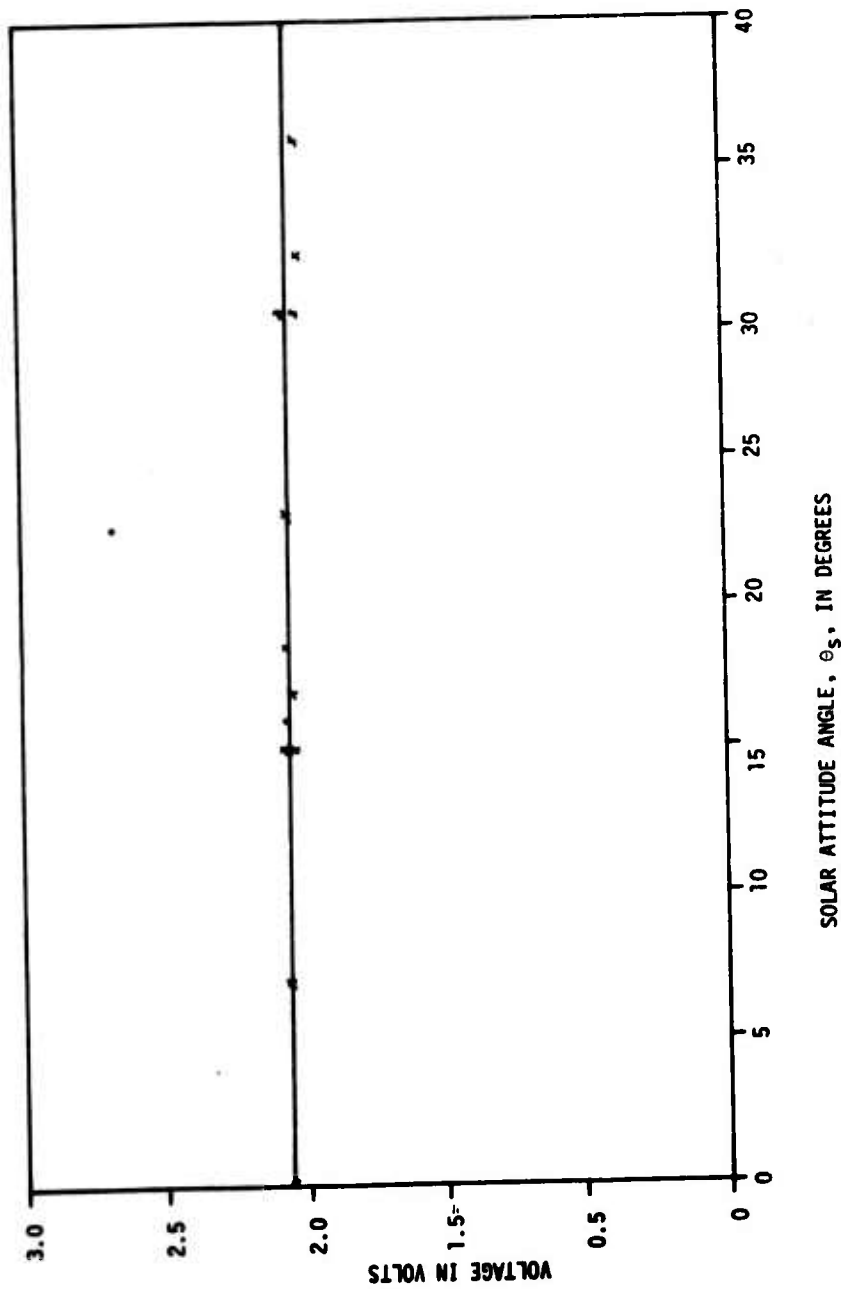


Figure 46. Module Group 2 Voltage vs. Solar Attitude Angle at Load Point Two

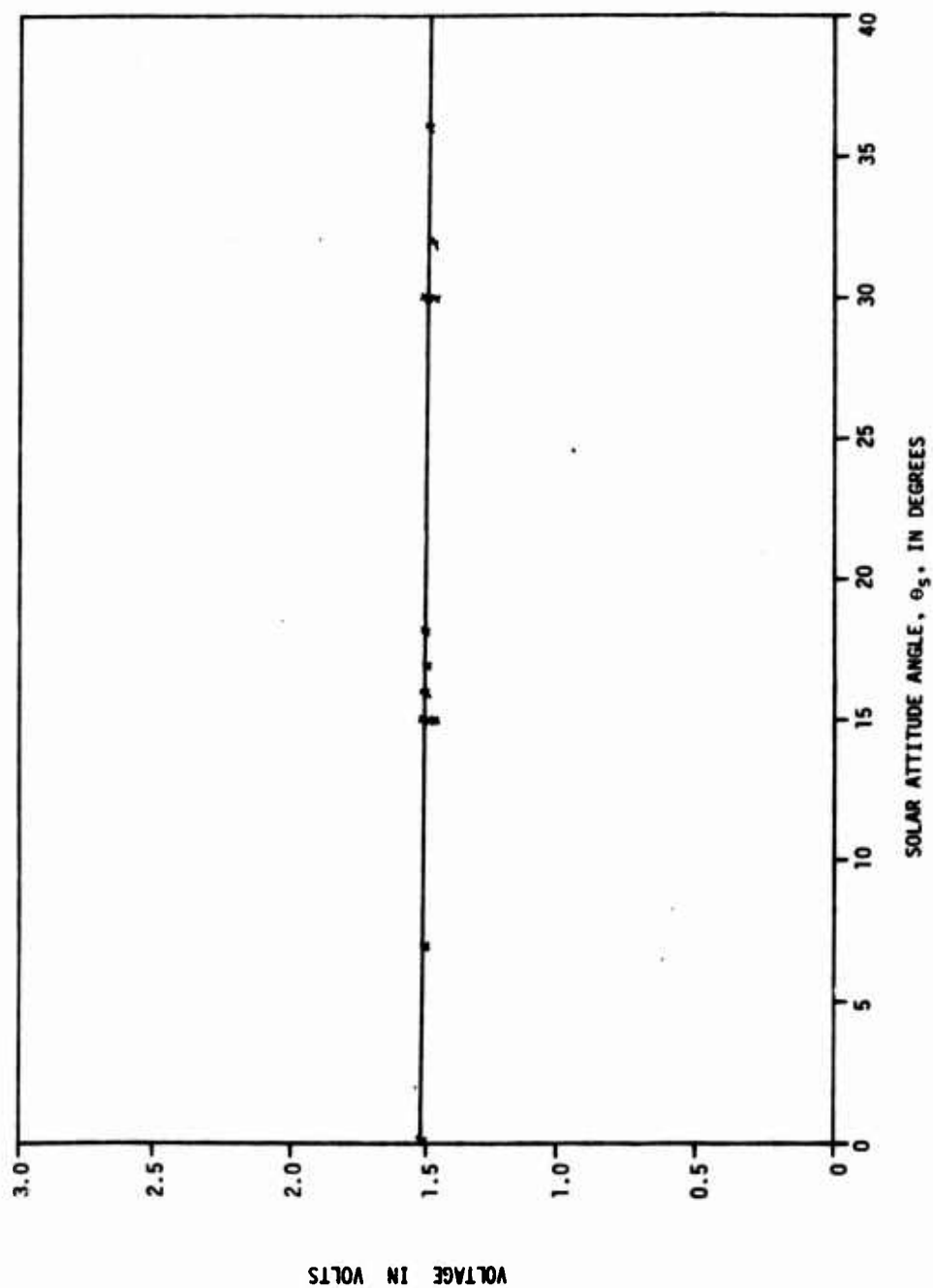


Figure 47. Module Group 3 Voltage vs. Solar Attitude Angle at Load Point Two

APPENDIX A

Derivation of Co-Ordinate Transformations for Calculations of Intensity Corrections.

Let us first define an inertial co-ordinate system as shown in Figure 48. The center of this system is the center of the ESP with the X-axis pointing toward the solar simulator, the Y axis pointing straight up, and the Z-axis to complete a right-handed system. The ESP was mounted on the goniometer in such a way that its center lies in the plane of rotation for both axes of rotation used in this experiment.

Next, we must define a local co-ordinate system that is fixed with respect to the ESP rather than inertial space. The easiest way to do this is to define the local system to be identical with the inertial system for the original panel position; however, this system moves with the panel during rotation.

To help clarify this explanation, two angles of rotation will now be defined. Pitch is defined as rotation about the inertial Z-axis with counter clockwise (CCW) rotation considered to be positive. Roll is defined as rotation about the local X-axis clockwise rotation considered to be positive. The transformation matrix associated with each of these maneuvers will now be derived.

Consider Figure 49. Elementary geometry shows that the unit vectors for the new co-ordinate system are as follows (\bar{i} , \bar{j} , and \bar{k} are the inertial unit vectors):

$$x_{Ba} = \cos \theta_p \bar{i} + \sin \theta_p \bar{j}$$

$$y_{Ba} = -\sin \theta_p \bar{i} + \cos \theta_p \bar{j}$$

$$z_{Ba} = \bar{k}$$

so that the transformation matrix is:

$$\begin{bmatrix} x_{Ba} \\ y_{Ba} \\ z_{Ba} \end{bmatrix} = \begin{bmatrix} \cos \theta_p & \sin \theta_p & 0 \\ -\sin \theta_p & \cos \theta_p & 0 \\ 0 & 0 & 1 \end{bmatrix} \begin{bmatrix} \bar{i} \\ \bar{j} \\ \bar{k} \end{bmatrix}$$

In a similar manner it can be seen from Figure 50 that:

$$x_{Bb} = \bar{i}$$

$$y_{Bb} = \cos \theta_R \bar{j} - \sin \theta_R \bar{k}$$

$$z_{Bb} = \sin \theta_R \bar{j} + \cos \theta_R \bar{k}$$

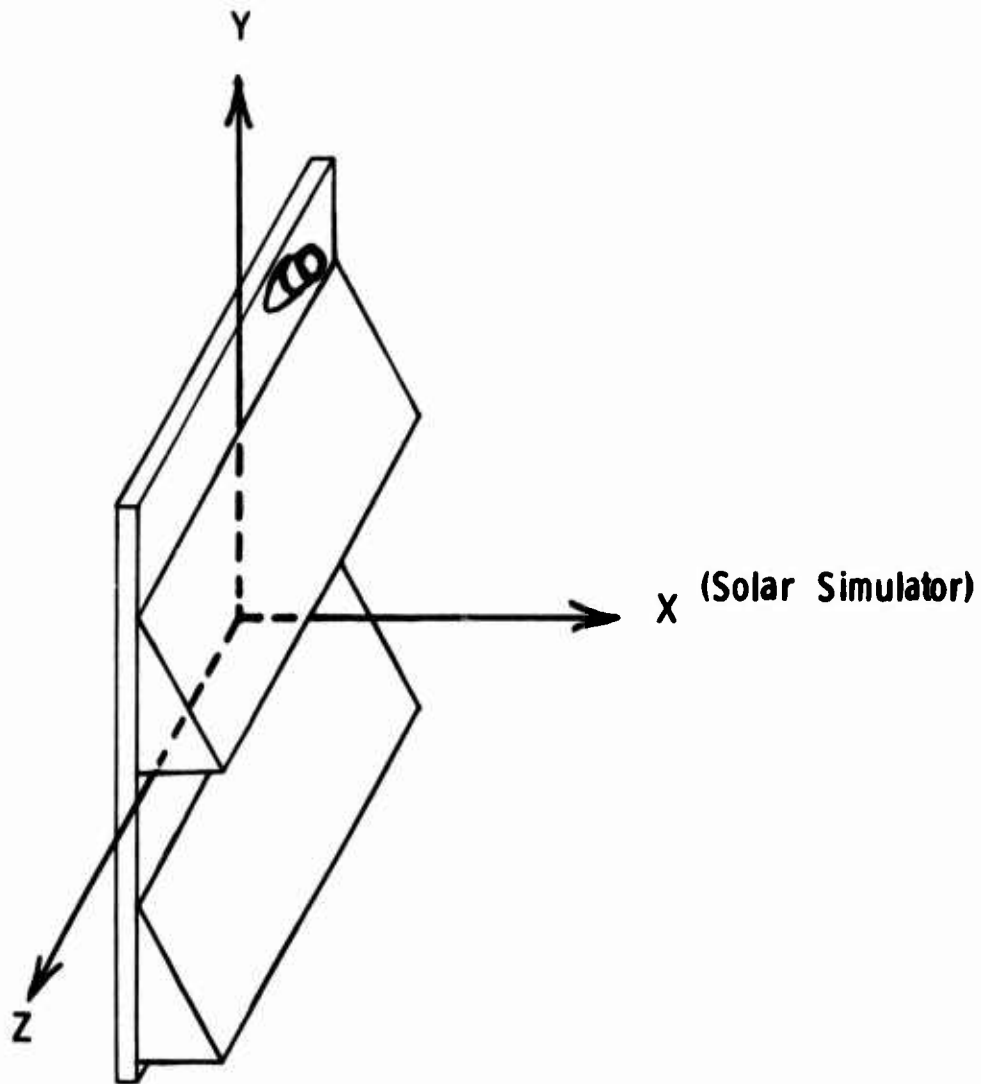


Figure 48. Inertial Coordinate System with Panel in the Unrotated Position

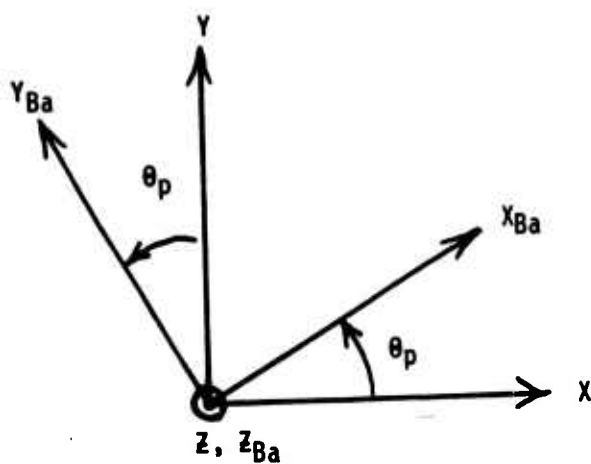


Figure 49. Pitch Rotation

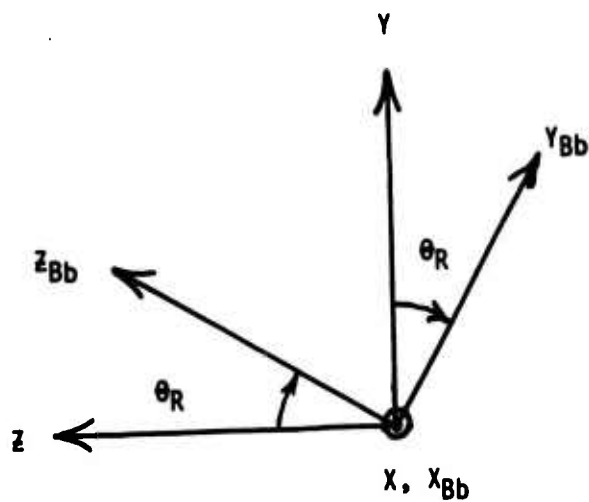


Figure 50. Roll Rotation

which yields this matrix:

$$\begin{bmatrix} x_{Bb} \\ y_{Bb} \\ z_{Bb} \end{bmatrix} = \begin{bmatrix} 1 & 0 & 0 \\ 0 & \cos \theta R & -\sin \theta R \\ 0 & \sin \theta R & \cos \theta R \end{bmatrix} \begin{bmatrix} \bar{i} \\ \bar{j} \\ \bar{k} \end{bmatrix}$$

For a given sequence of rotations, the final position can be described by the product of the matrices of each of the individual rotations. In the experiment, the goniometer was first rolled to a specified angle and then pitched from -90° to $+90^\circ$ while data was recorded by a strip chart recorder. Since the pitch rotation always takes place about the inertial Z-axis rather than the local Z-axis, the experimental procedure is equivalent to performing the pitch first (while local Z and inertial Z are identical) and then the roll.

With this argument in mind, we now compute the final transformation matrix:

$$\begin{bmatrix} x_B \\ y_B \\ z_B \end{bmatrix} = \begin{bmatrix} \text{roll matrix} \end{bmatrix} \begin{bmatrix} \text{pitch matrix} \end{bmatrix} \begin{bmatrix} \bar{i} \\ \bar{j} \\ \bar{k} \end{bmatrix}$$

$$\begin{bmatrix} x_B \\ y_B \\ z_B \end{bmatrix} = \begin{bmatrix} 1 & 0 & 0 \\ 0 & \cos \theta R & -\sin \theta R \\ 0 & \sin \theta R & \cos \theta R \end{bmatrix} \begin{bmatrix} \cos \theta p & \sin \theta p & 0 \\ -\sin \theta p & \cos \theta p & 0 \\ 0 & 0 & 1 \end{bmatrix} \begin{bmatrix} \bar{i} \\ \bar{j} \\ \bar{k} \end{bmatrix}$$

$$\begin{bmatrix} x_B \\ y_B \\ z_B \end{bmatrix} = \begin{bmatrix} \cos \theta p & \sin \theta p & 0 \\ \cos \theta R & \sin \theta p & \cos \theta R \cos \theta p \sin \theta R \\ \sin \theta R & \sin \theta p & \sin \theta R \cos \theta p \cos \theta R \end{bmatrix} \begin{bmatrix} \bar{i} \\ \bar{j} \\ \bar{k} \end{bmatrix}$$

$$x_B = \cos \theta p \bar{i} - \sin \theta p \bar{j}$$

$$y_B = \cos \theta R \sin \theta p \bar{i} + \cos \theta R \cos \theta p \bar{j} - \sin \theta R \bar{k}$$

$$z_B = \sin \theta R \sin \theta p \bar{i} + \sin \theta R \cos \theta p \bar{j} + \cos \theta R \bar{k}$$

Now that we have the transformation matrix to transform vectors from the local reference system to the inertial system we need only express the vector to the center of each module in terms of the local system. Using these vectors and knowing that the calibration plane for the experiment was 1.144 inches toward the simulator from the center of the inertial system, it is possible to calculate the actual distance of each module from the simulator and apply the necessary corrections. Since formulation of the local vectors to each module is a simple geometry problem they will not be derived here; however, the vectors are presented below for any interested party. (All dimensions are in inches.)

$$\begin{aligned}\bar{M}_1 &= .625X_B + 1.206Y_B + 2.500Z_B \\ \bar{M}_2 &= .625X_B + 1.206Y_B \\ \bar{M}_3 &= .625X_B + 1.206Y_B - 2.500Z_B \\ \bar{M}_4 &= .625X_B - 3.419Y_B + 2.500Z_B \\ \bar{M}_5 &= .625X_B - 3.419Y_B \\ \bar{M}_6 &= .625X_B - 3.419Y_B - 2.500Z_B\end{aligned}$$

It should be pointed out that the simulator beam is close enough to uniformity for any plane perpendicular to the beam to be well within experimental error for this experiment. Thus, it is necessary to calculate only the inertial X-axis component of the module vectors.

The solar attitude angle, θ_s , is computed in the following manner. We define a vector, \bar{p} , that is perpendicular to the surface of the modules (we will choose module 2 for simplicity). Since we know that the angle between the local X-axis and the module surface is 30° , it is obvious that:

$$\bar{p} = \cos 30^\circ X_B + \sin 30^\circ Y_B$$

$$\bar{p} = .866 X_B + .500 Y_B$$

Also we know that:

$$\bar{p} \cdot \bar{i} = |\bar{p}| \times |\bar{i}| \times \cos \theta_s$$

but

$$|\bar{p}| = |\bar{i}| = 1$$

so

$$\cos \theta_s = \bar{p} \cdot \bar{i}$$

$$\theta_s = \cos^{-1} [(.866) (\cos \theta_P \bar{i} + \sin \theta_P \bar{j}) + (.500) (-\cos \theta_R \sin \theta_P \bar{i} + \cos \theta_R \cos \theta_P \bar{j} - \sin \theta_R \bar{k})] \cdot \bar{i}$$

$$\theta_s = \cos^{-1} [.866 \cos \theta_P - .500 \cos \theta_P \sin \theta_P]$$

This completes the derivation of the information necessary to compute the data corrections described elsewhere in this report.

APPENDIX B

COMPUTER PROGRAM FOR TRIAD DATA REDUCTION

This program was written in FORTRAN Extended for use on the CDC 6600 computer. All of the compensating factors discussed in this paper were included. Figure 51 is the program logic flowchart. A printout of the program is included at the end of this Appendix as Figure 52.

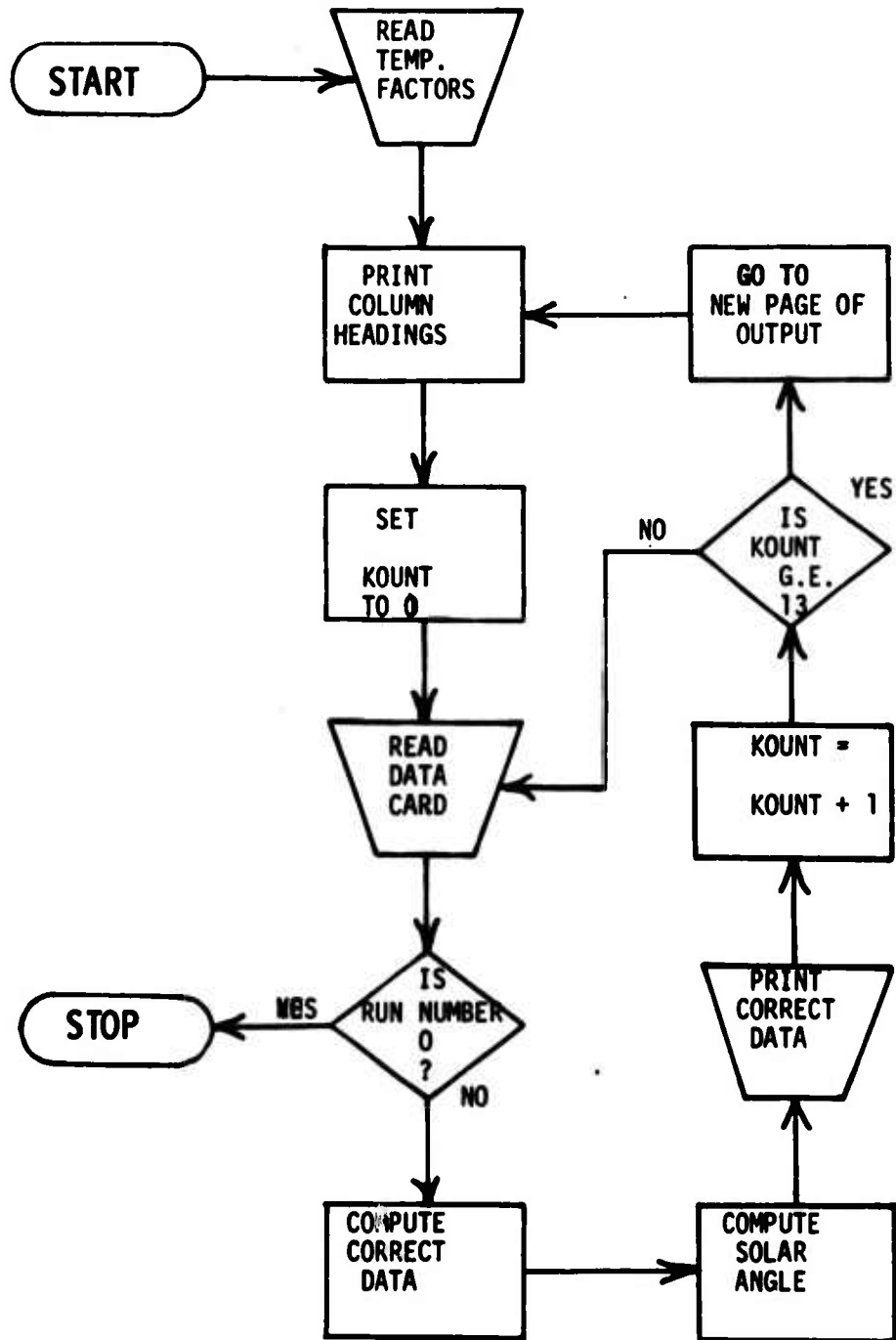


Figure 51. Computer Program Flowchart

AM TRIAD

COC 6600 FTN V3.J-320A OPT=1 12/29/77

```

PROGRAM TOIAR(INPUT,OUTPUT)
REAL M11,M21,M31,M41,M51,M61
DIMENSION T1(12),T2(12)
TREF=C
PI=3.14
100 FORMAT(2F6.3)
101 FCOMAT(T2,F4.0,F7.3,9F6.4,F5.1)
102 FCOMAT(1H0,1CY,12,7Y,F4.0,2Y,F4.0,2Y,F4.0,4F9.7,5F10.3,F8.1)
103 FCOMAT(1H1,1CX,3HOUN,1X,5HPITCH,2Y,4HPOLL,2X,4HSOLAR,2X,7HVOLTAGE,
12X,7HVOLTAGE,2X,7HVOLTAGE,2X,7HCURRENT,3X,7HCURRENT,3X,7HCURRENT,7
2X,7HCURRENT,3X,7HCURRENT,3X,7HCURRENT,4X,7HSAN)
104 FCOMAT(11Y,7HNO.,1X,5HANGLE,2Y,5HANGLE,1X,5HANGLE,2Y,7HGROUP 1,2X,
17HGROUP 2,2X,7HGROUP 3,2X,9HMODULE 1,2X,9HMODULE 2,2X,9HMODULE 3,2
2Y,9HMODULE 4,2X,9HMODULE 5,2X,9HMODULE 6,2X,5HANGLE)
105 FCOMAT(/)
70 200 I=1,12
READ 100,T1(I),T2(I)
200 CONTINUE
301 PRINT 103
PRINT 104
XCUNT=0
302 READ 101,T,FA,PA,V1,V2,V3,A1,A2,A3,A4,A5,A6,SA0
IF(I.LF.0) GO TO 400
IF(I.NF.1000) PRINT 105
TF=(PA-120.)*PI/180.
TF=PA*PI/180.
VF1=CCS(TF)
VF2=STN(TF)
VF3=0.
VF1=-COS(TF)*STN(TF)
VF2=CCS(TF)*CCS(TF)
VF3=-STN(TF)
ZF1=-STN(TF)*STN(TF)
ZF2=STN(TF)*CCS(TF)
ZF3=CCS(TF)
M11=0.625*VF1+1.206*VF2+2.50*ZF1
M21=0.625*VF1+1.206*VF2
M31=0.625*VF1+1.206*VF2-2.50*ZF1
M41=0.625*VF1-3.419*VF2+2.50*ZF1
M51=0.625*VF1-3.419*VF2
M61=0.625*VF1-3.419*VF2-2.50*ZF1
CM1=M11-1.144
CM2=M21-1.144
CM3=M31-1.144
CM4=M41-1.144
CM5=M51-1.144
CM6=M61-1.144
TUP=ACOS(1.466*STN(TF)+0.5*CCS(TF)*COS(TF))
TFUP=(00./66.0)*(TUP-24.0*PI/180.)
CA1=T2(I)*(A1/(1.0+0.0188*CM1))*(100./(101.5+1.225*COS(TPUP)))
CA2=T2(I)*(A2/(1.0+0.0188*CM2))*(100./(101.5+1.225*COS(TPUP)))
CA3=T2(I)*(A3/(1.0+0.0188*CM3))*(100./(101.5+1.225*COS(TPUP)))
CA4=T2(I)*(A4/(1.0+0.0188*CM4))*(100./(101.5+1.225*COS(TPUP)))
CA5=T2(I)*(A5/(1.0+0.0188*CM5))*(100./(101.5+1.225*COS(TPUP)))
CA6=T2(I)*(A6/(1.0+0.0188*CM6))*(100./(101.5+1.225*COS(TPUP)))

```

Figure 52. Program Printout

AFAPL-TR-73-106

AM TRIAD

CDC 6500 FTN V3.3-320A OPT=1 12/29/72

```
      CV1=T1(I)*V1
      CV2=T1(I)*V2
      CV3=T1(I)*V3
      S=35.0*(1.0-SAD/147.4)
      TS=(180./PI)*ACOS(0.966*COS(TF)-0.5*COS(TR)*SIN(TP))
      TPRF=T
      PRINT 102,I,PA,RA,TS,CV1,CV2,CV3,CA1,CA2,CA3,CA4,CA5,CA6,S
      KCUNT=KCUNT+1
      IF(KCUNT.GT.10) GO TO 301
      GO TO 302
400  CCNTINUE
      STOP
      END
```

UNCLASSIFIED

Security Classification

| DOCUMENT CONTROL DATA - R & D | | |
|--|------------------------|---|
| (Security classification of title, body of abstract and indexing annotation must be entered when the overall report is classified) | | |
| 1. ORIGINATING ACTIVITY (Corporate author) | | 2a. REPORT SECURITY CLASSIFICATION |
| Air Force Aero Propulsion Laboratory Aerospace Power Division | | UNCLASSIFIED |
| | | 2b. GROUP |
| 3. REPORT TITLE | | |
| An Evaluation of a Space Flight Test of Hardened Solar Array Technology | | |
| 4. DESCRIPTIVE NOTES (Type of report and inclusive dates) | | |
| Final Project Report January 72 through June 73 | | |
| 5. AUTHOR(S) (First name, middle initial, last name) | | |
| John M. Green, 1/Lt, USAF | | |
| 6. REPORT DATE | 7a. TOTAL NO. OF PAGES | 7b. NO. OF REFS |
| March 1974 | 82 | 0 |
| 8a. CONTRACT OR GRANT NO. | | 8b. ORIGINATOR'S REPORT NUMBER(S) |
| a. PROJECT NO. 3145 | | AFAPL-TR-73-106 |
| c. Task 314519 | | 9b. OTHER REPORT NO(S) (Any other numbers that may be assigned this report) |
| d. Work Unit 31451933 | | |
| 10. DISTRIBUTION STATEMENT | | |
| Distribution limited to U. S. Government Agencies Only: Test and Evaluation, September 1973. Other requests for this document must be referred to AF Aero Propulsion Laboratory (POE-2), WPAFB, Ohio, 45433. | | |
| 11. SUPPLEMENTARY NOTES | | 12. SPONSORING MILITARY ACTIVITY |
| | | Air Force Aero Propulsion Laboratory Wright-Patterson AFB, Ohio 45433 |
| 13. ABSTRACT | | |
| <p>Hardened solar array panel segments and experimental modules fabricated by TRW for the Air Force Aero Propulsion Laboratory are described. Preflight tests and data reduction techniques used for this experiment are explained and the results reported. The flight test, which was conducted by the Applied Physics Laboratory of Johns Hopkins University, yielded very little data due to a telemetry system failure of the host satellite (a Navy navigation satellite of the transit series). Data which was obtained in the 30 days of flight prior to the failure of presented and discussed.</p> | | |

DD FORM 1 NOV 65 1473

UNCLASSIFIED
Security Classification

UNCLASSIFIED
Security Classification

| 14. KEY WORDS | LINK A | | LINK B | | LINK C | |
|--|--------|----|--------|----|--------|----|
| | ROLE | WT | ROLE | WT | ROLE | WT |
| Solar Cells Hardened Solar Cells Flight Test of Hardened Solar Cells Aluminum Contacted Solar Cells Testing of Solar Cells | | | | | | |

UNCLASSIFIED
Security Classification